11-2020

Dissecting the Regulatory Network of Sphingolipid Biosynthesis in Plants

Ariadna Gonzalez-Solis
University of Nebraska-Lincoln, ariadna@huskers.unl.edu

DISSECTING THE REGULATORY NETWORK OF SPHINGOLIPID BIOSYNTHESIS IN PLANTS

by

Ariadna González Solís

A DISSERTATION

Presented to the Faculty of

The Graduate College at the University of Nebraska

In Partial Fulfillment of Requirements

For the Degree of Doctor of Philosophy

Major: Biochemistry

Under the Supervision of Professor Edgar Cahoon

Lincoln, Nebraska

November, 2020

DISSECTING THE REGULATORY NETWORK OF SPHINGOLIPID BIOSYNTHESIS IN PLANTS

Ariadna González Solís, Ph.D.

University of Nebraska, 2020

Advisor: Edgar Cahoon

Sphingolipids are a structurally diverse group of lipids recognized as important components of cellular membranes and regulators of processes during development and in response to environmental stresses. Much progress has been made characterizing the enzymes of the biosynthetic pathway revealing that sphingolipids are essential molecules in plants and that their synthesis and degradation needs to be tightly regulated. Serine palmitoyltransferase (SPT) catalyzes the first step in sphingolipid biosynthesis and is a primary regulatory point for homeostasis. ORM proteins have been identified as negative regulators of SPT activity, however the mechanistic details of the regulation and other functional roles of these proteins are only beginning to be understood. In this work, we show that ORM1 and ORM2 are essential for life cycle completion in *Arabidopsis thaliana*. Through the characterization of ORM gene-edited mutants we described that unregulated sphingolipid biosynthesis resulted in ceramide hyperaccumulation, altered organellar structures and increased senescence- and pathogenesis-related gene expression. Furthermore, the study of a structural ORM1 variant provided information about a transmembrane domain involved in the interaction with SPT.

In this thesis, we also provide insights into the physiological effects caused by mutations in SPT that induce the production of deoxysphingolipids. Our research

demonstrates that plants expressing these mutations showed early senescence and reduced sensitivity to the cell death induced by Fumonisin B1. These findings suggest functional roles of deoxysphingolipids that have not been explored in plants.

Finally, we describe a labeling approach to build a sphingolipid kinetic model to study the metabolic flux of sphingolipids during pathogen infection. This study considers a more comprehensive view of the sphingolipid metabolic network that changes dynamically when perturbed.

Overall, this study encompasses several aspects of sphingolipid biology in plants. From a directed understanding of the regulatory mechanism and how enzyme variants can lead to the synthesis of atypical sphingolipids to a more comprehensive understanding of the metabolic network. The combination of these approaches will provide important information to understand the regulation of sphingolipids homeostasis.

Acknowledgements

I would like to thank my advisor Edgar Cahoon for the opportunity to be part of his lab and all the support throughout my time at UNL. I would also like to acknowledge my committee members, Rebecca Roston, Jennifer Markham, Jim Alfano, Etsuko Moriyama and Rajib Saha for their guidance over the last years. Thanks also to Becky Cahoon and all the Cahoon Lab members that over the last years have been very helpful and supportive. In addition, I would like to thank Teresa Dunn and Gongshe Han for their help and insight during my graduate program.

This work was funded by the National Science Foundation (MCB 1818297) awarded to Edgar Cahoon and by the Mexican National Council of Science and Technology (Consejo Nacional de Ciencia y Tecnologia) awarded to Ariadna Gonzalez Solis.

Table of Contents

Table of Multimedia Objects

1 Chapter 1 Introduction

1. Sphingolipids

Sphingolipids are a ubiquitously distributed and diverse class of lipids that can be found in eukaryotic organisms and in some bacteria genus. Their amphiphilic nature given by a polar head group and two hydrophobic acyl chains make sphingolipids, along with glycerophospholipids and sterols, structural components of cellular membranes including plasma membrane (PM), endoplasmic reticulum (ER), Golgi apparatus, mitochondria and vacuole membranes (Moreau *et al.*, 1998). Crucial physiological processes that take place at the PM are mediated by glycosphingolipids that can form platforms for the organization and function of proteins involved in stimulus perception, signal transduction, protein translocation, endocytosis and cytoskeletal organization (Kraft et al, 2017; Laloi et al., 2007; Mongrand et al., 2004). Moreover, in plants, these glycosphingolipids enriched in the outer leaflet of the PM function as receptors of toxins produced by pathogens and are involved in sensing salt associated with environmental ionic stress (Jian et al., 2019; Lenarcic et al., 2017). Beyond their function as membrane components and receptors, other sphingolipid species play crucial roles as signaling molecules orchestrating environmental responses. Several reports have documented the roles of sphingolipids in response to drought, low temperatures, pathogenicity and as triggers of programed cell death and autophagy (Dutilleul et al., 2015; Huby et al., 2020; Magnin-Robert et al., 2015). In the last decades, a huge progress has been done in the plant sphingolipid biology field understanding the biosynthetic pathway and the functions of sphingolipid species in development and response to the environment. This knowledge

has opened new routes to discover how the cells sense sphingolipids levels and regulate the biosynthetic pathway in response to specific needs.

1.1.1 Sphingolipid Biosynthesis

In general, there is broad conservation in the way in which sphingolipids are synthesized in animals, yeast and plants. These lipids can be formed via two pathways: the *de novo* pathway, starting with the condensation of a serine with an acyl-CoA, and the salvage pathway, where complex sphingolipids are catabolized followed by channeling of the metabolites formed into the synthetic pathway (Merrill, 2002; Hannun & Obeid, 2008; Kitatani et al., 2008).

The unique and defining structural feature of sphingolipids is an amino alcohol backbone called long-chain base (LCB) or sphingoid base. The simplest and most common LCB, sphinganine (d18:0), derives from the condensation of serine and palmitoyl-CoA catalyzed by serine palmitoyltransferase (SPT) and subsequent reduction of the 3-ketosphinganine product. LCBs can be further modified by hydroxylation, desaturation, and phosphorylation to yield a range of structural variants (Figure 1.1) (Markham *et al.*, 2006; Chen, *et al*., 2009). In mammals, most sphingolipid structures contain sphingosine with Δ4 unsaturation (d18:1). In contrast, the most widely occurring LCBs in plants are sphinganine (d18:0), phytosphingosine (t18:0), 4-hydroxy-Δ8*cis/trans*-sphingenine (d18:1Δ8*trans/cis*) and Δ4trans, Δ8*cis/trans*-sphingadiene (d18:2Δ4,Δ8) (Figure 1.1) (Lynch and Dunn, 2004; Pruett et al., 2008).

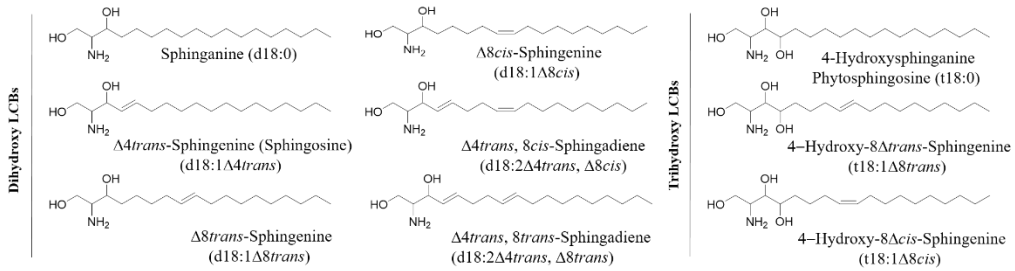

Figure 1.1 Chemical structures of long chain bases (LCBs).

Shown are examples of dihydroxy and trihydroxy LCBs commonly found in plants. Dihydroxy LCBs contain hydroxyl groups at C-1 and C-3 positions. Trihydroxy LCBs contain an additional hydroxyl group at C-4. Dihydroxy and trihidroxy LCBs can contain double bonds at Δ8 position in cis or trans configuration or in Δ4 position in trans configuration. The nomenclature d18:0 indicates that the LCB has two hydroxyl groups (d) and 18 carbons with no double bonds.

Free LCBs and their phosphorylated forms typically occur in low concentrations in eukaryotic cells. In mammals, free LCBs account for less than 1% of the total sphingolipids in tissues (Alecu *et al.*, 2017), however, they exert signaling functions such as modulating cell proliferation and apoptosis. In plant cells, free LCBs also serve as a trigger of programmed cell death (PCD) and are associated pathogen defense responses (Alden *et al.*, 2011; Zheng *et al.*, 2018; Huby *et al.*, 2019). The majority of LCBs occur in ceramides and more complex glycosylated sphingolipids.

The condensation of an LCB and a fatty acyl-CoA to form ceramides is catalyzed by ceramide synthases. Ceramide synthases have defined substrate specificities that result in ceramides with distinct pairings of structurally diverse LCBs and fatty acids (Markham *et al.*, 2011; Ternes *et al.*, 2011; Luttgeharm, et al., 2015a, Chen, *et al.*, 2015). In yeast, the two ceramide synthases, Lag1p and Lac1p, have specificity for C26-acyl CoAs to form ceramide (Guillas *et al.*, 2001). In contrast, six isoforms of ceramide synthases (CerS1-6) are expressed in mammals. Each isoform distinctly prefers to incorporate fatty acids of different chain lengths (C14-C32) into ceramides, this depends on the expression of the isoforms in certain cell type and environmental conditions (Levy and Futerman,

2010). In *Arabidopsis thaliana* (Arabidopsis), two classes of ceramide synthases have been identified. Class I, encoded by *Longevity Assurance Gene One Homolog2* (*LOH2*), mostly uses C16-acyl-CoAs to form ceramides and class II, encoded by *LOH1* and *LOH3*, act on acyl-CoAs containing more than 22 carbons (Ternes *et al.*, 2011; Luttgeharm *et al.*, 2015).

Ceramides provide the hydrophobic backbone to generate a variety of more complex sphingolipids. In yeast, ceramides can be further modified to yield abundant species including inositolphosphorylceramides (IPCs) and the glycosylated derivatives: mannose inositolphosphoceramide (MIPC) and mannose-(inositol-P)$_2$-ceramide M(IP)$_2$C (Dickson, 2010).

In plants, glucosylceramides (GlcCer) and glycosylinositolphosphoceramides (GIPCs) are the most abundant sphingolipids (Gronnier et al., 2016; Markham et al., 2006). GlcCer is the simplest glycosphingolipid that occurs broadly in eukaryotes, but not in *Saccharomyces cerevisiae*. GlcCer synthase is the ER-localized enzyme that catalyzes the condensation of ceramide with UDP-glucose (Leipelt *et al.,* 2001). GlcCer are enriched with C16-ceramides and dihydroxy-LCBs (Markham *et al.,* 2006). According to this composition, it has been suggested that the ceramide synthase Class I (LOH2) has preference for channeling the substrates to the formation of GlcCer. In contrast, GIPCs are enriched in ceramides with VLCFA and trihydroxy LCBs formed by the Class II ceramide synthases LOH1/LOH3 (Markham *et al.,* 2006). Similarly, in the case of mammalian cells, ceramides are the precursors of GlcCer, galactosylceramides (GalCer) and other numerous sphingolipids that are absent in plants and fungal cells including

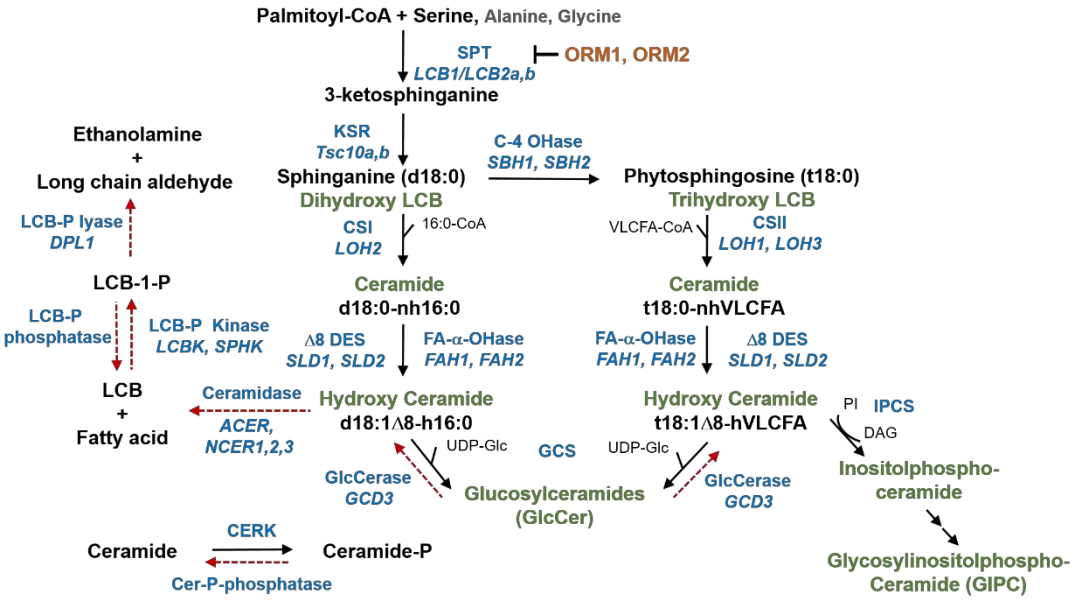

Figure 1.2 Sphingolipid biosynthesis in Arabidopsis.

Sphingolipid classes are indicated in green. Enzymes and the corresponding genes are indicated in blue. Solid arrows indicate biosynthesis steps and dashed arrows indicate catabolic steps. Abbreviations: LCB, Long chain base; SPT, serine palmitoyltransferase; KSR, 3-ketosphinganine reductase; C4-OHase, C4-LCB hydroxylase; CSI, ceramide synthase class I; CSII, ceramide synthase class II; VLCFA, very long chain fatty acid, Δ8 Des, D8 desaturase; GCS, glucosylceramide synthase; GlcCerase, glucosylceramidase; IPCS, inositol phosphoceramide synthase; PI, phosphatidylinositol; DAG, diacylglycerol; CERK, ceramide kinase.

sphingomyelin, characterized by the presence of a phosphorylcholine headgroup and gangliosides containing sialic acid residues.

Sphingolipid synthesis is compartmentalized between two organelles in the cell. The synthesis of LCBs, ceramides and GlcCer takes place in the ER, but further metabolic steps to generate GIPCs occurs in the Golgi apparatus. As noted earlier, GlcCer contain higher amounts of C16 fatty acids and dihydroxy LCBs, instead, GIPCs are enriched in ceramides containing VLCFA and trihydroxy LCBs. In this scenario a selective vesicular or non-vesicular transport would be needed to for the synthesis of GIPCs in the Golgi apparatus. In mammals, ceramide is transported from the ER, the site of synthesis, to Golgi by a non-vesicular mechanism mediated by CERT proteins (Kudo et al., 2008).

Ceramides can also be deacylated by ceramidases to generate fatty acids and LCBs which may then be phosphorylated by LCB kinases to produce LCB-P. In mammalian cells, the sphingosine generated by ceramidases can be then phosphorylated by an LCB kinase generating sphingosine-1 phosphate (d18:1-P), a potent intra- and extra-cellular signaling molecule (Mao and Obeid, 2008). While ceramide synthases are the main route to synthesize ceramides, reverse ceramidase activity also contributes to ceramide formation (Mao *et al.*, 2000). This ceramide synthase activity involves the condensation of a fatty acid and an LCB through an acyl-CoA-independent mechanism, this activity was first described in *Saccharomyces cerevisiae* for the ceramidases Ypc1 and Ydc1 (Mao et al., 2000). Arabidopsis has one alkaline ceramidase (ACER) and three neutral ceramidases (NCER1,2,3) that are involved in keeping sphingolipid homeostasis under environmental stresses (Li et al., 2015; Wu et al., 2015; Zheng et al., 2018), however, the ceramide synthesis activity has yet to be determined for these enzymes.

Finally, to exit the sphingolipid metabolic network, the phosphorylated forms of LCBs are substrate for LCB phosphate lyase also known as sphingosine-1-phosphate lyase (S1P-lyase or DPL1) the enzyme that catabolizes the sphingolipid backbone to produce ethanolamine phosphate and hexadecenal, both of which can enter the glycerolipid metabolism (Mao, Saba and Obeid, 1999; Tsegaye *et al.*, 2007).

The pool of different sphingolipid species is in constant dynamic flux and responds to the metabolic demands on the cell and the biotic and abiotic stresses from the environment. This balance not only considers the *de novo* biosynthesis but also the breakdown of more complex sphingolipid species to give rise to intermediates of the pathway with a functional role. How cells sense alterations in sphingolipids levels, in

response to developmental cues or environmental stimulus, and adjust the rates of the reactions to maintain homeostasis are vital mechanisms which are only recently beginning to be understood.

1.1.2 Serine Palmitoyltransferase

The *de novo* sphingolipid biosynthetic pathway begins with SPT, a CoA-dependent acyltransferase, which typically catalyzes the condensation of L-serine with palmitoyl coenzyme-A (palmitoyl-CoA) to form 3-ketosphinganine. Besides using L-serine as substrate to form the canonical LCBs, SPT also shows activity towards glycine and L-alanine to generate an atypical category designated 1-deoxysphigolipids (Chapter 4) (Penno *et al.*, 2010). The reaction catalyzed by SPT is highly conserved across multiple species even though the downstream enzymes have diverged in such a way to give rise to some sphingolipid species that are only found in mammals, plants or fungi.

In prokaryotes, SPT is a soluble homodimer with two catalytic sites at the interphase (Hanada, 2003; Ikushiro *et al.*, 2007; Yard *et al.*, 2007). In eukaryotes, SPT consists of a heterodimer with two major subunits (LCB1 and LCB2 in yeast; LCB1 and LCB2a or LCB2b in plants; SPTLC1 and SPTLC2 or SPTLC3 in mammals). A third subunit is a small protein required for optimal activity. In yeast there is a single isoform (Tscp3), not required for basal activity but it can increase it by 30 fold. In higher eukaryotes there are more subunits, in plants (ssSPTa and ssSPTb) or three in the case of mammals (Kimberlin et al., 2013; Han et al., 2009). These subunits confer acyl-CoA specificity and can increase the activity by 100 fold.

In mammalian cells, the subunit composition of SPT determines fatty-acyl-CoA substrates. For example, the complex formed by SPTCL3 and/or ssSPTb allow the use of

other shorter or longer acyl-CoAs to generate atypical LCBs (Han et al., 2009). While palmitoyl-CoA is the preferred substrate for the complex SPTLC1/2 ssSPTa, other combinations with SPTLC3 ssSPTb can use myristoyl (14:0)-CoA and stearoyl (18:0)-CoA.

Interestingly, in Arabidopsis, it is only 33 amino acids of ssSPTa which are required for activation of the SPT heterodimer and for conferring the acyl-CoA specificity (Kimberlin *et al.*, 2013). A single mutation in ssSPTa (Met25 to Gly) results in the change of substrate specificity from C16 acyl-CoA to longer substrates (C20). However, the exact molecular details of how these small proteins stimulate SPT activity are still unknown and what is the functional effect of the generation of atypical sphingolipids is also under investigation.

1.1.3 Regulatory Mechanisms of SPT Activity

Sphingolipid metabolism can be regulated at multiple levels, including enzyme expression, degradation and localization, post-translational modifications, protein-protein interactions and allosteric mechanisms. These regulatory mechanisms respond to intracellular sphingolipid levels and to extracellular stimuli. SPT, as the first enzyme of the pathway, controls the amounts of serine and palmitoyl-CoA that get channeled for sphingolipid biosynthesis, therefore this step is tightly regulated. The molecular mechanisms of governing the regulation of SPT are complex and constitute an active area of research.

The formation of higher order oligomers has been proposed as a mechanism for regulating SPT activity. In the case of the mammalian SPT, it has been shown that the functional complex is an octamer of catalytic heterodimers with a molecular mass of

~480 kDa. This highly organized complex includes the three SPT subunits (SPTLC1, SPTLC2 and SPTLC3) with a stoichiometry that is in dynamic change (Hornemann, Wei and Von Eckardstein, 2007). In addition to oligomerization of the SPT complex, changes in subcellular localization might also be related to the regulation of its activity. Based on localization studies, the repressed SPT resides to the peripheral ER and the active form in the perinuclear (Breslow *et al.*, 2010).

1.1.4 ORM Proteins are Regulators of SPT activity

Additional members of the SPT complex are the Orosomucoid or ORM proteins. There are two isoforms of ORM proteins in yeast (Orm1 and Orm2) and plants (ORM1 and ORM2) and three isoforms of ORMDLs in mammalian cells. These non-catalytic proteins play a role as negative regulators of SPT activity.

The first evidence of the role of Orm proteins in the regulation of sphingolipid synthesis revealed that the deletion of Orm1/2 resulted in an increase of sphingolipid levels compared to wild type cells in yeast (Breslow *et al.*, 2010). Interestingly, the *Δorm1Δorm2* mutant was more sensitive to DTT and tunicamycin, compounds known to induce unfolded protein response (UPR) and ER stress (Han *et al.*, 2010). Similar results were obtained using mammalian cells, where downregulation of the three ORMDL isoforms by siRNAs led to 3-fold increase in ceramide levels (Breslow *et al.*, 2010).

In *Saccharomyces cerevisiae*, SPT activity is regulated by Orms through post-transcriptional mechanisms in response to sphingolipids availability. This was established when the inhibition of SPT using myriocin triggered the phosphorylation of Orm proteins and caused a change in their subcellular localization from cortical to perinuclear ER (Breslow *et al.*, 2010). When sphingolipid levels are reduced, by decreasing SPT activity,

Orm proteins get phosphorylated at N-terminal serine residues by the Ypk1 kinase, downstream of TORC2, releasing SPT from Orm inhibition (Roelants *et al.*, 2011; Sun *et al.*, 2012). Once sphingolipids have been replenished the ceramide responsive phosphatase (PP2A) (Sun *et al.*, 2012) dephosphorylates Orms allowing the regulatory inhibition of SPT. A current model of sphingolipid synthesis regulation in yeast suggests the formation of higher-order oligomers including Orms and the SPT subunits Lcb1/2 that respond to specific requirements of sphingolipids by modulating SPT activity (Breslow *et al.*, 2010).

In addition, another layer of regulation is attributed to the phosphorylation at different serine residues by the kinase NPR1, downstream of TORC1, in response to limiting complex sphingolipids. In this case, the mechanisms activate complex sphingolipids synthesis and migration to the plasma membrane where they exert an effect on the permease to allow the internalization of nutrients (Shimobayashi *et al.*, 2013).

While multiple evidences show that plant and mammalian ORM proteins play a key role in regulating SPT activity, it is clear that the regulatory mechanisms differ from those in yeast due to the lack of the phosphorylation sites at the N-terminus of the plant ORM protein. In this context, recent studies using mammalian cell cultures suggested that the regulation of SPT by ORMDLs does not require cytosolic proteins or small molecules like ATP, ruling out the possibility of post-translational modifications like phosphorylation as a regulatory process (Davis *et al.*, 2019). Instead, the ORM-SPT regulation seems to respond to ceramide levels. Gupta et al. (2015) described how the induction of SPT activity increased ORMDL protein levels and blocking ceramide synthases suppressed this regulation. Additionally, incubation of isolated membranes with soluble ceramides

strongly inhibited *de novo* sphingolipid biosynthesis (Davis et al., 2019). These results indicate that ORMDL proteins might be regulated by an allosteric effect of ceramide or by a ceramide sensitive protein-protein interaction involving ORMs. However, although some evidences point to ceramides containing trihydroxy LCBs and VLCFAs as the main candidates to orchestrate this regulation, the mechanism is still unclear (Davis et al., 2019). Moreover, another open question is whether each ORMDL isoform is responding to ceramide levels and regulating SPT in the same way.

1.1.5 Localization and Topology of ORM proteins

ORMs are primarily localized to the ER (Kimberlin *et al.*, 2016). However, recent reports in plants showed ORMs can also localize in vesicles and in the PM to exert other functions related to protein degradation by autophagy playing a key role in plant immunity (Yang *et al.*, 2019).

The ORM proteins form stable complexes with SPT subunits to regulate its activity, direct binding of Orm1 and Orm2 with Lcb1, Lcb2, and Tsc3 has been reported in yeast, however the key regions involved in these interactions are not known. Different biochemical approaches have been used to determine the topology of ORM proteins with the final goal to predict regions involved in protein-protein interaction and to identify the allosteric ceramide binding domain. The topology of mammalian ORMDL3 and ORMDL1 proteins was determined using fluorescence-based protease protection assay and substituted cysteine accessibility method (SCAM), respectively (Davis, Suemitsu and Wattenberg, 2019). While the topology of the yeast Orm2 and the Arabidopsis ORM1 protein was studied using inserting glycosylation cassettes at specific sites of the protein

(Kimberlin *et al.*, 2016). These different approaches confirmed the existence of four transmembrane domains with the amino- and carboxy- termini facing the cytosol.

1.1.6 Degradation of ORM proteins

An additional mechanism for the regulation of SPT activity is the increased turnover of ORM proteins. In mammalian cells, the imbalance of PM lipid composition generated by adding exogenous cholesterol induced degradation of ORMDL1 protein, through autophagy, and resulted in increased SPT activity without changes in the levels of SPT subunits (Wang *et al.,* 2015). In yeast, a selective degradation of Orm2 by a novel route was shown to contribute to sphingolipid homeostasis. The phosphorylation of Orm2 via the TORC2-dependent Ypk1 kinase triggers its export from the ER to the Golgi. Once on Golgi and endosomes, Orm2 is poly-ubiquitinated by the ubiquitin ligase complex (Dsc). Then Cdc48/VCP extracts ubiquitinated Orm2 from membranes for proteasomal degradation (Schmidt *et al.*, 2019). This novel degradation pathway by EGAD (endosome and Golgi-associated degradation pathway) prevents the accumulation of Orm2 at the ER and promotes the controlled de-repression of sphingolipid biosynthesis. Interestingly, although Orm1 shares 72% amino acid identity with Orm2, this protein was not target of the Dsc complex for degradation.

Regulation of sphingolipids biosynthesis is crucial for growth and to respond to environmental stimuli. Several exciting discoveries have been made in this area of research in the last decade, however, many questions remain unanswered. For example, the mechanisms behind the SPT regulation by ORM proteins in multicellular eukaryotes remain unclear. While in the yeast model the post-translational modifications are essential for sensing and responding to sphingolipid availability, in plants and mammals the

allosteric regulation and protein-protein interactions appear to be the governing mechanisms. Although the yeast Orm double knockout has been characterized, the lack of a complete knockout in plants limits the study of the physiological implications of an unregulated sphingolipid biosynthesis in multicellular eukaryotes. In Chapter 2 of this thesis we show ORM1 and ORM2 are essential for life cycle completion in Arabidopsis. *orm1*$^{-/-}$ *orm2*$^{-/-}$ seeds were nonviable, accumulated ceramide levels, displayed aberrant embryo development, and had >80% reduced oil content versus wild-type seeds. This phenotype was mimicked in Arabidopsis seeds expressing the SPT subunit LCB1 lacking its first transmembrane domain, which is critical for ORM-mediated regulation of SPT. In Chapter 3, we provide some insights about the regulatory interaction of ORM proteins with the LCB1 subunit of SPT. This was possible by the characterization of the *orm1*$^{\Delta met/\Delta met}$ *orm2*$^{-/-}$ mutant, which expresses an ORM1 structural variant that is strongly compromised in the regulation of SPT activity. These plants that did not advance beyond the seedling stage and hyperaccumulated ceramides and other sphingolipids.

In addition, despite the compelling evidence of the functional redundancy of ORM isoforms in yeast, mammals and plants; recent reports point to potential individual roles and distinct regulation of each ORM isoform (Dang et al., 2017; Schmidt et al., 2019). In Chapter 2 we also uncovered phenotypical growth differences of *orm1*$^{+/-}$ *orm2*$^{-/-}$ *and* *orm1*$^{-/-}$ *orm2*$^{+/-}$ mutants that provide insights into potential differential roles of ORM1 and ORM2 in plant development. This area of study remains unexplored in the context of sphingolipid biosynthesis and other physiological processes.

1.2 Deoxysphingolipids

Sphingolipid metabolism has been extensively studied in humans due to the association of mutations in genes encoding enzymes of the sphingolipid pathway to diseases (Hannun and Obeid, 2018; Dunn et al., 2019). One example is the rare condition Hereditary Sensory and Autonomic Neuropathy type 1 (HSAN1) that has been associated the production of deoxysphingolipids (Penno *et al.*, 2010). Deoxysphingolipids are atypical sphingolipids that are generated when SPT utilizes alanine or glycine instead of serine. As mentioned before, in the sphingolipid biosynthesis pathway, the formation of the canonical LCB sphinganine (d18:0) requires the condensation of palmitoyl-CoA with L-serine. Instead, the use of L-alanine gives rise to 1-deoxysphinganine (1-deoxySA; m18:0) and glycine results in the formation of 1-deoxymethylsphinganine (1-deoxymethylSA; m17:0) (Lone *et al.*, 2019) (Figure 1.3).

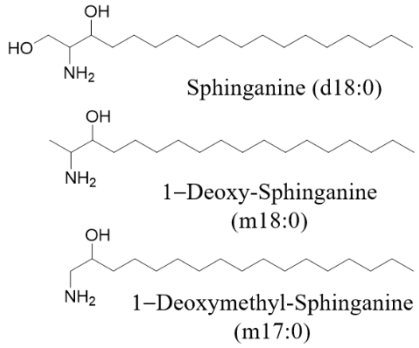

Figure 1.3 Chemical structures of deoxyLCBs.

Shown are the LCB sphinganine (d18:0) and the deoxyLCBs 1-deoxysphinganine (1-deoxySA; m18:0) and 1-deoxymethylsphinganine (1-deoxymethylSA; m17:0). The position of double bonds in plant deoxyLCBs is not known.

These LCBs, and the compounds derived from them, are called 1-deoxysphingolipids due to the lack of the hydroxyl group at C1 position which prevents the addition of a polar head group to the ceramide backbone to generate more complex sphingolipids which are the major forms in which LCBs occur in the cell. In addition, it is

important to note that the lack of the 1-hydroxyl group in these compounds precludes their canonical catabolism through the generation of LCB-1-phosphates.

In the last decade, great progress has been made understanding the metabolism and effects of deoxysphingolipids in the context of the HSAN1 condition in humans. However, even though these lipids have been also found in fungal species and marine organisms such as *Spisula polynyma* (Cuadros *et al.*, 2000), they remain largely unexplored in plants. In this section we present some of the advances understanding the synthesis and cellular effects of deoxysphingolipids in mammalian cells and yeast.

1.2.1 HSAN1 Mutations are Related to the Synthesis of Deoxysphingolipids

Even though wild-type SPT can generate deoxyLCBs, missense mutations in the SPTLC1 and SPTLC2 subunits have been linked to increased levels of deoxysphingolipids in the context of HSAN1 (Penno et al., 2010; Zitomer et al., 2009). Some of the most frequent mutations found in patients are SPTLC1 C133W, C133Y, S331F, S331F and SPTLC2 A182P, G382V, S384F, I504F (Bode et al., 2015); the analysis of structural models suggests these mutations induce a shift in the substrate specificity of SPT, from L-serine to L-alanine or glycine which leads to the formation of the two 1-deoxyLCBs (Penno et al., 2010; Bode et al., 2015). In contrast, other mutations localized to the surface of the protein (SPTLC1-S331Y and SPTLC2-I505F) are associated with a severe HSAN1 phenotype and could be involved in protein-protein interactions favoring the production of these atypical sphingolipids (Rotthier et al., 2010).

For ceramide formation, the N-acylation of LCBs and fatty acyl-CoAs of different chain length is defined by the ceramide synthase substrate preference. There is also a distinction in the N-acyl chain distribution of deoxyceramides. In mouse fibroblasts,

supplementation with m18:0 revealed this LCB was incorporated to a variety of acyl-CoAs from C16 to C24:1; while m18:1 was preferentially acylated to VLCFA (Alecu *et al.*, 2017). However, in contrast to the typical ceramides where the Δ4-desaturase (DEGS1) introduces a *trans* double bond at Δ4 position, in the deoxyceramides the double bond is at position Δ14, and the desaturase has not been identified (Steiner *et al.*, 2016).

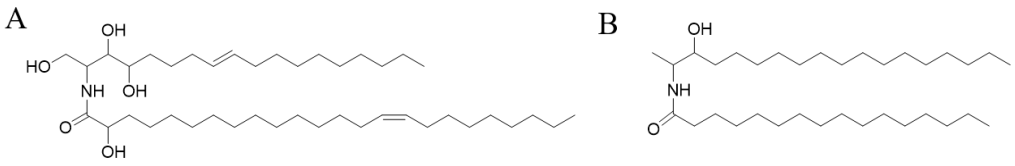

Figure 1.4 Chemical structures of ceramides.

Ceramides are formed by the condensation of a LCB and a fatty acyl-CoA through ceramide synthase. (**A**) Hydroxyceramide composed of the LCB t18:1 Δ8 *trans* and the fatty acid 24:1ω9*cis* hydroxylated at C-2 position. (**B**) Non-hydroxylated deoxyceramide composed of the LCB m18:0 and the fatty acid 16:0.

1.3 Cellular Effects of Deoxysphingolipids

Even though the underlying mechanisms behind the HSAN1 condition are not fully understood, the toxic effects on the neurons and other cells have been attributed to the accumulation of deoxysphingolipids. Some of the effects include altered Ca^{2+} levels related to changes in mitochondria and ER morphology (Alecu *et al.*, 2017); disassembly of actin fibers and other changes in cytoskeletal structures and (Cuadros *et al.*, 2000), changes in the physicochemical properties of membranes (Jiménez-Rojo *et al.*, 2014).

In mammalian cells, the accumulation of canonical ceramides, either by *de novo* synthesis or hydrolysis of complex sphingolipids, activates apoptosis (Bartke and Hannun, 2009). In addition to the activation of signaling pathways, another way the accumulation of ceramides may impact cell processes is by alterations in the biophysical properties of membranes. Saturated ceramides increase the order of the fluid membranes

and tend to form gel domains; while ceramides with VLCFA promote the formation of interdigitated phases (Pinto et al., 2011). In contrast to canonical sphingolipids, the lack of the hydroxyl group in position 1 make deoxyceramides more hydrophobic and limits their capacity to form hydrogen bonds with other membrane lipids. This results in poor miscibility with other membrane lipids, aggregation and a great influence in cellular membranes, especially the ER membrane in which these lipids are synthesized. Studies on giant unilamellar vesicles (GUVs) made with a mixture of sphingomyelin and deoxyceramides revealed that these lipids induce gel-fluid phase separation and are able to induce the vesiculation of these GUVs (Jimenez-Rojo et al., 2014). It is important to note that the impact on membrane integrity is also dependent on the abundance of these compounds. Interestingly, Jimenez-Rojo et al. (2014) found comparable amounts of 1-deoxyDHCers and ceramides in a murine macrophage cell line under normal conditions.

1.3.1 HSAN1-like Mutations Affect SPT Activity

Analysis of HSAN1 patients revealed the two most frequent mutations correspond to SPTLC1 at Cys133 (C133W or C133Y) and Val144 (V144D), these residues are in a highly conserved region of LCB1 that is predicted to be a catalytic domain. Gable et al. (2001) found that the corresponding mutations (C180W, C180Y, and V191D) in the LCB1 gene of *Saccharomyces cerevisiae* reduced SPT activity by 50 % and increased the levels of 1-deoxySA. Similarly, HSAN1-associated mutations were shown to confer dominant negative effects on the SPT activity in lymphoblasts even though the protein levels of LCB1 and LCB2 subunits did not change (Bejaoui *et al.*, 2002). Reduced SPT activity was also observed in transgenic mice expressing the $LCB1^{C133W}$ allele (McCampbell *et al.*, 2005), however, even though the composition of the ceramide pool

was altered, the total ceramide levels in these mice were unaffected. This suggests the activation of alternative mechanism to regulate ceramide degradation or the conversion to glycosylated sphingolipids. Interestingly, using a metabolic labeling approach the mutations in SPTLC1$^{S331F/Y}$ and SPTLC2^{I504F} resulted in increased SPT activity when expressed in HEK293 cells, and the rest of the seventeenth analyzed mutations did not induce any change in activity. However, under FB1 treatment eleven mutations induced a reduction in SPT activity (Bode *et al.*, 2015).

1.3.2 Degradation of Deoxysphingolipids

1-deoxyspingolipids lack the hydroxyl group at C1 which prevents the addition of a polar head group to the ceramide backbone to generate more complex sphingolipids. In addition, the lack of this hydroxyl group also blocks the phosphorylation of LCBs affecting the canonical degradation pathway by the enzyme LCB lyase that uses phosphorylated LCBs to generate phosphoethanolamine and hexadecenal, the breakdown products of sphingolipid catabolism.

The accumulation of 1-deoxysphingolipids has been used a strategy in yeast to indirectly measure the activity of SPT under the assumption that these structures accumulate and are not degraded. However, a recent report showed the reduction of intracellular concentration of 1-deoxysphingolipids over time suggesting alternative degradation/elimination pathways. 1-deoxysphingosine (m18:1) was metabolized to a variety of hydroxylated downstream metabolites that appeared to be formed by cytochrome P450 enzymes (Alecu *et al.*, 2017). Compared to the catabolism of the canonical LCBs that takes place in minutes to hours, the conversion of the newly identified metabolites is slower and can take up to several days (Alecu *et al.*, 2017).

In Chapter 4, we describe that the incorporation of HSNA1-like mutations into Arabidopsis resulted in early senescence and resistance to the cell death triggered by the mycotoxin Fumonisin B1.

1.4 Metabolic Modeling

Computational systems biology has emerged as a field to describe biological networks using mathematical models. Mathematical modeling allows to describe the behavior of complex biological systems characterized by a substantial larger number of parameters for predicting cellular phenotypes (Kim, Rocha and Maia, 2018). Some applications include the design of microbial strains for overproduction of metabolites of industrial interest. The process of model building is iterative, combining experimental testing for validation and *in silico* analysis for optimization (Gadkar, Gunawan and Doyle, 2005). A model can accelerate the process of hypothesis generation and testing by predicting plausible regulatory mechanisms that satisfy the observed experimental behavior of the system under different growth conditions. It can also allow the simulation of acute perturbations that are normally not amenable to try with experimentation.

Depending on the specific applications, mathematical models vary in their formulation and complexity. The two main categories of mathematical modeling applied to metabolism are: steady state and kinetic (Islam and Saha, 2018).

Flux balance analysis (FBA) is in the category of steady-state modeling and relies on genome-scale metabolic models and the stoichiometry of the metabolic networks to predict the optimal flux distribution and the impact of perturbations (e.g. gene knock-out/overexpression) (Varma and Palsson, 1994). This approach allows the quantitative interpretation of the metabolic physiology to provide a method for the design and

optimization of bioprocesses. However, steady-state/stoichiometric models do not capture essential information like metabolite concentration, enzyme kinetics and regulatory processes.

Meanwhile, the use of dynamic models including metabolic and regulatory processes through kinetic expressions (rate equations of enzyme reactions), increases the accuracy of the phenotype predictions in terms of the temporal behavior of the metabolic network (Zielinski and Rohwer, 2012). However, practical applications of this approach are often not feasible due to the lack of defined enzyme kinetic parameters for all enzymes in the network.

To overcome this limitation, ensemble kinetic modeling (EM) (Tran, Rizk and Liao, 2008) was developed to build accurate predictive models by sampling through the entire allowable kinetic solution space. A strategy to reduce the allowable solution space that needs to be spanned is enforcing thermodynamic feasibility constraints on the metabolic reactions (Henry, Broadbelt and Hatzimanikatis, 2007; Tran, Rizk and Liao, 2008). The model is then filtered using measured parameters of the system's response to different genetic perturbations (Rizk and Liao, 2009). In addition, EM can be used to predict regulatory interactions occurring in biochemical pathways (Khazaei, McGuigan and Mahadevan, 2012).

Most of the metabolic modeling for biotechnological purposes has been done in prokaryotes. Some reasons for the scarcity of eukaryotic models are derived from the complexity of these organisms in terms of subcellular localization of proteins/metabolites, intra and extra cellular transporters, limited knowledge of gene annotation, interactions with different tissues/organs.

1.4.1 Modeling Sphingolipid Metabolism

Currently, only few models of sphingolipid metabolism are available in the literature. In part, this is due to the challenges given by the diversity in sphingolipid composition and the complexity of the numerous interconnected reactions that happen in various subcellular compartments. A mathematic model of the sphingolipid biosynthesis was first reported in yeast. This model allowed simulations of metabolic fluxes, included the connection with phospholipid metabolism and was able to predict outcomes when enzyme where deleted (Alvarez-Vasquez *et al.*, 2005). A second study in yeast developed a comprehensive kinetic model which can predict changes in enzyme activity based on changes in metabolic concentrations that result from genetic perturbations. This model included pathways for the synthesis of fatty acids to determine potential genes that impact the distribution of sphingolipid species (Savoglidis *et al.*, 2016). Beyond yeast, (Gupta *et al.*, 2011) proposed a model including data from lipidomic and transcriptomic analyses to describe the sphingolipid pathway in mammalian cells. In addition, a recent study described a model of sphingolipid metabolism in human tissue that simulates the molecular scenarios in the context of Alzheimer disease including different subcellular compartments (Wronowska *et al.*, 2015).

It is important to note how various regulatory processes, at the transcriptional and protein levels are important for the homeostasis of the sphingolipid synthesis. The previously reported sphingolipid models did not consider regulatory parameters in the kinetic models or assumed a defined regulatory network. The inclusion of the regulation schemes by ORMs and other proteins in the models can have an impact on the analysis of the network response and thus can lead to different conclusions and hypotheses.

Previous efforts on modeling the sphingolipid pathway have used *Saccharomyces cerevisiae* and mammalian cells, however, there are no models based on data from plant sphingolipid metabolism. It is important to note that the sphingolipid levels typically reported in the literature correspond to steady state measurements, the result of the synthesis and turnover of metabolites that cannot be distinguished with the analytical tools. In Chapter 5, we provide some advances towards building a sphingolipid kinetic model with measurements derived from metabolic labeling. It is then intent of such model to provide a basis for understanding synthesis and turnover of sphingolipids in the context of cellular responses during pathogen infection.

1.5 References

Alden, K.P., Dhondt-Cordelier, S., McDonald, K.L., Reape, T.J., Ng, C.K., McCabe, P.F., and Leaver, C.J. (2011). Sphingolipid long chain base phosphates can regulate apoptotic-like programmed cell death in plants. Biochem. Biophys. Res. Commun. 410: 574–580.

Alecu, I., Othman, A., Penno, A., Saied, E.M., Arenz C., von Eckardstein, A., Hornemann, T. (2017) Cytotoxic 1-deoxysphingolipids are metabolized by a cytochrome P450-dependent pathway, J. Lipid Res. 58:60–71.

Alecu, I., Tedeschi, A., Behler, N., Wunderling, K., Lamberz, C., Lauterbach, M.A., Gaebler, A., Ernst, D., Van Veldhoven, P.P., Al-Amoudi, A., Latz, E., Othman, A., Kuerschner, L., Hornemann, T., Bradke, F., Thiele, C., Penno, A. (2017) Localization of 1-deoxysphingolipids to mitochondria induces mitochondrial dysfunction, J. Lipid Res. 58:42–59.

Alvarez-Vasquez, F., Sims, K.J., Cowart, L.A., Okamoto, Y., Voit, E.O., Hannun, Y.A. (2005) Simulation and validation of modelled sphingolipid metabolism in *Saccharomyces cerevisiae*. Nature. 433:425–430.

Bartke, N., & Hannun, Y. A. (2009). Bioactive sphingolipids: metabolism and function. J Lipid Res, 50:S91–S96.

Bejaoui, K., Uchida, Y., Yasuda, S., Ho, M., Nishijima, M., Brown, R.H. Jr, Holleran, W.M., Hanada, K. (2002) Hereditary sensory neuropathy type 1 mutations confer dominant negative effects on serine palmitoyltransferase, critical for sphingolipid synthesis. J. Clinical Invest. 110:1301–1308.

Bode, H., Bourquin, F., Suriyanarayanan, S., Wei, Y., Alecu, I., Othman, A., Von Eckardstein, A., Hornemann, T. (2016) HSAN1 mutations in serine palmitoyltransferase reveal a close structure-function-phenotype relationship, Hum. Mol. Genet. 25:853–865.

Breslow, D.K., Collins, S.R., Bodenmiller, B., Aebersold, R., Simons, K., Shevchenko, A., Ejsing, C.S., and Weissman, J.S. (2010). Orm family proteins mediate sphingolipid homeostasis. Nature 463: 1048–1053.

Chen, M., Han, G., Dietrich, C.R., Dunn, T.M., and Cahoon, E.B. (2006). The essential nature of sphingolipids in plants as revealed by the functional identification and characterization of the Arabidopsis LCB1 subunit of serine palmitoyltransferase. Plant Cell 18: 3576–3593.

Chen, M., Cahoon, E.B., Saucedo-García, M., Plasencia, J., and Gavilanes-Ruíz, M. (2009). Plant Sphingolipids: Structure, Synthesis and Function. In Lipids in

Photosynthesis: Essential and Regulatory Functions, H. Wada, and and N. Murata, eds (Dordrecht: Springer Netherlands), pp. 77–115.

Clarke, B.A., et al. (2019). The Ormdl genes regulate the sphingolipid synthesis pathway to ensure proper myelination and neurologic function in mice. eLife 8: e51067

Coursol, S., Fan, L.M., Le Stunff, H., Spiegel, S., Gilroy, S., and Assmann, S.M. (2003). Sphingolipid signalling in Arabidopsis guard cells involves heterotrimeric G proteins. Nature 423: 651–654.

Cuadros, R., Montejo de Garcini, E., Wandosell, F., Faircloth, G., Fernández-Sousa, J.M., Avila, J. (2000) 'The marine compound spisulosine, an inhibitor of cell proliferation, promotes the disassembly of actin stress fibers. Cancer Lett, 152: 23–29.

Dang J, Bian X, Ma X, Li J, Long F, Shan S, Yuan Q, Xin Q, Li Y, Gao F, Gong Y, Liu Q. (2017) ORMDL3 Facilitates the Survival of Splenic B Cells via an ATF6α-Endoplasmic Reticulum Stress-Beclin1 Autophagy Regulatory Pathway. J Immunol. 199:1647-1659.

Davis, D.L., Gable, K., Suemitsu, J., Dunn, T.M., and Wattenberg, B.W. (2019). The ORMDL/Orm-serine palmitoyltransferase (SPT) complex is directly regulated by ceramide: Reconstitution of SPT regulation in isolated membranes. J. Biol. Chem. 294: 5146–5156.

Davis, D., Suemitsu, J. and Wattenberg, B. (2019) Transmembrane topology of mammalian ORMDL proteins in the endoplasmic reticulum as revealed by the substituted cysteine accessibility method (SCAM^{TM}) Biochim Biophys Acta Proteins Proteom. 1867:382–395.

Dickson, R. C. (2010) Roles for sphingolipids in *Saccharomyces cerevisiae*. Adv Exp Med Biol. 688, pp. 217–231.

Dietrich, C.R., Han, G., Chen, M., Berg, R.H., Dunn, T.M., and Cahoon, E.B. (2008). Loss-of-function mutations and inducible RNAi suppression of Arabidopsis LCB2 genes reveal the critical role of sphingolipids in gametophytic and sporophytic cell viability. Plant J. 54: 284–298.

Dunn TM, Tifft CJ, Proia RL. (2019) A perilous path: the inborn errors of sphingolipid metabolism. J Lipid Res. 60:475-483.

Dutilleul C, Chavarria H, Reze N, Sotta B, Baudouin E, Guillas I (2015) Evidence for ACD5 ceramide kinase activity involvement in Arabidopsis response to cold stress. Plant, Cell & Environment 38: 2688–2697.

Esaki K, Sayano T, Sonoda C, Akagi T, Suzuki T, Ogawa T, Okamoto M, Yoshikawa T, Hirabayashi Y, Furuya S. (2015) L-Serine Deficiency Elicits Intracellular Accumulation of Cytotoxic Deoxysphingolipids and Lipid Body Formation. J Biol Chem. 290:14595-609.

Gable, K., Slife, H., Bacikova, D., Monaghan, E., and Dunn, T.M. (2000). Tsc3p is an 80-amino acid protein associated with serine palmitoyltransferase and required for optimal enzyme activity. J. Biol. Chem. 275: 7597–7603.

Gable, K., Han, G., Monaghan, E., Bacikova, D., Natarajan, M., Williams, R., Dunn, T. M. (2002) Mutations in the yeast LCB1 and LCB2 genes, including those corresponding to the Hereditary Sensory Neuropathy type I mutations, dominantly inactivate serine palmitoyltransferase J. Biol. Chem. 277:10194–10200.

Gable, K., Gupta, S.D., Han, G., Niranjanakumari, S., Harmon, J. M., Dunn, T.M. (2010) A Disease-causing Mutation in the Active Site of Serine Palmitoyltransferase Causes Catalytic Promiscuity J. Biol. Chem., 285:22846–22852.

Gadkar, K. G., Gunawan, R. and Doyle, F. J. (2005) Iterative approach to model identification of biological networks. *BMC Bioinformatics*. 6:155.

Garofalo, K., Penno, A. and Schmidt, B.P. (2011) Oral L-serine supplementation reduces production of neurotoxic deoxysphingolipids in mice and humans with hereditary sensory autonomic neuropathy type 1. J. Clin. Invest. 14–16.

Gronnier J, Germain V, Gouguet P, Cacas JL, Mongrand S. (2016) GIPC: Glycosyl Inositol Phospho Ceramides, the major sphingolipids on earth. Plant Signal Behav. 11(4):e1152438.

Guillas I, Kirchman PA, Chuard R, Pfefferli M, Jiang JC, Jazwinski SM, Conzelmann A. (2001) C26-CoA-dependent ceramide synthesis of *Saccharomyces cerevisiae* is operated by Lag1p and Lac1p. EMBO J. 20:2655-65.

Gupta S, Maurya MR, Merrill AH Jr, Glass CK, Subramaniam S. (2011) Integration of lipidomics and transcriptomics data towards a systems biology model of sphingolipid metabolism. BMC Syst Biol. 8:5-26.

Gupta, S.D., Gable, K., Alexaki, A., Chandris, P., Proia, R.L., Dunn, T.M., and Harmon, J.M. (2015). Expression of the ORMDLS, modulators of serine palmitoyltransferase, is regulated by sphingolipids in mammalian cells. J. Biol. Chem. 290: 90–98.

Han G, Gupta SD, Gable K, Niranjanakumari S, Moitra P, Eichler F, Brown RH Jr, Harmon JM, Dunn TM. (2009) Identification of small subunits of mammalian serine palmitoyltransferase that confer distinct acyl-CoA substrate specificities. Proc Natl Acad Sci USA. 106:8186-91.

Han, S., Lone, M.A., Schneiter, R., and Chang, A. (2010). Orm1 and Orm2 are conserved endoplasmic reticulum membrane proteins regulating lipid homeostasis and protein quality control. Proc. Natl. Acad. Sci. USA 107: 5851–5856.

Han, G., Gupta, S.D., Gable, K., Bacikova, D., Sengupta, N., Somashekarappa, N., Proia, R.L., Harmon, J.M., and Dunn, T.M. (2019). The ORMs interact with transmembrane domain 1 of Lcb1 and regulate serine palmitoyltransferase oligomerization, activity and localization. Biochim. Biophys. Acta Mol. Cell Biol. Lipids 1864: 245–259.

Hanada, K. (2003) Serine palmitoyltransferase, a key enzyme of sphingolipid metabolism. Biochim. Biophys. Acta 1632:16–30.

Hannun, Y. A. and Obeid, L. M. (2018) Sphingolipids and their metabolism in physiology and disease, Nat Rev Mol Cell Biol., pp. 175–191.

Henry CS, Broadbelt LJ, Hatzimanikatis V. (2007) Thermodynamics-based metabolic flux analysis. Biophys J. 92:1792-805.

Hornemann, T., Wei, Y. and Von Eckardstein, A. (2007) Is the mammalian serine palmitoyltransferase a high-molecular-mass complex? Biochem. J. 405:157–164.

Huby, E., Napier, J.A., Baillieul, F., Michaelson, L.V., and Dhondt-Cordelier, S. (2020). Sphingolipids: Towards an integrated view of metabolism during the plant stress response. New Phytol. 225: 659–670.

Ikushiro H, Islam MM, Tojo H, Hayashi H. (2007) Molecular characterization of membrane-associated soluble serine palmitoyltransferases from *Sphingobacterium multivorum* and *Bdellovibrio stolpii*. *J. Bacteriol*. American Society for Microbiology Journals, 189:5749–5761.

Islam, M. M. and Saha, R. (2018) Computational Approaches on Stoichiometric and Kinetic Modeling for Efficient Strain Design BT - Synthetic Metabolic Pathways: Methods and Protocols', in Jensen, M. K. and Keasling, J. D. (eds). New York, NY: Springer New York, pp. 63–82.

Jiang, Z., Zhou, X., Tao, M. et al. (2019) Plant cell-surface GIPC sphingolipids sense salt to trigger Ca^{2+} influx. Nature 572:341–346.

Jiménez-Rojo, N., Sot, J., Busto, J.V., Shaw, W,A., Duan, J., Merrill, A.H. Jr, Alonso, A., Goñi, F.M. (2014) Biophysical Properties of Novel 1-Deoxy-(Dihydro)ceramides Occurring in Mammalian Cells. Biophys. J. 107: 2850–2859.

Khazaei, T., McGuigan, A. and Mahadevan, R. (2012) Ensemble modeling of cancer metabolism' Frontiers in physiology. 3:135.

Kim, O. D., Rocha, M. and Maia, P. (2018) A Review of Dynamic Modeling Approaches and Their Application in Computational Strain Optimization for Metabolic Engineering. Front Microbiol. 9:1690.

Kimberlin, A.N., Han, G., Luttgeharm, K.D., Chen, M., Cahoon, R.E., Stone, J.M., Markham, J.E., Dunn, T.M., and Cahoon, E.B. (2016). ORM expression alters sphingolipid homeostasis and differentially affects ceramide synthase activity. Plant Physiol. 172: 889–900

Kimberlin, A.N., Majumder, S., Han, G., Chen, M., Cahoon, R.E., Stone, J.M., Dunn, T.M., and Cahoon, E.B. (2013). Arabidopsis 56- amino acid serine palmitoyltransferase-interacting proteins stimulate sphingolipid synthesis, are essential, and affect mycotoxin sensitivity. Plant Cell 25: 4627–4639.

Kraft, M. L. (2017) Sphingolipid organization in the plasma membrane and the mechanisms that influence it. Front Cell Dev Biol. 154.

Laloi, M., Perret, A. M., Chatre, L., Melser, S., Cantrel, C., Vaultier, M. N., Zachowski, A., Bathany, K., Schmitter, J. M., Vallet, M., Lessire, R., Hartmann, M. A., & Moreau, P. (2007). Insights into the role of specific lipids in the formation and delivery of lipid microdomains to the plasma membrane of plant cells. Plant Physiol. 143:461–472.

Lenarčič T, Albert I, Böhm H, Hodnik V, Pirc K, Zavec AB, Podobnik M, Pahovnik D, Žagar E, Pruitt R, Greimel P, Yamaji-Hasegawa A, Kobayashi T, Zienkiewicz A, Gömann J, Mortimer JC, Fang L, Mamode-Cassim A, Deleu M, Lins L, Oecking C, Feussner I, Mongrand S, Anderluh G, Nürnberger T. (2017) Eudicot plant-specific sphingolipids determine host selectivity of microbial NLP cytolysins. Science. 15:1431-1434.

Levy, M. and Futerman, A. H. (2010) Mammalian ceramide synthases. IUBMB Life. 62:347–356.

Li, J., Bi, F.C., Yin, J., Wu, J.X., Rong, C., Wu, J.L., Yao, N. (2015) An Arabidopsis neutral ceramidase mutant *ncer1* accumulates hydroxyceramides and is sensitive to oxidative stress. Front Plant Sci. 19:460.

Li, J., Yin, J., Rong, C., Li, K.E., Wu, J.X., Huang, L.Q., Zeng, H.Y., Sahu, S.K., and Yao, N. (2016). Orosomucoid proteins interact with the small subunit of serine palmitoyltransferase and contribute to sphingolipid homeostasis and stress responses in Arabidopsis. Plant Cell 28: 3038–3051.

Liang, H., Yao, N., Song, J.T., Luo, S., Lu, H., and Greenberg, J.T. (2003). Ceramides modulate programmed cell death in plants. Genes Dev. 17: 2636–2641

Lone, M.A., Santos, T., Alecu, I., Silva, L.C., Hornemann, T. (2019) 1-Deoxysphingolipids. Biochim Biophys Acta Mol Cell Biol Lipids.1864:512-521

Luttgeharm, K.D., Chen, M., Mehra, A., Cahoon, R.E., Markham, J.E., and Cahoon, E.B. (2015a). Overexpression of Arabidopsis ceramide synthases differentially affects growth, sphingolipid metabolism, programmed cell death, and mycotoxin

resistance. Plant Physiol. 169: 1108–1117.

Luttgeharm, K.D., Kimberlin, A.N., Cahoon, R.E., Cerny, R.L., Napier, J.A., Markham, J.E., and Cahoon, E.B. (2015b). Sphingolipid metabolism is strikingly different between pollen and leaf in Arabidopsis as revealed by compositional and gene expression profiling. Phytochemistry 115: 121–129.

Magnin-Robert M, Le Bourse D, Markham J, Dorey S, Clément C, Baillieul F, Dhondt-Cordelier S. (2015) Modifications of Sphingolipid Content Affect Tolerance to Hemibiotrophic and Necrotrophic Pathogens by Modulating Plant Defense Responses in Arabidopsis. Plant Physiol. 169:2255-74.

Mao C, Xu R, Bielawska A, Obeid LM. (2000) Cloning of an alkaline ceramidase from *Saccharomyces cerevisiae*. An enzyme with reverse (CoA-independent) ceramide synthase activity. J Biol Chem. 275:6876-84.

Mao, C., and Obeid, L. M. (2008). Ceramidases: Regulators of cellular responses mediated by ceramide, sphingosine, and sphingosine-1-phosphate. Biochim Biophys Acta, 1781:424–434.

Mao C, Saba JD, Obeid LM. (1999) The dihydrosphingosine-1-phosphate phosphatases of Saccharomyces cerevisiae are important regulators of cell proliferation and heat stress responses. Biochem J. 342:667-75.

Markham JE, Li J, Cahoon EB, Jaworski JG. 2006Separation and identification of major plant sphingolipid classes from leaves. J Biol Chem. Aug 11;281(32):22684-94. doi: 10.1074/jbc.M604050200. Epub 2006 Jun 12. PMID: 16772288.

Markham, J.E., and Jaworski, J.G. (2007). Rapid measurement of sphingolipids from *Arabidopsis thaliana* by reversed-phase highperformance liquid chromatography coupled to electrospray ionization tandem mass spectrometry. Rapid Commun. Mass Spectrom. 21: 1304–1314.

Markham, J.E., Molino, D., Gissot, L., Bellec, Y., Hématy, K., Marion, J., Belcram, K., Palauqui, J.C., Satiat-Jeunemaître, B., and Faure, J.D. (2011). Sphingolipids containing very-long-chain fatty acids define a secretory pathway for specific polar plasma membrane protein targeting in Arabidopsis. Plant Cell 23: 2362–2378.

McCampbell A, Truong D, Broom DC, Allchorne A, Gable K, Cutler RG, Mattson MP, Woolf CJ, Frosch MP, Harmon JM, Dunn TM, Brown RH Jr. (2005) Mutant SPTLC1 dominantly inhibits serine palmitoyltransferase activity in vivo and confers an age-dependent neuropathy. Hum Mol Genet. 14:3507-21.

Moreau P, Bessoule JJ, Mongrand S, Testet E, Vincent P, Cassagne C. (1998) Lipid trafficking in plant cells. Prog Lipid Res. 37:371-91.

Peer, M., Stegmann, M., Mueller, M.J., and Waller, F. (2010). Pseudomonas syringae infection triggers de novo synthesis of phytosphingosine from sphinganine in *Arabidopsis thaliana*. FEBS Lett. 584: 4053–4056.

Penno, A., Reilly, M.M., Houlden, H., Laura, M., Rentsch, K., Niederkofler, V., Stoeckli, E.T., Nicholson, G., Eichler, F., Brown, R.H. Jr., von Eckardstein A., Hornemann T. (2010) Hereditary sensory neuropathy type 1 is caused by the accumulation of two neurotoxic sphingolipids, J. Biol. Chem. 285:11178−11187.

Pinto SN, Silva LC, Futerman AH, Prieto M. (2011) Effect of ceramide structure on membrane biophysical properties: the role of acyl chain length and unsaturation. Biochim Biophys Acta. 1808:2753-60.

Pruett ST, Bushnev A, Hagedorn K, Adiga M, Haynes CA, Sullards MC, Liotta DC, Merrill AH Jr. (2008) Biodiversity of sphingoid bases ("sphingosines") and related amino alcohols. J Lipid Res. 49:1621-39.

Roelants, F.M., Breslow, D.K., Muir, A., Weissman, J.S., Thorner, J. (2011) Protein kinase Ypk1 phosphorylates regulatory proteins Orm1 and Orm2 to control sphingolipid homeostasis in *Saccharomyces cerevisiae*. Proc Natl Acad Sci USA 108:19222–7.

Rotthier, A., Penno, A., Rautenstrauss, B., Auer-Grumbach, M., Stettner, G.M., Asselbergh, B., Van Hoof K., Sticht, H., Levy, N., Timmerman, V., Hornemann, T., Janssens K. (2011) Characterization of two mutations in the SPTLC1 subunit of serine palmitoyltransferase associated with hereditary sensory and autonomic neuropathy type I, Hum. Mutat. 32:E2211−E2225.

Sassa, T., Suto, S., Okayasu, Y., Kihara, A. (2012) A shift in sphingolipid composition from C24 to C16 increases susceptibility to apoptosis in HeLa cells. Biochim Biophys Acta. 1821:1031–1037.

Saucedo-García M, Guevara-García A, González-Solís A, Cruz-García F, Vázquez-Santana S, Markham JE, Lozano-Rosas MG, Dietrich CR, Ramos-Vega M, Cahoon EB, Gavilanes-Ruíz M. (2011) MPK6, sphinganine and the LCB2a gene from serine palmitoyltransferase are required in the signaling pathway that mediates cell death induced by long chain bases in Arabidopsis. New Phytol. 191:943-57.

Savoglidis G, da Silveira Dos Santos AX, Riezman I, Angelino P, Riezman H, Hatzimanikatis V. (2016) A method for analysis and design of metabolism using metabolomics data and kinetic models: Application on lipidomics using a novel kinetic model of sphingolipid metabolism. Metab Eng. 37:46–62.

Schmidt O, Weyer Y, Baumann V, Widerin MA, Eising S, Angelova M, Schleiffer A, Kremser L, Lindner H, Peter M, Fröhlich F, Teis D. (2019) Endosome and Golgi-associated degradation (EGAD) of membrane proteins regulates sphingolipid metabolism. EMBO J. 38:e101433.

Shimobayashi, M., Oppliger, W., Moes, S., Jenö, P., Hall, M.N. (2013) TORC1-regulated protein kinase Npr1 phosphorylates Orm to stimulate complex sphingolipid synthesis. Mol Biol Cell. 24:870–881.

Steiner R, Saied EM, Othman A, Arenz C, Maccarone AT, Poad BL, Blanksby SJ, von Eckardstein A, Hornemann T. (2016) Elucidating the chemical structure of native 1-deoxysphingosine. J Lipid Res. 57:1194–1203.

Sun, Y., Miao, Y., Yamane, Y., Zhang, C., Shokat, K.M., Takematsu, H., Kozutsumi, Y., Drubin, D.G. (2012) Orm protein phosphoregulation mediates transient sphingolipid biosynthesis response to heat stress via the Pkh-Ypk and Cdc55-PP2A pathways. Mol Biol Cell. 23:2388–2398.

Tamura, K., Musuhashi, M., Hara-Nishimura, I., and Imai, H. (2001). Characterization of an Arabidopsis cDNA encoding a subunit of serine palmitoyltransferase, the initial enzyme in sphingolipid biosynthesis. Plant Cell Physiol. 42:1271–1281.

Teng, C., Dong, H., Shi, L., Deng, Y., Mu, J., Zhang, J., Yang, X., and Zuo, J. (2008). Serine palmitoyltransferase, a key enzyme for de novo synthesis of sphingolipids, is essential for male gametophyte development in Arabidopsis. Plant Physiol. 146: 1322–1332.

Ternes, P., Feussner, K., Werner, S., Lerche, J., Iven, T., Heilmann, I., Riezman, H., and Feussner, I. (2011). Disruption of the ceramide synthase LOH1 causes spontaneous cell death in Arabidopsis thaliana. New Phytol. 192: 841–854.

Tran, L. M., Rizk, M. L. and Liao, J. C. (2008) Ensemble modeling of metabolic networks. Biophys J. 95:5606–5617.

Tsegaye Y, Richardson CG, Bravo JE, Mulcahy BJ, Lynch DV, Markham JE, Jaworski JG, Chen M, Cahoon EB, Dunn TM. (2007) Arabidopsis mutants lacking long chain base phosphate lyase are fumonisin-sensitive and accumulate trihydroxy-18:1 long chain base phosphate. J Biol Chem. 282:28195-206.

Varma, A. and Palsson, B. O. (1994) Metabolic flux balancing: Basic concepts, scientific and practical use. Nat Biotechnol.12:994–998.

Wronowska, W., Charzyńska, A., Nienałtowski, K., Gambin, A. (2015) Computational modeling of sphingolipid metabolism. BMC Syst Biol. 9:47.

Wu, J.X., Li, J., Liu, Z., Yin, J., Chang, Z.Y., Rong, C., Wu, J.L., Bi, F.C., Yao, N. (2015) The Arabidopsis ceramidase AtACER functions in disease resistance and salt tolerance. Plant J. 81:767-80.

Yang, F., Kimberlin, A.N., Elowsky, C.G., Liu, Y., Gonzalez-Solis, A., Cahoon, E.B., and Alfano, J.R. (2019). A plant immune receptor degraded by selective autophagy. Mol. Plant 12: 113–123.

Yard BA, Carter LG, Johnson KA, Overton IM, Dorward M, Liu H, McMahon SA, Oke M, Puech D, Barton GJ, Naismith JH, Campopiano DJ. (2007) The Structure of Serine Palmitoyltransferase; Gateway to Sphingolipid Biosynthesis. J Mol Biol. 370:870–886.

Zheng P, Wu JX, Sahu SK, Zeng HY, Huang LQ, Liu Z, Xiao S, Yao N. (2018) Loss of alkaline ceramidase inhibits autophagy in Arabidopsis and plays an important role during environmental stress response. Plant Cell Environ. 41:837–849.

Zielinski, D.C., Palsson, B.Ø. (2012) Kinetic Modeling of Metabolic Networks BT - Systems Metabolic Engineering. In: Wittmann C, Lee SY, editors. Dordrecht: Springer Netherlands; 2012. p. 25–55.

Zitomer, N.C., Mitchell, T., Voss, K.A, Bondy, G.S., Pruett, S.T., Garnier-Amblard, E.C., Liebeskind, L.S., Park, H., Wang, E., Sullards, M.C., Merrill Jr A.H., Riley R.T. (2009) Ceramide synthase inhibition by fumonisin B1 causes accumulation of 1-deoxysphinganine: a novel category of bioactive 1-deoxysphingoid bases and 1-deoxydihydroceramides biosynthesized by mammalian cell lines and animals, J. Biol. Chem. 284:4786–4795.

2 Chapter 2 Unregulated Sphingolipid Biosynthesis in Gene-Edited Arabidopsis ORM Mutants Results in Nonviable Seeds.

The content of this chapter has been published.

Ariadna Gonzalez-Solis, Gongshe Han, Lu Gan, Yunfeng Li, Jonathan E. Markham, Rebecca E. Cahoon, Teresa M. Dunn, Edgar B. Cahoon. Unregulated Sphingolipid Biosynthesis in Gene-Edited Arabidopsis ORM Mutants Results in Nonviable Seeds with Strongly Reduced Oil Content. The Plant Cell Aug 2020, 32 (8) 2474-2490; DOI: 10.1105/tpc.20.00015.

2.1 Abstract

Orosomucoid-like proteins (ORMs) interact with serine palmitoyltransferase (SPT) to negatively regulate sphingolipid biosynthesis, a reversible process critical for balancing the intracellular sphingolipid levels needed for growth and programmed cell death. Here, we show that ORM1 and ORM2 are essential for life cycle completion in Arabidopsis (*Arabidopsis thaliana*). Seeds from *orm1*$^{-/-}$ *orm2*$^{-/-}$ mutants, generated by crossing CRISPR/Cas9 knockout mutants for each gene, accumulated high levels of ceramides, indicative of unregulated sphingolipid biosynthesis. *orm1*$^{-/-}$ *orm2*$^{-/-}$ seeds were nonviable, displayed aberrant embryo development, and had >80% reduced oil content versus wild-type seeds. This phenotype was mimicked in Arabidopsis seeds expressing the SPT subunit LCB1 lacking its first transmembrane domain, which is critical for ORM-mediated regulation of SPT. In this study we also uncovered phenotypical growth differences of *orm1*$^{+/-}$ *orm2*$^{-/-}$ *and orm1*$^{-/-}$ *orm2*$^{+/-}$ mutants that provide insights into potential different roles of ORM1 and ORM2 in plant development.

2.2 Introduction

Sphingolipids are essential and abundant endomembrane and plasma membrane lipids that contribute to membrane function, vesicular trafficking, and mediation of cellular processes in eukaryotes (Coursol *et al.*, 2003; Liang *et al.*, 2003; Chen *et al.*,

2006; Markham *et al.*, 2011). Serine palmitoyltransferase (SPT), the first step in sphingolipid biosynthesis, is highly regulated in eukaryotes to modulate the requirement of sphingolipids for growth and membrane function, while limiting accumulation of LCBs and ceramides until needed to trigger specific cellular functions, such as PCD-mediated pathogen defense in plants (Peer *et al.*, 2010). SPT is comprised of LCB1 and LCB2 subunits and the accessory protein known as small subunit of SPT (ssSPT) or TSC3 in *Saccharomyces cerevisiae* (*S. cerevisiae*) (Gable *et al.*, 2000; Kimberlin *et al.*, 2013). SPT is primarily regulated by post-translational mechanisms in order to rapidly respond to perturbations in intracellular sphingolipid concentrations. ORMs or orosomucoid-like proteins (or ORMDL in mammals) are now recognized as non-catalytic proteins that negatively regulate SPT (Breslow *et al.*, 2010; Han *et al.*, 2010). In *S. cerevisiae,* Orm1p and Orm2p suppress SPT activity in response to elevated sphingolipid levels through physical interaction that requires the first transmembrane domain of LCB1 (Han *et al.*, 2019). Sphingolipid-responsive regulation of the ORM-SPT interaction in *S. cerevisiae* is mediated by phosphorylation/dephosphorylation of the N-terminal domain of the ORMs (Breslow *et al.*, 2010). This domain is absent from ORM/ORMDL of higher eukaryotes suggesting alternative regulation of the ORM-SPT interaction, such as a recently demonstrated mechanism of direct binding of a ceramide molecule to mammalian ORMDL and yeast ORM to confer negative SPT regulation (Davis *et al.*, 2019). In addition, ORMDL expression levels vary with sphingolipid availability in mammalian cells (Gupta *et al.*, 2015).

S. cerevisiae cells are viable after knockout of the two ORM genes, but accumulate increased amounts of LCBs and ceramides and are sensitive to tunicamycin,

an inducer of ER stress (Breslow *et al.*, 2010). However, to date, a full understanding of the biochemical and physiological functions of ORM or ORMDL porteins in multi-cellular eukaryotes is only beginning to emerge. A recent report showed that ORMDL proteins are critical for nerve myelination and for suppressing accumulation of toxic sphingolipid biosynthetic intermediates in mice (Clarke *et al.,* 2019). Studies in Arabidopsis have previously shown that downregulation of *ORM2* using an artificial miRNA in an *ORM1* T-DNA mutant yields fertile plants with increased accumulation of LCBs and ceramides and early senescence (Li *et al.*, 2016). In addition, RNAi suppression of Arabidopsis *ORM1* and *ORM2* resulted in plants with normal appearance but with increased sensitivity to the ceramide synthase inhibitor fumonisin B1 and increased LOH2 ceramide synthase activity (Kimberlin *et al.*, 2016). Beyond Arabidopsis, RNAi of *ORM* genes in rice was linked to reduced pollen viability (Chueasiri *et al.*, 2014).

The lack of complete ORM knockout mutants in Arabidopsis or other plants has precluded assessment of SPT regulation in the absence of ORM proteins. To advance our understanding of ORM-mediation of sphingolipid biosynthesis we generated *ORM1/ORM2* double mutants using CRISPR/Cas9. Our findings show that in full ORM1/ORM2 knockout mutants removing sphingolipid biosynthesis regulation results in nonviable seeds with impaired embryo development, ceramide accumulation and strongly reduced oil content. We obtained the same phenotypes by removing the first transmembrane domain of the LCB1 subunit of SPT which is known to be essential for ORM-SPT interaction.

2.3 Materials and Methods

2.3.1 Plant Materials and Growth Conditions

Arabidopsis (*Arabidopsis thaliana*) Columbia-0 (Col-0) was used as the wild-type reference in this study. Arabidopsis seedlings were grown on Murashige and Skoog (MS) medium supplemented with 1% (w/v) Sucrose and 0.8% (w/v) agar, pH 5.7, with 16-h-light (100 mmol/ m^{-2} s^{-1})/8-h-dark conditions at 22°C. The light source for growth chamber–grown seedlings was supplied by standard wide-spectrum fluorescent bulbs type F32/841/ ECO 32 W (maximum intensity, 480 to 570 nm). For Arabidopsis plants in soil, seeds were sown, and after 2 d of stratification at 4°C, plants were grown at 22°C with 16-h-light (100 mmol/ m^{-2} s^{-1})/8-h-dark conditions.

2.3.2 Generation of CRISPR/Cas9 ORM Mutants

For CRISPR/Cas9-mediated gene editing of *ORM1* and *ORM2*, designed target sites (Figure 2.1A) were fused with a single guide RNA and expressed under the control of the U6 promoter. The egg cell–specific EC1 promoter was used to drive Cas9 expression as previously reported by Wang et al. (2015). In short, *BsaI* sites were incorporated by PCR into the ORM target sequences (primers P1 to P4; Supplemental Table 1 in Appendix A). The purified PCR products were digested with *BsaI* and ligated to the *BsaI*-linearized binary vector pHEE401E. The final CRISPR/Cas9 binary vector was electroporated into *Agrobacterium tumefaciens* strain GV3101 and then transformed into the Arabidopsis Col-0 wild-type plants via the floral dip method (Clough and Bent, 1998). The seeds were screened for hygromycin resistance on MS plates containing 25 mg/L hygromycin. For genotyping, fragments including the target regions of ORM1 and ORM2 were amplified by PCR from the genomic DNA of transgenic plants (primers P5 to P8; Supplemental

Table 1 in Appendix A). Amplicons were digested with the restriction enzymes *BslI* (*ORM1*) and *DraIII* (*ORM2*). The specific indels were identified by DNA sequencing. To analyze for nontransgenic plants, progeny of hygromycin-selected and confirmed homozygous (CRISPR/Cas9 mutation) T1 plants were sown directly on soil without hygromycin selection. These plants were then screened by PCR (P9+P10; Supplemental Table 1 in Appendix A) for the lack of the *Cas9* gene with the presence of the CRISPR mutation, in the T2 generation. The plants lacking *Cas9* but containing the CRISPR mutation were kept and used for further studies as mutated but not transgenic lines.

2.3.3 Generation of the LCB1ΔTMD1 Mutant

LCB1ΔTMD1 was generated by deleting coding sequence for 17 amino acids corresponding to the first transmembrane domain of AtLCB1 (amino acids 35 to 51). *LCB1ΔTMD1* under the control of the *LCB1* native promoter was cloned into the pBinGlyRed3 binary vector, which was transformed into *A. tumefaciens* GV3101 by electroporation. Heterozygous LCB1/lcb1- knockout mutants (SALK_077745) were transformed by the floral dip method (Clough and Bent, 1998).

2.3.4 Pollen Staining

Anthers of mature plants were isolated and smeared on a glass slide. The pollen was stained using Alexander staining method (Alexander, 1969) for 1 h at 25°C. Pollen imaging was performed using the EVOS FL Auto Cell Imaging System.

2.3.5 Sphingolipid Extraction and Analysis

Sphingolipids were extracted as described in Markham and Jaworski (2007). Briefly, leaves from 20- to 30-d-old Arabidopsis plants grown on soil were collected and

lyophilized. Ten to 30 mg of tissue was homogenized and extracted with isopropanol:heptane:water (55:20:25, v/v/v). We used 1 to 4 mg of plant material for each biological replicate for sphingolipid analysis from seeds. Internal standards for the different sphingolipid classes were added. The supernatants were dried and deesterified with methylamine in ethanol:water (70:30, v/v). The lipid extract was re-suspended in tetrahydrofuran:methanol:water (5:2:5, v/v/v) containing 0.1% (v/v) formic acid. The sphingolipid species were analyzed using a Shimadzu Prominence ultra-performance liquid chromatography system and a 4000 QTRAP mass spectrometer (AB SCIEX). Data analysis and quantification were performed using the software Analyst 1.5 and MultiQuant 2.1 as described by Markham and Jaworski (2007), Kimberlin et al. (2013), and Davis et al. (2020).

2.3.6 Lipid Extraction Analysis

To quantify the TAG content, lipids were extracted from ~1 mg of seeds using a method based on that of Bligh and Dyer (1959). Seeds were ground using a glass rod in 13x100-mm glass screw cap tubes with 3 mL of methanol:chloroform (2:1, v/v). Triheptadecanoin (17:0-TAG) was added to the seeds as an internal standard prior to extraction. After 1 h of incubation at 25°C, 1 mL of chloroform and 1.9 mL of water were added. The solution was mixed thoroughly and centrifuged at 400g for 10 min. The lower organic phase containing total lipids was transferred to a new glass tube and solvent evaporated under a N_2 stream with heating at 40°C. The sample was redissolved in 1 mL of heptane and loaded onto a solid phase extraction column (Supelco Supelclean LC-Si SPE column; Sigma-Aldrich) pre-equilibrated with heptane. A purified TAG fraction was eluted from the column and converted to fatty acid methyl esters, which were analyzed

by gas chromatography as previously described (Zhu et al., 2016). TAG fatty acid content was quantified relative to 17:0 fatty acid methyl ester from the internal standard.

2.3.7 Statistical Analyses

Two-tailed Student's t test was performed to evaluate statistically significant differences compared to the control (wild type). One-way ANOVA followed by Tukey's test was used to determine the differences among the five genotypes for a given variable. Values of $P < 0.05$ were considered statistically significant. The statistical analyses were done using GraphPad Prism 8.3.0.

2.4 Results

2.4.1 ORMs Are Essential for Plant Development

We designed two single guide RNAs to target regions in the coding sequence of each of the two Arabidopsis ORM genes (Figure 2.1A). We introduced these constructs into Arabidopsis via *Agrobacterium tumefaciens*–mediated transformation to generate CRISPR/Cas9-induced knockouts of the *ORM1* and O*RM2* genes. We screened T1 and T2 transformants by restriction enzyme digestion of the PCR amplicons encompassing the *ORM1* and *ORM2* target sites to obtain homozygous lines with mutations in each gene. These lines were also verified by PCR to lack Cas9 transgenes. These homozygous single mutants were visually indistinguishable from wild-type plants under optimal growth conditions (Figure 2.1B).

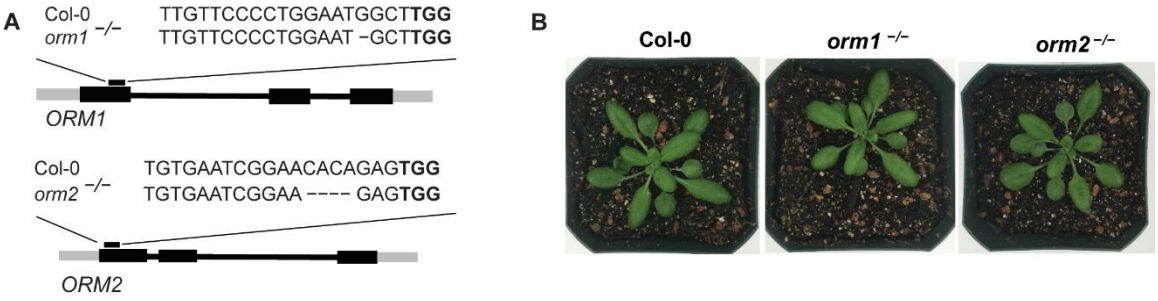

Figure 2.1 Gene-edited ORM Arabidopsis mutants.

(**A**) Schematic representation of CRISPR/Cas9-induced mutations in *ORM* genes. Gene structures of *ORM1* and *ORM2*; black boxes represent exons. The CRISPR/Cas9 target site is indicated as well as the nucleotide deletions for each gene in the single mutants. (**B**) Representative images of 25-d-old wild-type Col-0, *orm1*$^{-/-}$, and *orm2*$^{-/-}$ plants.

The population of mutants obtained contained nucleotide deletions resulting in frameshifts and premature stop codons, as determined by PCR–restriction enzyme digestion and sequencing (Supplemental Figure 1 in Appendix A). To obtain double knockout mutants, we crossed the *orm1*$^{-/-}$ and *orm2*$^{-/-}$ single mutants. No progeny with homozygous knockout mutations in both genes were obtained after analyzing 155 plants from the F2 generation and 60 plants from the F3 generation. To gain more insight into the basis for the apparent lethality associated with the double mutant, we performed viability staining on pollen from plants genotyped as *orm1*$^{+/-}$ *orm2*$^{+/-}$ (Supplemental Figure 2A in Appendix A). Nearly all of the pollen from these mutants was viable, similar to pollen from the wild-type plants (Figures 2.2A and 2.2C), rather than 25% nonviability that would be expected for pollen lethality in this mutant. Instead, a population of seeds from these plants had dark colored seed coats and were severely wrinkled. Strikingly, free ceramide concentrations in pooled abnormal seeds were; 40-fold higher than those in wild-type seeds and; 8-fold higher than in the normal-appearing seed segregants from *orm1*$^{+/-}$ *orm2*$^{+/-}$ plants (Figure 2.3C).

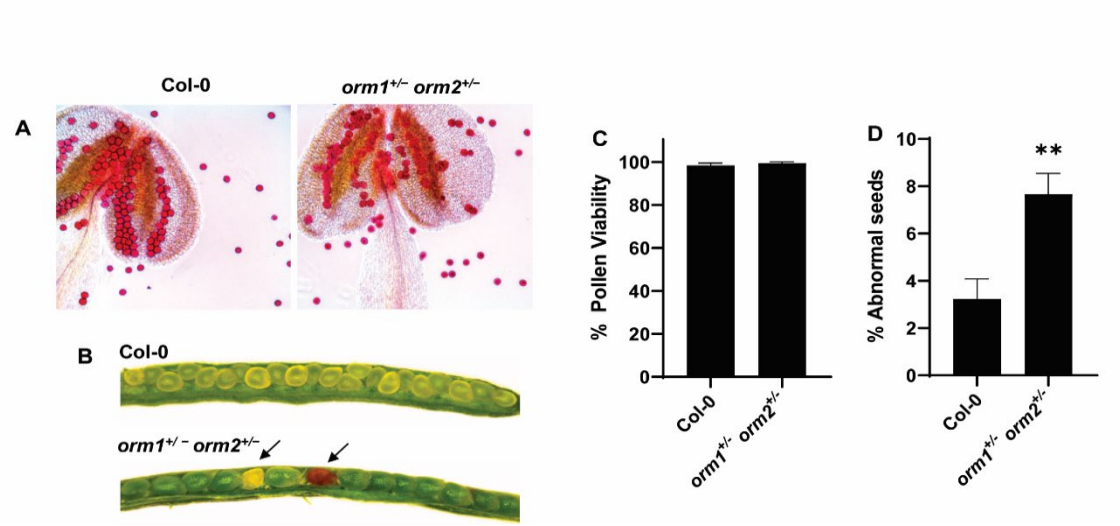

Figure 2.2 Pollen Viability and Seed Development from *orm1*$^{+/-}$ *orm2*$^{+/-}$ Plants.

(**A**) Representative images of pollen and anthers (treated with Alexander stain) collected from wild-type Col-0 and *orm1*$^{+/-}$ *orm2*$^{+/-}$ plants. (**B**) Viability of pollen determined by counts of ~100 pollen grains from five randomly selected flowers from independent Col-0 and *orm1*$^{+/-}$ *orm2*$^{+/-}$ plants. Shown are the mean ± SD. (**C**) Developing seeds in siliques from wild-type Col-0 and *orm1*$^{+/-}$ *orm2*$^{+/-}$ plants. Shriveled, brown (abnormal) seeds are indicated by arrows. (**D**) Percentage of shriveled and brown (abnormal) seeds in siliques determined by counts of an average of 200 developing seeds from 10 randomly selected siliques of the independent wild-type Col-0 and *orm1*$^{+/-}$ *orm2*$^{+/-}$ plants. Shown are the mean ± SD. Asterisks denote significant differences as determined by two-tailed Student's t test, with a significance of P ≤0.01.

This phenotype was observed for 7% of seeds collected from the F2 *orm1*$^{+/-}$ *orm2*$^{+/-}$ plants of *orm1*$^{-/-}$ and *orm2*$^{-/-}$ crosses, which is consistent with the expected 6.25% Mendelian ratio for the occurrence of homozygous double mutants. The remaining seeds were visually indistinguishable from wild-type seeds (Figures 2.2B and 2.2D). Of the seeds in these two populations, dark, wrinkled seeds did not germinate, whereas seeds with normal appearance showed no impairment in germination on solid Sucrose-containing medium (Figures 2.3A and 2.3B) and soil.

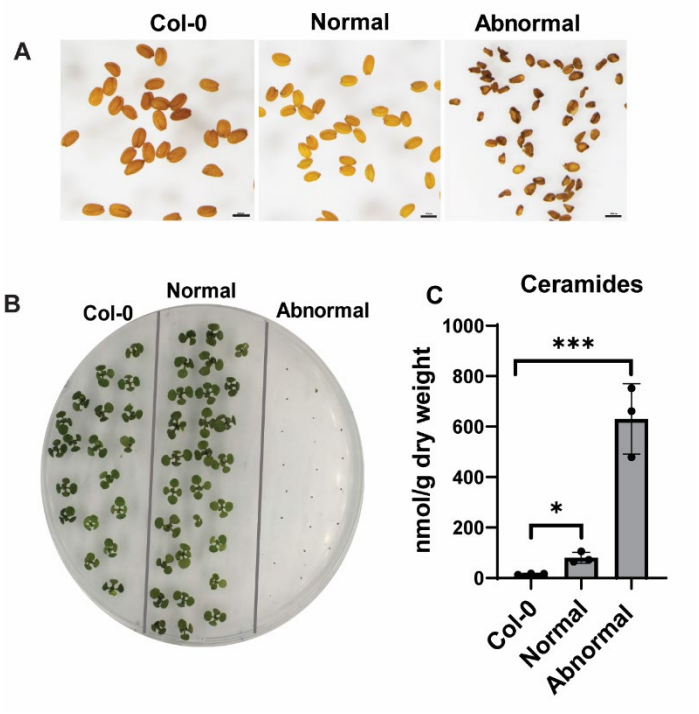

Figure 2.3 The ORM Double Knockout is Seed Lethal.

(**A**) Seeds from wild-type Col-0; seeds from *orm1*$^{+/-}$ *orm2*$^{+/-}$ were separated and classified into normal and the darker, shriveled seeds as abnormal. Bars = 1 mm. (**B**) Phenotypes of 10-d-old seedlings from wild-type Col-0 seeds and normal and abnormal seeds from *orm1*$^{+/-}$ *orm2*$^{+/-}$. Abnormal seeds did not germinate. (**C**) Ceramide content in seeds from wild-type Col-0 and normal and abnormal seeds from *orm1*$^{+/-}$ *orm2*$^{+/-}$. Shown are the mean ± SD, n 5 3. Asterisks indicate significant differences based on one-way ANOVA followed by Tukey's multiple comparisons test, with a significance of *, P ≤0.05 and ***, P ≤0.001.

2.4.2 LCB1-ΔTMD1 Mimics the Phenotype of the ORM-null Mutant

We also observed a similar seed phenotype in *Atlcb1*$^{+/-}$ plants expressing a version of the LCB1 subunit of SPT lacking its first transmembrane domain (LCB1ΔTMD1) that is required for SPT-ORM regulatory interactions (Han et al., 2019). In these experiments, the segregating seeds from *Atlcb1*$^{+/-}$ plants expressing LCB1ΔTMD1 included a population of shrunken, nonviable seeds with a 14-fold increase in ceramide levels compared with wild-type seeds (Figure 2.4).

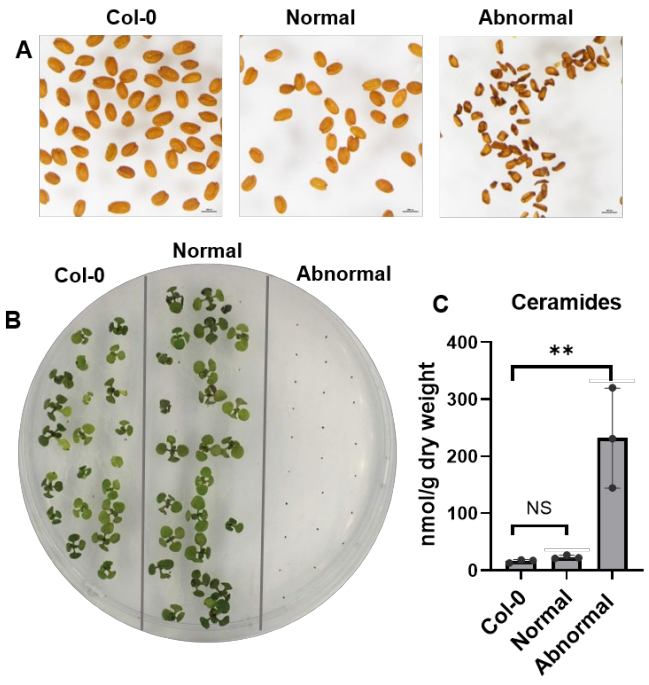

Figure 2.4 *Atlcb1*$^{+/-}$ Plants Expressing LCB1ΔTMD1 Phenocopy the ORM Double Knockout Mutant.

Figure 2.4. (**A**) Seeds from wild-type Col-0; seeds from *Atlcb1*$^{+/-}$ plants expressing LCB1ΔTMD1 were separated and classified into normal and abnormal darker and shriveled seeds. Bars = 1 mm. (**B**) Phenotypes of 10-d-old seedlings from wild-type Col-0 seeds and normal and abnormal seeds from *Atlcb1*$^{+/-}$ expressing LCB1ΔTMD1. Abnormal seeds did not germinate. (**C**) Ceramide content in seeds from wild-type Col-0 and normal and abnormal seeds from LCB1ΔTMD1. Shown are the mean ± SD, n = 3. Asterisks indicate significant difference based on one-way ANOVA followed by Tukey's multiple comparisons test, with a significance of **, $P \leq 0.01$. NS, not significant.

We examined seeds from the *orm1*$^{-/-}$ and *orm2*$^{-/-}$ crosses and LCB1ΔTMD1 in more detail to understand the basis for the loss of viability. The weight of mature nonviable, abnormal seeds was 80 to 90% lower than that of normal seed segregants from these lines (Figure 2.5E). Embryos dissected from the abnormal seeds had variable appearance ranging from cell clusters with undifferentiated appearance to embryo-like structures that were up to one-third the size of those from normal seeds (Figures 2.5A to 2.5D).

Underlying this phenotype, oil content of the abnormal seeds, as measured by the fatty acid content of purified triacylglycerols (TAG), was 85 to 90% lower than that of normal seed segregants (Figure 2.5F).

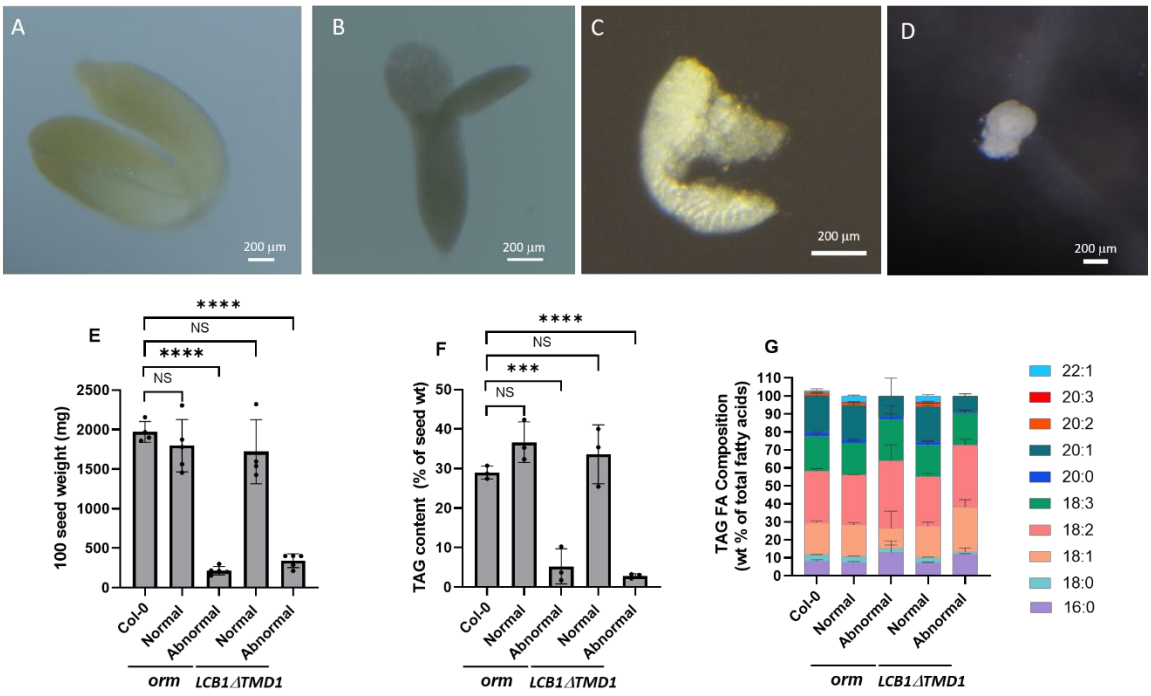

Figure 2.5 Abnormal Seeds from ORM and LCB1ΔTMD1 Mutant Plants Have Altered Embryo Morphology and Reduced TAG Concentrations.

(A) to **(D)** Morphology of embryos from the wild-type seeds (**A**) and abnormal seeds from *orm1*$^{+/-}$ *orm2*$^{+/-}$. plants (see [**B**] to [**D**]) showing that the embryo is not fully developed. Embryos were dissected from mature seeds. **(E)** The 100 seed weight. Values are the mean ± SD of seeds harvested from four independent plants. Asterisks indicate significant difference based on oneway ANOVA followed by Tukey's multiple comparisons test, with a significance of ****, $P \leq 0.0001$. NS, not significant; TMD, transmembrane domain. **(F)** TAG content in seeds from wild-type Col-0 and normal and abnormal seeds from *orm1*$^{+/-}$ *orm2*$^{+/-}$. and *Atlcb1*$^{+/-}$ expressing LCB1ΔTMD1. Values are the mean ± SD of three independent lipid extractions. Asterisks indicate significant difference based on one-way ANOVA followed by Tukey's multiple comparisons test, with a significance of ***, $P \leq 0.001$ and ****, $P \leq 0.0001$. NS, not significant; TMD, transmembrane domain. **(G)** Composition of TAG as weight percent of fatty acid in seeds from wild-type Col-0 and normal and abnormal seeds from *orm1*$^{+/-}$ *orm2*$^{+/-}$. and *Atlcb1*$^{+/-}$ expressing LCB1ΔTMD1. Values are the mean ± SD of three independent samples. TMD, transmembrane domain.

The most striking difference in fatty acid composition of TAG from the abnormal seeds was a reduction in the overall content of C20 and C22 very long chain fatty acids derived from ER-localized elongation reactions. Notably, the fatty acids 20:2, 20:3, and 22:1

were not detectable in TAG from the abnormal seeds (Figure 2.5G). Overall, these results indicate that ORMs are essential for the completion of a full life cycle in Arabidopsis. Lethality due to the absence of ORM proteins is associated with the recovery of nonviable seeds with undeveloped embryos that accumulate excessive ceramide concentrations and have strongly reduced TAG levels. This was phenocopied in plants with deregulated SPT activity due to the loss of the transmembrane domain of LCB1 that abolishes ORM regulation of SPT (Han et al., 2019). The identification of nearly the same phenotype in ORM-null mutants and LCB1-ΔTMD1 lines also indicated that the loss of seed viability is associated with the role of ORM proteins in sphingolipid metabolism, rather than other reported functions of ORM in Arabidopsis (Yang et al., 2019).

2.4.3 The *orm1*$^{+/-}$ *orm2*$^{-/-}$ *and* *orm1*$^{-/-}$ *orm2*$^{+/-}$ Mutants Have Distinct Growth Phenotypes

The availability of progeny from *orm1*$^{-/-}$ and *orm2*$^{-/-}$ crosses also allowed us to assess the contributions of each ORM gene to the viability and growth of Arabidopsis plants. In addition to our inability to obtain homozygous double mutants for these genes, we observed that *orm1*$^{-/-}$ *orm2*$^{+/-}$ mutants were strongly dwarfed and senesced prior to flowering (Figure 2.6A). By contrast, *orm1*$^{+/-}$ *orm2*$^{-/-}$ mutants had a distinct bushy phenotype with overproliferation of shoots and inflorescences, delayed flowering time compared to wild-type and an extended life span of 7 months (Figures 2.6B and 2.6C). The seeds from these plants were viable and rendered 82 % plants genotyped as *orm1*$^{+/+}$ *orm2*$^{-/-}$, 22 % *orm1*$^{+/-}$ *orm2*$^{-/-}$ and 0 % *orm1*$^{-/-}$ *orm2*$^{-/-}$.

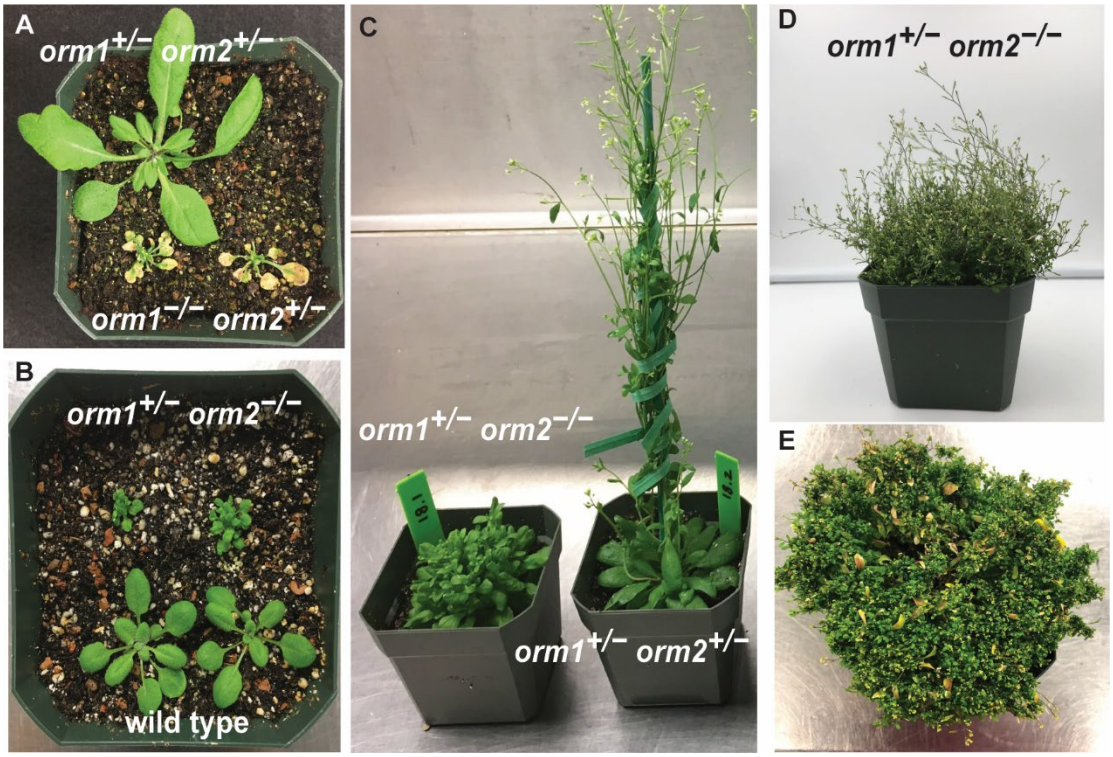

Figure 2.6 *orm1*$^{+/-}$ *orm2*$^{-/-}$ and *orm1*$^{-/-}$ *orm2*$^{+/-}$ Plants Have Distinct Growth Phenotypes.

(**A**) Representative image of 35-d-old *orm1*$^{+/-}$ *orm2*$^{-/-}$ and *orm1*$^{-/-}$ *orm2*$^{+/-}$ plants. The *orm1*$^{-/-}$*orm2*$^{+/-}$ plants showed reduced size and yellow regions corresponding to cell death. (**B**) Representative image of 18-d-old wild-type Col-0 and *orm1*$^{+/-}$*orm2*$^{-/-}$ plants. Mutants showed reduced size, abnormal leaf shape, and a bushy phenotype. (**C**) Representative image of 50-d-old *orm1*$^{+/-}$*orm2*$^{-/-}$ and *orm1*$^{+/-}$*orm2*$^{+/-}$ plants. The *orm1*$^{+/-}$ *orm2*$^{-/-}$ plants showed a bushy phonotype and delayed flowering. (**D**) Representative image of 80-d-old *orm1*$^{+/-}$*orm2*$^{-/-}$ plant. (**E**) Representative image of 120-d-old *orm1*$^{+/-}$*orm2*$^{-/-}$ plant.

Sphingolipidomic profiling revealed little differences in the concentrations of free LCBs, the LCB-phosphate (LCB-P) and ceramides among the wild-type, *orm1*$^{+/-}$ *orm2*$^{+/-}$, *orm1*$^{-/+}$ *orm2*$^{-/-}$ and one plant of the genotype *orm1*$^{-/-}$*orm2*$^{+/-}$. However, one plant genotyped *orm1*$^{-/-}$*orm2*$^{+/-}$ (2) showed increased levels of LCBs and ceramides (Fig 2.7A, 2.7B and 2.7C). The ceramide profile of this plant with increased sphingolipid levels showed accumulation of C16, C22, C24 and C26 ceramides compared to wild type.

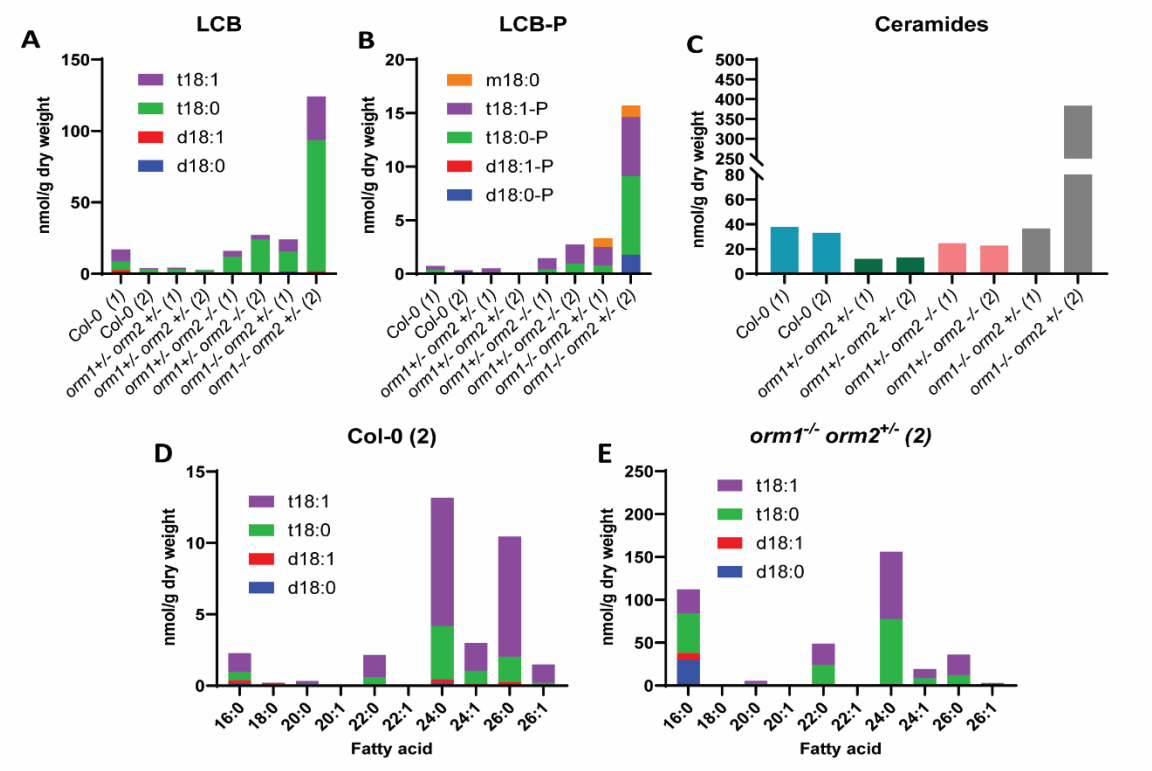

Figure 2.7 LCB and Ceramide Profiles in *orm1*$^{+/-}$ *orm2*$^{+/-}$, *orm1*$^{+/-}$ *orm2*$^{-/-}$ and *orm1*$^{-/-}$ *orm2*$^{+/-}$ Plants.

(**A**) Free LCB composition (d18:0, d18:1, t18:0, t18:1), (**B**) free LCB-phosphate (LCB-P) and (**C**) total ceramide content in two representative plants of each genotype: wild-type Col-0, *orm1*$^{+/-}$ *orm2*$^{+/-}$, *orm1*$^{+/-}$ *orm2*$^{-/-}$*and orm1*$^{-/-}$ *orm2*$^{+/-}$. (**D**) and (**E**) Ceramide molecular species compositions representing the exact pairings of LCB and fatty acid for the wild-type (D), *orm1*$^{-/-}$ *orm2*$^{+/-}$*(*E) plants.

2.5 Discussion

Our findings identified the essential role of sphingolipid biosynthetic regulation at the level of SPT for seed viability, which was previously unclear due to the lack of complete knockout mutants for ORM genes in plants. We showed that *orm1*$^{-/-}$ *orm2*$^{-/-}$ seeds have impaired embryo development accompanied by hyperaccumulation of the cytotoxic sphingolipid biosynthetic intermediates ceramides. Strongly enhanced ceramide accumulation was also observed in the *S. cerevisiae orm1Δ/orm2Δ* mutant (Breslow et al., 2010; Han et al., 2010) and recently in *Ormdl1/3* mutant mice (Clarke et al., 2019). We also confirmed that impaired seed viability in the mutant is due solely to the function

of ORMs in SPT regulation, rather than other ascribed ORM functions (Yang et al., 2019). This was achieved by mimicking this phenotype by removing the first transmembrane domain of LCB1, which is required for ORM binding to SPT (Han et al., 2019).

This study emphasizes that the full significance of ORMs to plant viability can only be assessed by complete knockout of the corresponding genes. By contrast, Arabidopsis ORM suppressed plants previously generated by RNAi or artificial microRNA methods were fully viable, although the response to bacterial pathogens was altered in these plants and early senescence was observed with the most extreme suppression of ORM expression (Kimberlin et al., 2016; Li et al., 2016). Similar to our findings, a recent report revealed the inability to recover mice lacking all three ORMDL genes (Clarke et al., 2019). However, we were able to more precisely determine that lethality occurs during seed development rather than during gametogenesis. This finding contrasts with those from previous studies of plants with strongly reduced sphingolipid biosynthetic capacity due to impaired SPT activity (Dietrich et al., 2008; Teng et al., 2008; Kimberlin et al., 2013). In these mutants, pollen is defective in endomembrane formation and is unable to complete maturation. Sphingolipids accumulate to exceptionally high levels in Arabidopsis pollen relative to leaves (Luttgeharm et al., 2015b; Ischebeck, 2016). As such, it is likely that pollen is able to tolerate unregulated sphingolipid synthesis that results from complete ORM knockout.

The use of gene editing also allowed us to assess the redundancy of ORM1 and ORM2. Notably, single mutants and progeny from the crosses that genotype as *orm1*$^{+/-}$ *orm2*$^{+/-}$ had an appearance similar to the wild-type plants under normal conditions.

However, *orm1*$^{-/-}$ *orm2*$^{+/-}$ seedlings displayed early senescence and did not flower. Sphingolipid analyses revealed increased ceramides and LCBs levels in one of the plants of this genotype (Figure 2.7). Consistent with previous reports and our findings (Chapter 3), the accumulation of ceramides likely triggers enhanced expression of PCD-related genes. It is possible that the differences in sphingolipids content within the biological replicates was due to sample variation in terms of temporal PCD elicitation.

By comparison, *orm1*$^{+/-}$ *orm2*$^{-/-}$ plants were fertile but had a highly bushed appearance, were strongly delayed in flowering (>80 d to flowering) and had a prolonged life span of ~7 months. Despite the phenotypic differences no changes were seen in the levels of sphingolipids in the *orm1*$^{+/-}$ *orm2*$^{-/-}$ mutants compared to wild type. It is important to note that the sphingolipid measurements were performed using leaves, perhaps significant changes in sphingolipid concentrations can be detected in specific cells like axillary buds that are groups of meristematic cells located in the leaf axis.

The normal appearance of mutants genotyped as *ORM1/orm2*$^{-/-}$ and *orm1*$^{-/-}$*/ORM2* suggests that ORM1 and ORM2 are functionally redundant, despite the phenotypic differences observed in *orm1*$^{-/-}$ *orm2*$^{+/-}$ and *orm1*$^{+/-}$ *orm2*$^{-/-}$ seedlings. However, it is possible that ORM1 and ORM2 have specific roles allowing a fine tuning of SPT activity through different mechanisms under specific physiological demands. Our studies indicate that ORM1 may be a more potent inhibitor of SPT or perhaps the stronger phenotype associated with the complete *ORM1* knockout in the *ORM2* heterozygous background reflects the finding that *ORM1* is more highly expressed than *ORM2* throughout the plant except in pollen (Kimberlin et al., 2016). The phenotype of the *orm1*$^{+/-}$ *orm2*$^{-/-}$ mutant suggests that ORM2 could contribute to the prolonged life cycle of an Arabidopsis plant

perhaps by cell type-specific function to fine-tune sphingolipid levels or through a nonsphingolipid-related function. It has been shown that mutations that lead to prolonged shoot apical meristems (SAM) activity, continuous generation of new shoots and arrest senescence of tissues are associated with extended longevity of Arabidopsis (Gan, 2003; Nooden and Penney, 2001). Moreover, in future work we will determine changes in phytohormones levels in the mutants. The roles of the hormones auxin and cytokinins are essential for apical dominance and the suppression of axillary buds (Guo and Gan, 2011). In this context it is possible that ORM2 has a functional role at the meristematic cells related to the transport of phytohormones.

AUTHOR CONTRIBUTIONS

A.G.S., G.H., T.M.D., and E.B.C. designed the study; A.G.S., Y.L., R.E.C. performed the experiments and analyzed the data, along with G.H., T.M.D., and E.B.C.; and A.G.S., G.H., T.M.D., and E.B.C. wrote the article.

2.6 References

Alexander, M.P. (1969). Differential staining of aborted and nonaborted pollen. Stain Technol. 44: 117–122.

Bligh, E.G., and Dyer, W.J. (1959). A rapid method of total lipid extraction and purification. Can. J. Biochem. Physiol. 37: 911–917.

Breslow, D.K., Collins, S.R., Bodenmiller, B., Aebersold, R., Simons, K., Shevchenko, A., Ejsing, C.S., and Weissman, J.S. (2010). Orm family proteins mediate sphingolipid homeostasis. Nature 463: 1048–1053.

Chen, M., Han, G., Dietrich, C.R., Dunn, T.M., and Cahoon, E.B. (2006). The essential nature of sphingolipids in plants as revealed by the functional identification and characterization of the Arabidopsis LCB1 subunit of serine palmitoyltransferase. Plant Cell 18: 3576–3593.

Chueasiri, C., Chunthong, K., Pitnjam, K., Chakhonkaen, S., Sangarwut, N., Sangsawang, K., Suksangpanomrung, M., Michaelson, L.V., Napier, J.A., and Muangprom, A. (2014). Rice ORMDL controls sphingolipid homeostasis affecting fertility resulting from abnormal pollen development. PloS One 5: e106386.

Clarke, B.A., et al. (2019). The Ormdl genes regulate the sphingolipid synthesis pathway to ensure proper myelination and neurologic function in mice. eLife 8: e51067

Clough, S.J., and Bent, A.F. (1998). Floral dip: A simplified method for Agrobacterium-mediated transformation of Arabidopsis thaliana. Plant J. 16: 735–743.

Coursol, S., Fan, L.M., Le Stunff, H., Spiegel, S., Gilroy, S., and Assmann, S.M. (2003). Sphingolipid signalling in Arabidopsis guard cells involves heterotrimeric G proteins. Nature 423: 651–654.

Davis, D.L., Gable, K., Suemitsu, J., Dunn, T.M., and Wattenberg, B.W. (2019). The ORMDL/Orm-serine palmitoyltransferase (SPT) complex is directly regulated by ceramide: Reconstitution of SPT regulation in isolated membranes. J. Biol. Chem. 294: 5146–5156

Davis, J.A., et al. (2020). The lipid flippases ALA4 and ALA5 play critical roles in cell expansion and plant growth. Plant Physiol. 182: 2111–2125.

Dietrich, C.R., Han, G., Chen, M., Berg, R.H., Dunn, T.M., and Cahoon, E.B. (2008). Loss-of-function mutations and inducible RNAi suppression of Arabidopsis LCB2 genes reveal the critical role of sphingolipids in gametophytic and sporophytic cell viability. Plant J. 54: 284–298.

Gan, S. (2003) Mitotic and Postmitotic Senescence in Plants. Sci. Aging Knowl. Environ. 2003:re7.

Gable, K., Slife, H., Bacikova, D., Monaghan, E., and Dunn, T.M. (2000). Tsc3p is an 80-amino acid protein associated with serine palmitoyltransferase and required for optimal enzyme activity. J. Biol. Chem. 275: 7597–7603.

Guo, Y., Gan, S. (2011). AtMYB2 regulates whole plant senescence by inhibiting cytokinin-mediated branching at late stages of development in Arabidopsis. Plant Physiol. 156: 1612–1619.

Gupta, S.D., Gable, K., Alexaki, A., Chandris, P., Proia, R.L., Dunn, T.M., and Harmon, J.M. (2015). Expression of the ORMDLS, modulators of serine palmitoyltransferase, is regulated by sphingolipids in mammalian cells. J. Biol. Chem. 290: 90–98.

Han, G., Gupta, S.D., Gable, K., Bacikova, D., Sengupta, N., Somashekarappa, N., Proia, R.L., Harmon, J.M., and Dunn, T.M. (2019). The ORMs interact with transmembrane domain 1 of Lcb1 and regulate serine palmitoyltransferase oligomerization, activity and localization. Biochim. Biophys. Acta Mol. Cell Biol. Lipids 1864: 245–259.

Han, S., Lone, M.A., Schneiter, R., and Chang, A. (2010). Orm1 and Orm2 are conserved endoplasmic reticulum membrane proteins regulating lipid homeostasis and protein quality control. Proc. Natl. Acad. Sci. USA 107: 5851–5856.

Ischebeck, T. (2016). Lipids in pollen - They are different. Biochim. Biophys. Acta 1861 (9 Pt B): 1315–1328.

Kimberlin, A.N., Han, G., Luttgeharm, K.D., Chen, M., Cahoon, R.E., Stone, J.M., Markham, J.E., Dunn, T.M., and Cahoon, E.B. (2016). ORM expression alters sphingolipid homeostasis and differentially affects ceramide synthase activity. Plant Physiol. 172: 889–900

Kimberlin, A.N., Majumder, S., Han, G., Chen, M., Cahoon, R.E., Stone, J.M., Dunn, T.M., and Cahoon, E.B. (2013). Arabidopsis 56- amino acid serine palmitoyltransferase-interacting proteins stimulate sphingolipid synthesis, are essential, and affect mycotoxin sensitivity. Plant Cell 25: 4627–4639.

Li, J., Yin, J., Rong, C., Li, K.E., Wu, J.X., Huang, L.Q., Zeng, H.Y., Sahu, S.K., and Yao, N. (2016). Orosomucoid proteins interact with the small subunit of serine palmitoyltransferase and contribute to sphingolipid homeostasis and stress responses in Arabidopsis. Plant Cell 28: 3038–3051.

Liang, H., Yao, N., Song, J.T., Luo, S., Lu, H., and Greenberg, J.T. (2003). Ceramides modulate programmed cell death in plants. Genes Dev. 17: 2636–2641

Luttgeharm, K.D., Kimberlin, A.N., Cahoon, R.E., Cerny, R.L., Napier, J.A., Markham, J.E., and Cahoon, E.B. (2015b). Sphingolipid metabolism is strikingly different between pollen and leaf in Arabidopsis as revealed by compositional and gene expression profiling. Phytochemistry 115: 121–129.

Markham, J.E., and Jaworski, J.G. (2007). Rapid measurement of sphingolipids from *Arabidopsis thaliana* by reversed-phase highperformance liquid chromatography coupled to electrospray ionization tandem mass spectrometry. Rapid Commun. Mass Spectrom. 21: 1304–1314.

Markham, J.E., Molino, D., Gissot, L., Bellec, Y., Hématy, K., Marion, J., Belcram, K., Palauqui, J.C., Satiat-Jeunemaître, B., and Faure, J.D. (2011). Sphingolipids containing very-long-chain fatty acids define a secretory pathway for specific polar plasma membrane protein targeting in Arabidopsis. Plant Cell 23: 2362–2378.

Noodén, L.D., Penney, J.P. (2001) Correlative controls of senescence and plant death in *Arabidopsis thaliana* (Brassicaceae). J Exp Bot 52: 2151–2159.

Peer, M., Stegmann, M., Mueller, M.J., and Waller, F. (2010). Pseudomonas syringae infection triggers de novo synthesis of phytosphingosine from sphinganine in Arabidopsis thaliana. FEBS Lett. 584: 4053–4056.

Tantikanjana, T., Yong, J.W.H., Letham, D.S., Griffith, M., Hussain, M., Ljung, K., Sandberg, G., and Sundaresan, V. (2001). Control of axillary bud initiation and shoot architecture in Arabidopsis through the SUPERSHOOT gene. Genes Dev. 15: 1577–1588

Teng, C., Dong, H., Shi, L., Deng, Y., Mu, J., Zhang, J., Yang, X., and Zuo, J. (2008). Serine palmitoyltransferase, a key enzyme for de novo synthesis of sphingolipids, is essential for male gametophyte development in Arabidopsis. Plant Physiol. 146: 1322–1332

Wang, Z.P., Xing, H.L., Dong, L., Zhang, H.Y., Han, C.Y., Wang, X.C., and Chen, Q.J. (2015). Egg cell-specific promoter-controlled CRISPR/Cas9 efficiently generates homozygous mutants for multiple target genes in Arabidopsis in a single generation. Genome Biol. 16: 144.

Yang, F., Kimberlin, A.N., Elowsky, C.G., Liu, Y., Gonzalez-Solis, A., Cahoon, E.B., and Alfano, J.R. (2019). A plant immune receptor degraded by selective autophagy. Mol. Plant 12: 113–123.

Zhu, L.H., et al. (2016). Dedicated industrial oilseed crops as metabolic engineering platforms for sustainable industrial feedstock production. Sci. Rep. 6: 22181.

3 Chapter 3. Compromised regulation of SPT activity leads to hyperaccumulation of selected sphingolipids, altered organellar structures and transcriptional regulation.

The content included in this chapter has been published.

Ariadna Gonzalez-Solis, Gongshe Han, Lu Gan, Yunfeng Li, Jonathan E. Markham, Rebecca E. Cahoon, Teresa M. Dunn, Edgar B. Cahoon. Unregulated Sphingolipid Biosynthesis in Gene-Edited Arabidopsis ORM Mutants Results in Nonviable Seeds with Strongly Reduced Oil Content. The Plant Cell Aug 2020, 32 (8) 2474-2490; DOI: 10.1105/tpc.20.00015.

3.1 Abstract

Serine palmitoyltransferase, the first enzyme of sphingolipid biosynthesis, is negatively regulated by ORM proteins. However, in multicellular eukaryotes the mechanisms of this regulation are not fully understood, especially the details of the SPT-ORMs interaction are not known. In this study, through gene editing, we recovered the *orm1*$^{\Delta met/\Delta met}$ *orm2*$^{-/-}$ mutant, which expresses an ORM1 structural variant lacking one amino acid (Met-51). This mutant did not advance beyond the seedling stage, hyperaccumulated ceramides, and showed altered organellar structures and increased senescence- and pathogenesis-related gene expression. These seedlings also showed upregulated expression of genes for sphingolipid catabolic enzymes, pointing to additional mechanisms for maintaining sphingolipid homeostasis. Moreover, ORM1 lacking Met-51 had strongly impaired interactions with LCB1 in a yeast (*Saccharomyces cerevisiae*) model, providing structural clues about regulatory interactions between ORM and SPT.

3.2 Introduction

Sphingolipids have been recognized as abundant membrane components that play several roles in plant cells. Besides their importance in endomembrane trafficking and formation of plasma membrane domains, sphingolipids are also bioactive molecules that participate

in signaling pathways during the pathogen-induced hypersensitive response, abiotic stress and ABA-dependent guard cell closure (Coursol et al., 2003; Magnin-Robert et al., 2015). Therefore, the study of sphingolipid metabolism has become an active are of research in the last decades, especially the emphasis on the regulatory processes that ensure homeostasis during cell development and responses to the environment. As the first step in the pathway, serine palmitoyltransferase (SPT) is considered a target for regulation. Small subunits of SPT (ssSPT) interact with the core subunits of SPT, LCB1 and LCB2, and have an activating effect on the activity (Kimberlin et al., 2013). Whereas, ORM proteins are negative regulators. Studies of yeast mutants have shown ORMs are downstream of a Torc2/Ypk1 kinase signaling pathway that senses sphingolipid availability and regulates SPT activity accordingly (Roelants et al., 2011). In the yeast regulatory scenario, under sphingolipid depletion ORMs get phosphorylated relieving SPT inhibition. However, in multicellular eukaryotes, the lack of the N-terminal domain containing the phosphorylation sites suggests the regulation of SPT by ORMs occurs through different mechanisms that have not been fully elucidated. Here, we describe an Arabidopsis mutant expressing an ORM1 structural variant that is strongly compromised in the regulation of SPT activity. This mutant provided valuable insights into changes in sphingolipid levels and the effects in the cell. These effects included compromised organellar structures, the induction of catabolic genes to maintain sphingolipid homeostasis and pathogenesis-related genes. In addition, this mutant provided clues about the structural requirements of ORMs for interaction with LCB1 for the regulation of SPT activity.

3.3 Materials and Methods

3.3.1 Plant Materials and Growth Conditions

Arabidopsis (*Arabidopsis thaliana*) Columbia-0 (Col-0) was used as the wild-type reference in this study. Arabidopsis seedlings were grown on Murashige and Skoog (MS) medium supplemented with 1% (w/v) Sucrose and 0.8% (w/v) agar, pH 5.7, with 16-h-light (100 mmol/ m^{-2} s^{-1})/8-h-dark conditions at 22°C. The light source for growth chamber–grown seedlings was supplied by standard wide-spectrum fluorescent bulbs type F32/841/ ECO 32 W (maximum intensity, 480 to 570 nm). For Arabidopsis plants in soil, seeds were sown, and after 2 d of stratification at 4°C, plants were grown at 22°C with 16-h-light (100 mmol/ m^{-2} s^{-1})/8-h-dark conditions.

3.3.2 Generation of CRISPR/Cas9 ORM Mutants

For CRISPR/Cas9-mediated gene editing of *ORM1* and *ORM2*, designed target sites (Fig 2.1A) were fused with a single guide RNA and expressed under the control of the U6 promoter. The egg cell–specific EC1 promoter was used to drive Cas9 expression as previously reported by Wang et al. (2015). In short, *BsaI* sites were incorporated by PCR into the ORM target sequences (primers P1 to P4; Supplemental Table 1 in Appendix A). The purified PCR products were digested with *BsaI* and ligated to the *BsaI*-linearized binary vector pHEE401E. The final CRISPR/Cas9 binary vector was electroporated into *Agrobacterium tumefaciens* strain GV3101 and then transformed into the Arabidopsis Col-0 wild-type plants via the floral dip method (Clough and Bent, 1998). The seeds were screened for hygromycin resistance on MS plates containing 25 mg/L hygromycin. For genotyping, fragments including the target regions of ORM1 and ORM2 were amplified by PCR from the genomic DNA of transgenic plants (primers P5 to P8; Supplemental

Table 1 in Appendix A). Amplicons were digested with the restriction enzymes *BslI* (*ORM1*) and *DraIII* (*ORM2*). The specific indels were identified by DNA sequencing. To analyze for nontransgenic plants, progeny of hygromycin-selected and confirmed homozygous (CRISPR/Cas9 mutation) T1 plants were sown directly on soil without hygromycin selection. These plants were then screened by PCR (P9+P10; Supplemental Table 1 in Appendix A) for the lack of the *Cas9* gene with the presence of the CRISPR mutation, in the T2 generation. The plants lacking *Cas9* but containing the CRISPR mutation were kept and used for further studies as mutated but not transgenic lines.

3.3.3 Genetic Complementation of *orm1*$^{\Delta met/\Delta met}$ *orm2*$^{-/-}$

For genetic complementation of the mutant *orm1*$^{\Delta met/\Delta met}$ *orm2*$^{-/-}$, *ORM1* cDNA was synthesized with included silent mutations of the *ORM1* gRNA target sequence to mitigate possible editing of the transgene. The cDNA was amplified by overlapping PCR and cloned into the *EcoRI* and *XbaI* sites of binary vector pBinGlyRed3 under the control of the native *ORM1* promoter 600-bp region upstream of the *ORM1* start codon (primers P11 to P16; Supplemental Table 1 in Appendix 1). *orm1*$^{\Delta met/\Delta met}$ *orm2*$^{-/-}$ plants were transformed with the pBinGlyRed3-ORM1 construct by the floral dip method (Clough and Bent, 1998). Transformants were selected based on *Discosoma* red fluorescent protein fluorescence and genotyped. Mutation was confirmed by sequencing.

3.3.4 RNA Isolation and Quantitative RT-PCR

RNA was extracted from 12- to 15-d-old Arabidopsis seedlings grown on solid MS medium. Each replicate corresponds to pooled seedlings from independent plates. RNA extraction was performed using an RNeasy Kit (Qiagen) according to the manufacturer's protocol. The isolated RNA (1mg) was treated with DNase I (Invitrogen). cDNA

conversion was performed with a RevertAid cDNA synthesis kit (Thermo Fisher Scientific). SYBR Green was used as the fluorophore in a qPCR supermix (Qiagen). PP2AA3 and UBIQUITIN (UBQ) were used as internal reference genes. qPCR was performed using a Bio-Rad MyiQ iCycler qPCR instrument. The thermal cycling conditions were an initial step of 95°C for 10 min followed by 45 cycles at 95°C for 15 s, 60°C for 30 s, and 72°C for 30 s. Primers used in this study are listed in Supplemental Table 1 in Appendix 1.

3.3.5 Electron Microscopy

Ten-day-old wild-type and *orm1*$^{\Delta met/\Delta met}$ *orm2*$^{-/-}$ seedlings were used for TEM. The samples were cut and fixed with 2.5% (v/v) glutaraldehyde and 2.0% (v/v) paraformaldehyde in 0.1 M cacodylate buffer. The samples were subjected to postfixation with 1% (w/v) osmium tetroxide in 0.1 M cacodylate buffer, dehydrated with ethanol and acetone, and embedded with a Spurr's Embedding Kit. Ultrathin sections (100 nm) were cut and stained with uranyl acetate and lead citrate. Samples were imaged on a Hitachi H7500 transmission electron microscope at an accelerating voltage of 80 kV.

3.3.6 Sphingolipid Extraction and Analysis

Sphingolipids were extracted as described in Markham and Jaworski (2007). Briefly, 12- to 15-d-old Arabidopsis seedlings grown on solid medium were collected from independent plates for each biological replicate. The seedlings were lyophilized, and 10 to 30 mg of tissue was homogenized and extracted with isopropanol:heptane:water (55:20:25, v/v/v). We used 1 to 4 mg of plant material for each biological replicate for sphingolipid analysis from seeds. Internal standards for the different sphingolipid classes were added. The supernatants were dried and deesterified with methylamine in

ethanol:water (70:30, v/v). The lipid extract was re-suspended in tetrahydrofuran:methanol:water (5:2:5, v/v/v) containing 0.1% (v/v) formic acid. The sphingolipid species were analyzed using a Shimadzu Prominence ultra-performance liquid chromatography system and a 4000 QTRAP mass spectrometer (AB SCIEX). Data analysis and quantification were performed using the software Analyst 1.5 and MultiQuant 2.1 as described by Markham and Jaworski (2007), Kimberlin et al. (2013), and Davis et al. (2020).

3.3.7 *Saccharomyces cerevisiae* Cell Growth and Expression Plasmids

Saccharomyces cerevisiae strain TDY9113 (Mata *tsc3*D:NAT*lcb1*D:KAN *ura*3 *leu*2 *lys*2 *trp1*D) lacking endogenous SPT was used for the expression of Arabidopsis SPT subunits and ORM proteins as described by Kimberlin et al. (2016). For DoxSA quantification, *S. cerevisiae* strain TDY9113 expressing AtLCB1^{C144W} was grown in 1.5% (w/v) Gal and 0.5% (w/v) Glc supplemented with 40 mM Ala. Plasmids for the expression of AtLCB1-FLAG, Myc-AtLCB2a, and HA-AtssSPTa in *S. cerevisiae* were as described by Kimberlin et al. (2013) and for HA-AtORM1 as described by Kimberlin et al. (2016). AtLCB1^{C144W} was generated by QuikChange mutagenesis (Agilent Technologies) and confirmed by sequencing. The open reading frame of AtORM1$^{\Delta Met51}$ was amplified by PCR and inserted into pPR3-N (Dualsystems Biotech) for expression with an N-terminal HA tag. LCB and DoxSA quantifications were performed as previously described by Kimberlin et al. (2016).

3.3.8 Immunoprecipitation

Microsomal membrane proteins were prepared from *S. cerevisiae* cells expressing FLAG-tagged AtLCB1, Myc-tagged AtLCB2a, HA-tagged AtssSPTa, and HA-tagged

AtORM1 or AtORM1$^{\Delta Met51}$. Microsomal membrane proteins were solubilized in 1.5% digitonin at 4°C for 2.5 h and incubated with FLAG-beads (Sigma-Aldrich) overnight. The bound proteins were eluted in immunoprecipitation buffer (50 mM Hepes-KOH, pH 6.8, 150 mM potassium acetate, 2 mM magnesium acetate, 1 mM calcium chloride, and 15% [v/v] glycerol) containing 0.25% (w/v) digitonin and 200 mg/mL FLAG peptide, resolved on a 4 to 12% (w/v) Bis-Tris NuPAGE gel (Invitrogen), and detected by immunoblotting with anti-HA (1:5000 dilution; Covance), anti-Myc (1:3000 dilution; Sigma-Aldrich), and antiFLAG (1:5000 dilution; GenScript) antibodies.

3.3.9 Membrane Topology Mapping of AtORM1$^{\Delta Met51}$

AtORM1 or AtORM1$^{\Delta Met51}$-encoding synthetic cDNAs with an in-frame glycosylation cassette (GC) inserted after codon 46, 82 or 121 were synthesized by GenScript and ligated into pPR3-N for expression with an N-terminal HA tag. The HA-ORM1-GC–tagged proteins were expressed (along with AtLCB1-FLAG, MYC-AtLCB2a, and HA-AtssSPTa) in *S. cerevisiae* strain TDY9113. Isolation of microsomal proteins, digestion with endoglycosidase H, and immunodetection of the AtORM1 proteins were performed as previously described (Kimberlin et al., 2016).

3.3.10 Statistical Analyses

Two-tailed Student's t test was performed to evaluate statistically significant differences compared to the control (wild type). One-way ANOVA followed by Tukey's test was used to determine the differences among the five genotypes for a given variable. Values of $P \leq 0.05$ were considered statistically significant. The statistical analyses were done using GraphPad Prism 8.3.0.

3.4 Results

3.4.1 *orm1*$^{\Delta met/\Delta met}$ *orm2*$^{-/-}$ Mutant Does Not Survive Beyond the Seedling Stage

Screening of gene-edited lines revealed a mutant with an in frame deletion of a single codon that resulted in a deletion of the Met residue at amino acid 51 relative to the wild-type ORM1 (Figure 3.1B). This line also carried nucleotide deletions in *ORM2* that led to a frameshift and premature stop codon (Supplemental Figures 1 and 2B in Appendix 1). Seedlings with the genotype *orm1*$^{\Delta met/\Delta met}$ *orm2*$^{+/-}$ showed a phenotype like the wild type and the single mutants under normal growth conditions (Figure 3.1A). However, we could only recover plants of the genotype *orm1*$^{\Delta met/\Delta met}$ *orm2*$^{-/-}$ in solid medium supplemented with Sucrose. The resulting seedlings were severely dwarfed and had a proliferation of small, deformed chlorotic leaves. These plants persisted in a visually viable state for 20 to 25 d after planting, but did not progress beyond the seedling stage, indicating that the *orm1*$^{\Delta met/\Delta met}$ *orm2*$^{-/-}$ mutation is seedling lethal (Figures 3.1A and 3.1C to 3.1F). Complementation of this mutant with the Arabidopsis ORM1 cDNA under the control of its native promoter was sufficient to rescue the seedling lethality and recover fertile plants, although many of the independent complemented mutant lines were smaller than wild-type plants, which is similar to the phenotype of *orm1*$^{+/-}$ *orm2*$^{-/-}$ plants, as described above (Supplemental Figure 3 in Appendix 1).

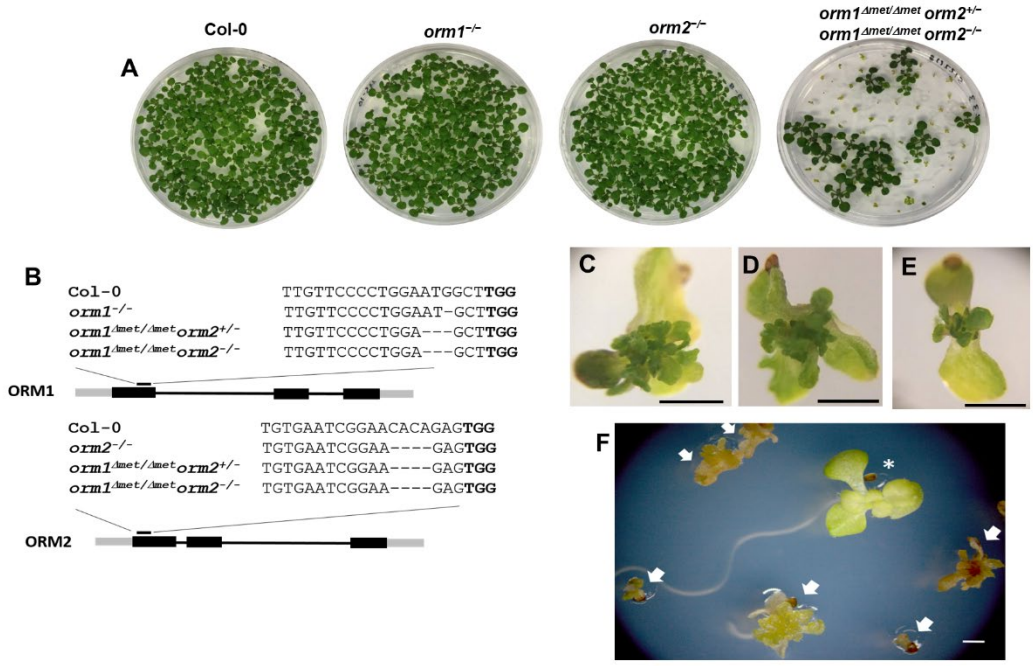

Figure 3.1 ***orm1*$^{\Delta met/\Delta met}$** ***orm2*$^{-/-}$** **Plants Exhibit Developmental Defects and Do Not Progress beyond the Seedling Stage.**

(**A**) and (**C**) to (**E**) Representative images (**A**) of the 12-d-old wild-type Col-0, *orm1*$^{-/-}$, *orm2*$^{-/-}$, *orm1*$^{\Delta met/\Delta met}$ *orm2*$^{+/-}$, and *orm1*$^{\Delta met/\Delta met}$ *orm2*$^{-/-}$seedlings. Seedlings with the same phenotype as the wild type correspond to *orm1*$^{\Delta met/\Delta met}$ *orm2*$^{+/-}$; small seedlings showing developmental defects correspond to *orm1*$^{\Delta met/\Delta met}$ *orm2*$^{-/-}$; enlarged images are shown in (**C**) to (**E**). Bars = 1 mm. (**B**) CRISPR/Cas9-induced mutations in *ORM1* and *ORM2*. Structures of the *ORM* genes; black boxes represent exons. The position of the CRISPR target site is marked as well as the nucleotide deletions in each mutant. (**F**) Phenotypes of 18-d-old seedlings; arrows indicate *orm1*$^{\Delta met/\Delta met}$ *orm2*$^{-/-}$and asterisk indicates *orm1*$^{\Delta met/\Delta met}$ *orm2*$^{+/-}$. Bar = 1 mm.

3.4.2 *orm1*$^{\Delta met/\Delta met}$ *orm2*$^{-/-}$ Mutant Hyperaccumulates Selected Sphingolipids

Based on the finding that downregulating ORM expression triggers sphingolipid accumulation (Breslow et al., 2010; Kimberlin et al., 2016; Li et al., 2016), we conducted extensive sphingolipidomic profiling of our gene-edited mutants from seedlings grown on Suc medium at 12 to 15 d after planting.

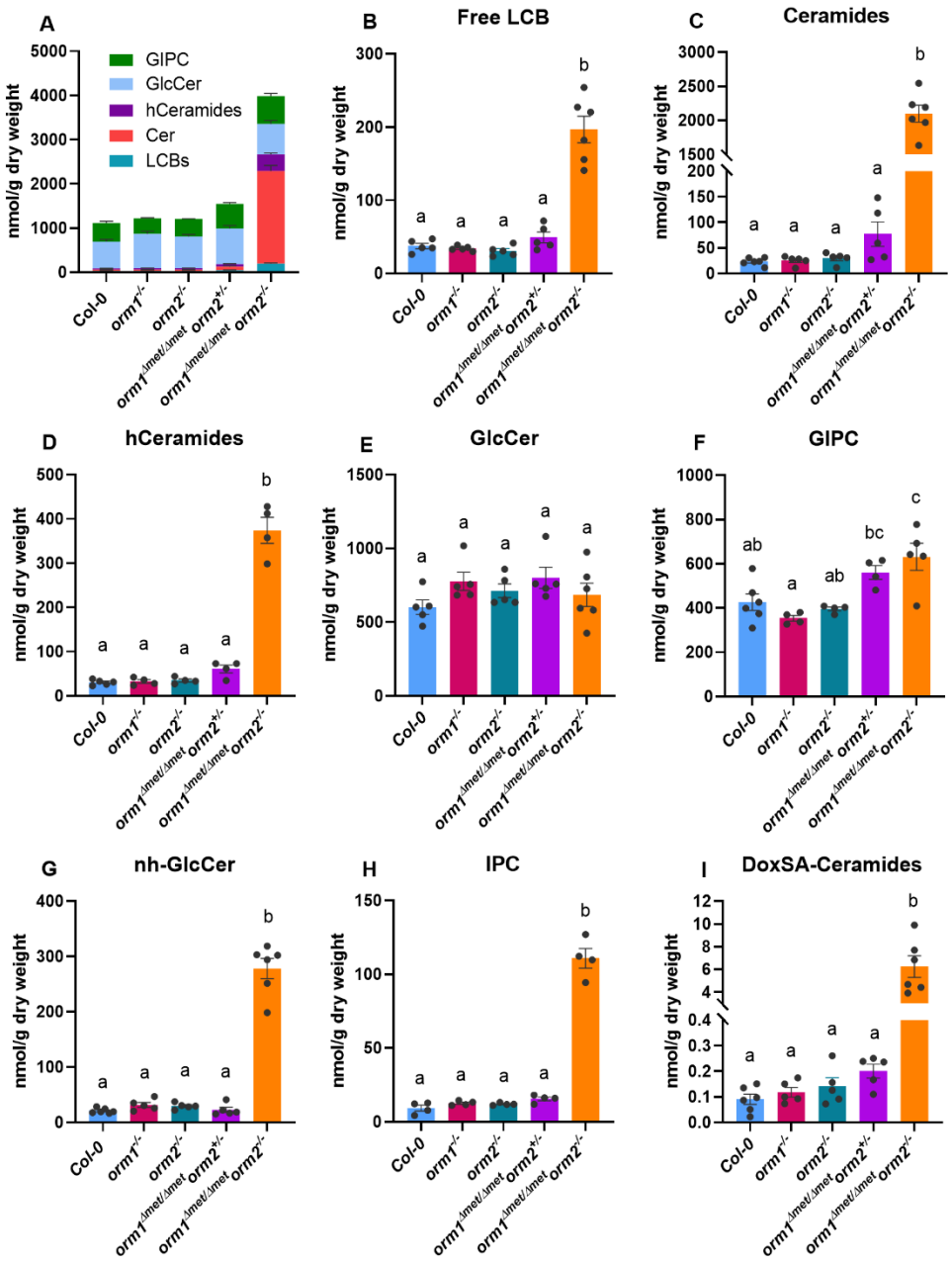

Figure 3.2 Selected Sphingolipid Classes Highly Accumulate in the *orm1*$^{\Delta met/\Delta met}$ *orm2*$^{-/-}$ Mutant.

(**A**) to (**G**) Total sphingolipid content (**A**) in wild-type, *orm1*$^{-/-}$, *orm2*$^{-/-}$, *orm1*$^{\Delta met/\Delta met}$ *orm2*$^{+/-}$, and *orm1*$^{\Delta met/\Delta met}$ *orm2*$^{-/-}$. Content of the following sphingolipid classes in the mutants: free LCBs (**B**), Cer (Ceramides; see [**C**]), hCer (hCeramides; see [**D**]), GlcCer (**E**), and GIPCs (**F**). Content of atypical sphingolipids nh-GlcCer (**G**) and IPCs (**H**). (**I**) Content of atypical deoxyLCB m18:0 in ceramides. Normally, SPT condenses Ser with palmitoyl-CoA to form d18:0. However, the unusual condensation of Ala gives rise to a deoxyLCB, DoxSA m18:0. Measurements are the average of four to six replicates consisting of pooled 12- to 15-d-old seedlings grown on different plates. Bars represent SE of the mean. Different letters indicate significant difference based on one-way ANOVA followed by Tukey's multiple comparisons test ($P \leq 0.05$).

The *orm1*$^{\Delta met/\Delta met}$ *orm2*$^{-/-}$ mutant accumulated 3.7-fold more sphingolipids than wild-type seedlings (Figure 3.2A). No significant differences in the levels of free LCBs, ceramides with nonhydroxylated fatty acids (Cer), or other sphingolipid classes were detected in the *orm1*$^{-/-}$, *orm2*$^{-/-}$, or *orm1*$^{\Delta met/\Delta met}$ *orm2*$^{+/-}$ mutants compared to wild-type plants (Figures 3.2B to 3.2E and 3.G to 3.2I). In strong contrast, *orm1*$^{\Delta met/\Delta met}$ *orm2*$^{-/-}$ seedlings showed heightened accumulation of LCB (5-fold), Cer (90-fold), and ceramides with hydroxylated fatty acids (hCer; 12-fold) compared to wild-type seedlings of similar age (Figures 3.2B and 3.2D; Supplemental Figure 4 in Appendix 1). Although no changes were detected in GlcCer concentrations, the levels of GlcCer containing nonhydroxylated fatty acids (nhGlcCer), not typically found in abundance in Arabidopsis, were 13-fold higher in *orm1*$^{\Delta met/\Delta met}$ *orm2*$^{-/-}$ seedlings than in wildtype seedlings (Figures 6E and 6G; Supplemental Figures 5 and 6). GIPC levels increased by 48% in the *orm1*$^{\Delta met/\Delta met}$ *orm2*$^{-/-}$ mutant compared to wild-type seedlings (Figure 3.2F; Supplemental Figure 7 in Appendix 1). The LCB composition of the single mutants and *orm1*$^{\Delta met/\Delta met}$ *orm2*$^{+/-}$ did not change significantly compared to wild type (Figures 3.3A and 3.3B). However, in *orm1*$^{\Delta met/\Delta met}$ *orm2*$^{-/-}$, the levels of free and phosphorylated forms of d18:0 were the most strongly increased, with lesser increases in the amounts of t18:0 and t18:1 free and phosphorylated species (Figures 3.3A and 3.3B). Cer profiles of the single mutants were similar to those of the wild type (Figures 3.3C to 3.3E). By contrast, the *orm1*$^{\Delta met/\Delta met}$ *orm2*$^{+/-}$ mutant had increased amounts of Cer with C16 fatty acids relative to wild-type and single mutant plants (Figure 3.3F). This phenotype was more accentuated in *orm1*$^{\Delta met/\Delta met}$ *orm2*$^{-/-}$ seedlings, which primarily accumulated Cer species with C16 fatty acids linked to the dihydroxy LCB d18:0 and d18:1 (Figure 3.3G). Increased amounts of

Cer with C22, C24, and C26 fatty acids as well as atypical C18 and C20 fatty acid–containing species were also detected in *orm1*$^{\Delta met/\Delta met}$ *orm2*$^{-/-}$ seedlings relative to wild-type plants and mutants of either ORM gene (Figure 3.3G).

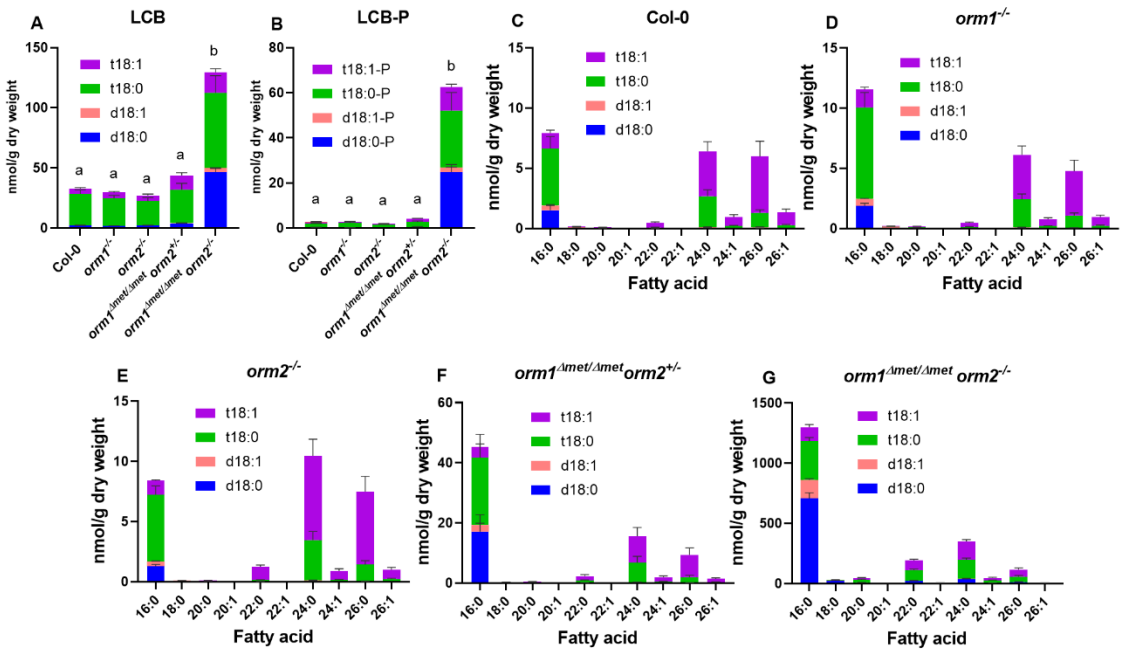

Figure 3.3 Free LCB and Ceramide Compositions and Concentrations Are Strongly Affected in the *orm1*$^{\Delta met/\Delta met}$ *orm2*$^{-/-}$ Mutant.

(**A**) to (**G**) Free LCB composition (d18:0, d18:1, t18:0, t18:1, [**A**]) and free LCB-phosphate (LCB-P) composition in the wild-type, *orm*1$^{-/-}$, *orm2*$^{-/-}$, *orm1*$^{\Delta met/\Delta met}$ *orm2*$^{+/-}$, and *orm1*$^{\Delta met/\Delta met}$ *orm2*$^{-/-}$. (**B**). Bars show averages of four to six replicates consisting of 12- to 15-d-old pooled seedlings grown on different plates. Error bars represent the SE of the mean. Different letters indicate significant difference, for each LCB, based on one-way ANOVA followed by Tukey's multiple comparisons test ($P \leq 0.05$). Ceramide molecular species compositions representing the exact pairings of LCB and fatty acid for the wild-type (**C**), *orm*1$^{-/-}$, (**D**), *orm2*$^{-/-}$, (**E**), *orm1*$^{\Delta met/\Delta met}$ ***orm2***$^{+/-}$, (**F**), and *orm1*$^{\Delta met/\Delta met}$ *orm2*$^{-/-}$ (**G**) plants. Measurements for all panels are the average of four to six replicates consisting of 12- to 15-d-old pooled seedlings grown on different plates. Bars represent SE of the mean.

Overall, the primary change in the composition of all sphingolipid classes, especially Cer, hCer, and nhGlcCer, in the *orm1*$^{\Delta met/\Delta met}$ *orm2*$^{-/-}$ seedlings was the change in the total and/or relative amounts of those containing C16 fatty acids bound to dihydroxy LCB, which are derived from the LOH2 ceramide synthase (Figure 3.3G; Supplemental Figures 4 and 6; Markham et al., 2011; Ternes et al., 2011; Luttgeharm et al., 2015a). The

orm1$^{\Delta met/\Delta met}$ *orm2*$^{-/-}$ plants also contained aberrant forms of hCer and GIPCs with currently undefined structures based on liquid chromatography–mass spectrometry ionization as well as Cer with the LCB deoxysphinganine (DoxSA), which is derived from the condensation of Ala, rather than Ser, to palmitoylCoA by SPT (Figure 6I). In addition, the concentration of inositolphosphorylceramides (IPCs), the precursors of GIPCs, increased nearly 12-fold in small *orm1*$^{\Delta met/\Delta met}$ *orm2*$^{-/-}$ seedlings versus the wild type (Figure 6H). Overall, these findings are consistent with the notion that SPT regulation by the ORM1$^{\Delta met}$-encoded polypeptide is deficient and that the flux of excess LCB occurs through the LOH2 ceramide synthase to produce Cer backbones with C16 fatty acids and dihydroxy LCB, a portion of which are channeled to GIPCs but accumulate as IPC intermediates.

3.4.3 Integrity of Cellular Component Is Compromised in the *orm1*$^{\Delta met/\Delta met}$ *orm2*$^{-/-}$ Mutant

Given that sphingolipids are abundant endomembrane and plasma membrane components that contribute to vesicular trafficking, we used transmission electron microscopy (TEM) to evaluate the subcellular phenotypes associated with enhanced sphingolipid accumulation in 10-d-old *orm1*$^{\Delta met/\Delta met}$ *orm2*$^{-/-}$ seedlings relative to the wild-type seedlings of the same age. Mesophyll cells from the wild-type seedlings showed large vacuoles with turgor pressure pushing organelles to the periphery (Figure 3.4A). Chloroplasts of the wild-type cells had the typical oval shape and well-defined thylakoid membranes (Figures 3.4A and 3.4B). By contrast, the *orm1*$^{\Delta met/\Delta met}$ *orm2*$^{-/-}$ mutant cells

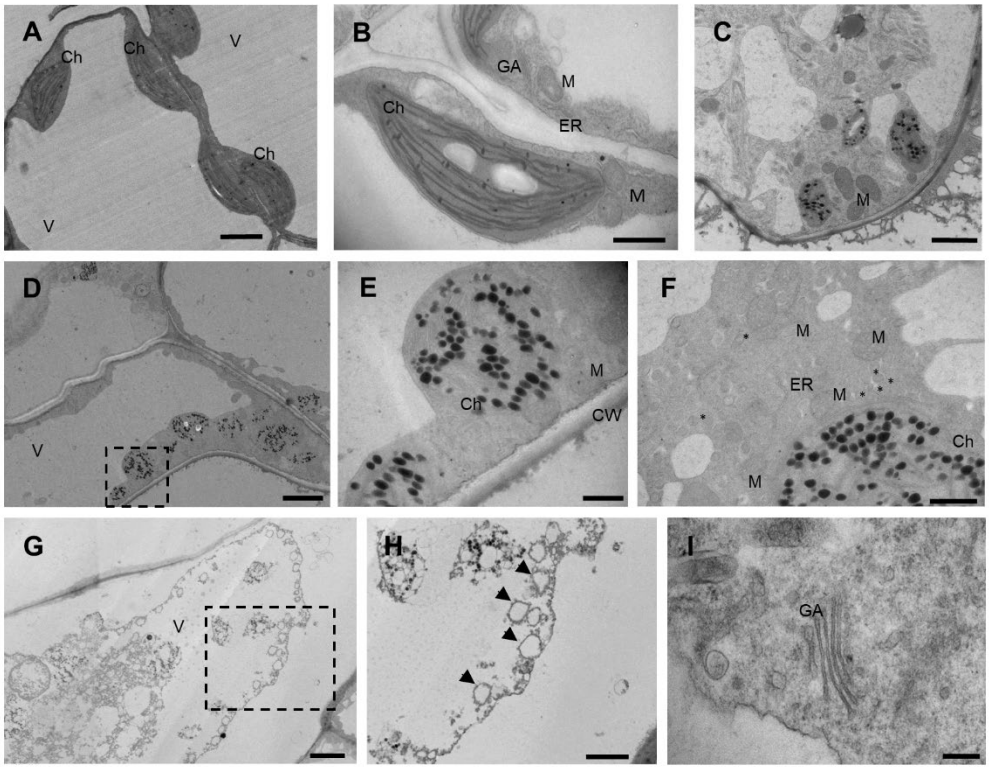

Figure 3.4 Subcellular Features are Strongly Altered in the *orm1*$^{\Delta met/\Delta met}$ *orm2*$^{-/-}$ Mutant.

(**A**) to (**H**) Representative TEM images of the wild-type seedlings (see [**A**] and [**B**]) and *orm1*$^{\Delta met/\Delta met}$ *orm2*$^{-/-}$. (see [**C**] to [**I**]). Longitudinal sections of leaves from 10-d-old seedlings were prepared for TEM analysis. Boxes represent sections enlarged in (**E**) and (**H**). Asterisks indicate vesicles and arrows autophagosomes. Bar = 200 nm in (**I**); bars = 800 nm in (**E**) and (**F**); bar = 1mm in (B); bars = 2mm in (A) and(**C**); and bars = 4mm in (**D**) and (**G**). Ch, Chloroplast; CW, cell wall; GA, Golgi apparatus; M, mitochondrion; V, vacuole.

displayed a lack of vacuolar turgor (Figure 3.4D). In addition, chloroplasts of *orm1*$^{\Delta met/\Delta met}$ *orm2*$^{-/-}$ cells were round and showed marked disintegration of thylakoids and highly abundant osmiophilic structures that resemble plastoglobuli (Figures 3.4C to 3.4F). Notably, increased vesicle numbers were observed around the ER network in *orm1*$^{\Delta met/\Delta met}$ *orm2*$^{-/-}$ cells (Figure 3.4F). Furthermore, electrodense material and double membrane vesicles consistent with autophagosomes were detected inside the vacuoles of these cells. Moreover, entire chloroplasts were engulfed and appeared to be in the process

of degradation (Figures 3.4G and 3.4H). Despite these large defects, Golgi stacks were detectable in *orm1*$^{\Delta met/\Delta met}$ *orm2*$^{-/-}$ cells (Figure 3.4I).

3.4.4 Genes for Ceramide Synthases, LCB Kinase, and LCB-Phosphate Lyase Are Upregulated in the *orm1*$^{\Delta met/\Delta met}$ *orm2*$^{-/-}$ Mutant

Given the increased concentrations of most sphingolipid classes in *orm1*$^{\Delta met/\Delta met}$ *orm2*$^{-/-}$, we examined the expression of genes in 12-d-old seedlings for key sphingolipid biosynthetic and catabolic enzymes, including the SPT-associated polypeptides LCB1 and ssSPTa, ceramide synthases (LOH1, LOH2, and LOH3), sphingosine kinases (SPHK1 and SPHK2), and the LCB catabolic enzyme LCB-phosphate lyase (or DPL1). No significant differences were detected in the expression of genes for LCB1, ssSPTa, or LOH1 in any mutant analyzed (Supplemental Figures 8A to 8C in Appendix 1). However, consistent with the increased amounts of ceramides in *orm1*$^{\Delta met/\Delta met}$ *orm2*$^{-/-}$, the ceramide synthase gene *LOH2* showed a 2.5-fold increase in expression and the ceramide synthase gene *LOH3* showed a 2-fold increase in *orm1*$^{\Delta met/\Delta met}$ *orm2*$^{-/-}$ plants compared to the wild type and the other mutants examined (Figures 3.5A and 3.5B). Most notably, the expression of the key sphingolipid catabolism-associated genes *SPHK2* and *DPL1* increased by approximately six- to sevenfold, respectively, in orm1$^{\Delta met/\Delta met}$ orm2$^{-/-}$ plants relative to the wild type and other ORM mutants (Figures 3.5C and 3.5D). This result is consistent with the notion that the induction of LCB catabolism is one route (in addition to ceramide biosynthesis) for the mitigation of unregulated LCB production in the *orm1*$^{\Delta met/\Delta met}$ *orm2*$^{-/-}$ mutant.

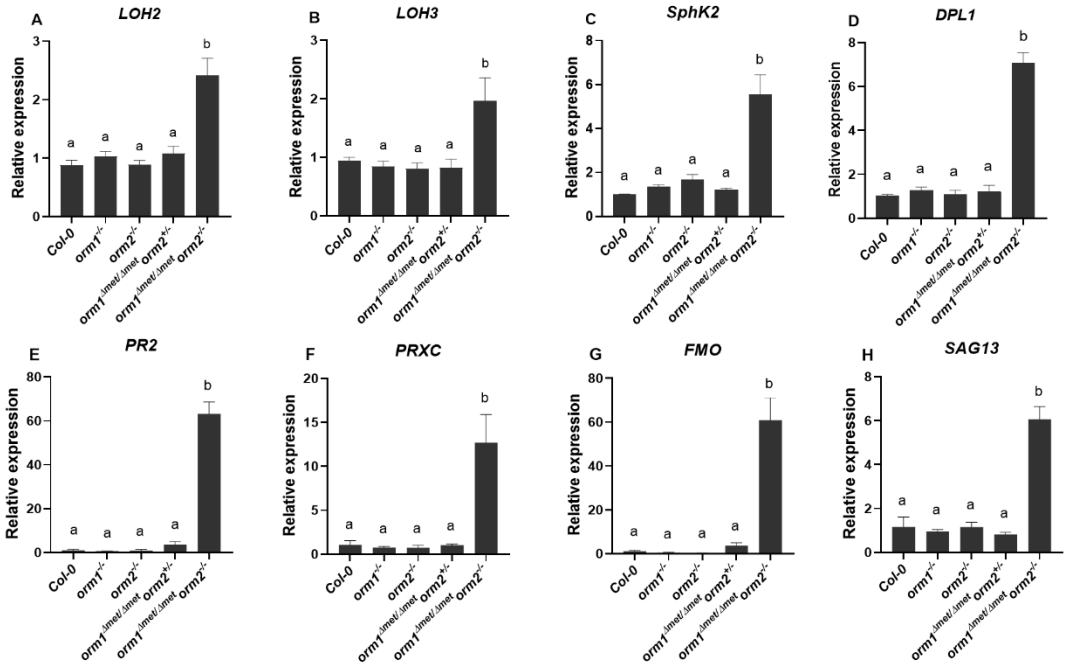

Figure 3.5 Expression of Genes Associated with Sphingolipid Homeostasis, Plant Defense Responses, and Senescence are Upregulated in the *orm1*$^{\Delta met/\Delta met}$ *orm2*$^{-/-}$ Mutant.

(**A**) to (**H**) Wild-type, *orm*1$^{-/-}$, *orm2*$^{-/-}$, *orm1*$^{\Delta met/\Delta met}$ *orm2*$^{+/-}$, and *orm1*$^{\Delta met/\Delta met}$ *orm2*$^{-/-}$. seedlings of 12-d-old plants were used to examine gene expression by qPCR to monitor genes encoding enzymes in sphingolipid biosynthetic and catabolic pathways: ceramide synthase gene *LOH2* (**A**), ceramide synthase gene *LOH3* (**B**), sphingosine kinase 2 gene *SPHK2* (**C**), and LCB-phosphate lyase gene *DPL1* (**D**) and selected pathogenesis- and senescence-related genes: β-1,3-glucanase gene *PR2* (**E**), class III peroxidase gene *PRXC* (**F**), flavin monooxygenase gene *FMO* (**G**), and senescence-related 13 gene *SAG13* (**H**). *PP2AA3* transcript levels were used as a control for the sphingolipid genes and *UBQ* for the pathogenesis- and senescence-related genes. Specific primers used for this analysis are shown in the Supplemental Table 1 in Appendix 1. Gene expression levels are normalized to those in wild-type seedlings. Values are the mean ± SD (n = 6 to 12). Different letters indicate significant difference based on one-way ANOVA followed by Tukey's multiple comparisons test ($P \leq 0.05$).

3.4.5 Defense and Senescence Genes Are Upregulated in the *orm1*$^{\Delta met/\Delta met}$ *orm2*$^{-/-}$ Mutant

The accumulation of ceramides has been linked to the activation of signaling pathways that lead to PCD (Liang et al., 2003; Bi et al., 2014). To examine whether the high amounts of ceramides in *orm1*$^{\Delta met/\Delta met}$ *orm2*$^{-/-}$ activate PCD, we performed qPCR of marker genes using RNA extracted from 12-d-old seedlings. The expression of the pathogenesis-related genes (*PR-2, PRXC, FMO, PR3*) was significantly higher in

orm1$^{\Delta met/\Delta met}$ *orm2*$^{-/-}$ than in the wild type and the other mutants (Figures 3.5E to 3.5G; Supplemental Figure 8E in Appendix 1). A similar expression pattern was also observed for the senescence-related gene *SAG13* (Figure 3.5H).

3.4.6 ORM1$^{\Delta Met51}$ Fails to Interact with LCB1 to Suppress SPT Activity

Our results clearly show that ORM1 lacking Met-51 is strongly impaired in repressing SPT activity. This amino acid is located in the ER luminal domain immediately adjacent to the second transmembrane domain of ORM1 (Supplemental Figure 9 in Appendix 1). We hypothesized that, without this amino acid, the conformation of the second transmembrane domain of ORM1 is altered such that the interaction with LCB1 for the repression of SPT activity is disrupted.

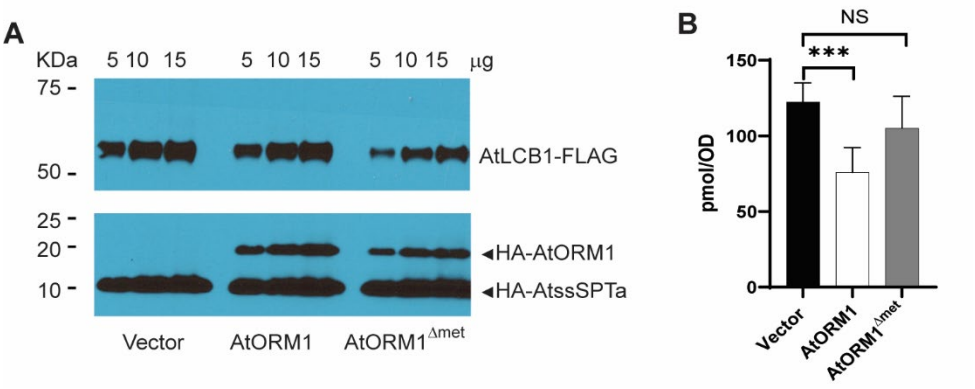

Figure 3.6 Expression of AtORM1$^{\Delta Met51}$ in yeast

(**A**) AtORM1$^{\Delta Met51}$ was stably expressed in *S. cerevisiae* with the native SPT complex replaced by the Arabidopsis SPT complex (see Methods). AtLCB1- FLAG, MYC-AtLCB2a, and HA-AtssSPTa without or with HA-AtORM1 or HA-AtORM1$^{\Delta Met51}$were expressed in *S. cerevisiae* strain *lcb1 tsc3*. Five, 10, and 15 mg of microsomal proteins was loaded and analyzed by SDS-PAGE (4 to 12%; Invitrogen) and detected with anti-LCB1 (1:3000) and anti-HA (Covance) antibodies. (**B**) DoxSA levels were determined from cells expressing AtLCB1^{C144W} and AtLCB2a, HA-AtssSPTa along with vector, HA-AtORM1 wild-type, or HAAtORM1$^{\Delta Met51}$. Shown are the mean ± SD of DoxSA levels from six independent colonies for each strain. Asterisks denote significant differences, as determined by two-tailed Student's t test with a significance of $P \leq 0.001$; NS, not significant, n=6.

To better understand this regulatory mechanism, we stably expressed the Arabidopsis ORM1$^{\Delta Met51}$ mutant protein in an *S. cerevisiae* mutant background in which AtLCB1,

AtLCB2, and AtssSPTa replaced the corresponding *S. cerevisiae* SPT-associated polypeptides, as confirmed by immunoblotting (Figure 3.6A).

We assessed in vivo SPT activity by measuring the DoxSA produced when expressing AtLCB1^{C144W} (Figure 3.6B). DeoxyLCBs cannot be phosphorylated/degraded and are used as a readout for in situ SPT activity (Gable et al., 2010; Kimberlin et al., 2016). When expressed in this *S. cerevisiae* background, the wild-type Arabidopsis ORM1 was able to suppress DoxSA production, which is consistent with its function as a negative regulator of SPT activity. By contrast, DoxSA concentrations in AtORM1$^{\Delta Met51}$-expressing cells were similar to those in vector control cells lacking ORM1, which is consistent with a lack of repressed SPT activity. ORMs interact with the first transmembrane domain of LCB1 to repress SPT activity in *S. cerevisiae* (Han et al., 2019), although the structural components of ORM associated with this interaction have not been defined. To test whether AtORM1$^{\Delta Met51}$ physically interacts with AtLCB1, as does the wild-type ORM1, we performed coimmunoprecipitation of FLAG-tagged AtLCB1 with solubilized microsomes from *S. cerevisiae* cells expressing Myc-AtLCB2a, hemagglutinin (HA)-AtssSPTa, and HA-AtORM1 or HA-AtORM1$^{\Delta Met51}$.

Pull-downs of AtLCB1 resulted in coimmunoprecipitation of AtLCB2a and AtORM1, but not ELO3, an ER protein that does not interact with SPT. By contrast, only trace amounts of HA-AtORM1$^{\Delta Met51}$ were detected in the AtLCB1 pulldowns (Figure 3.7A). This finding indicates that Met-51 is critical for the ORM-LCB1 physical interaction to regulate SPT activity. To determine whether the impaired ORM-LCB1 interaction is due to gross or subtle alterations in the secondary structure of ORM induced by the Met51 deletion, we compared the membrane topology of AtORM1 and AtORM1$^{\Delta Met51}$.

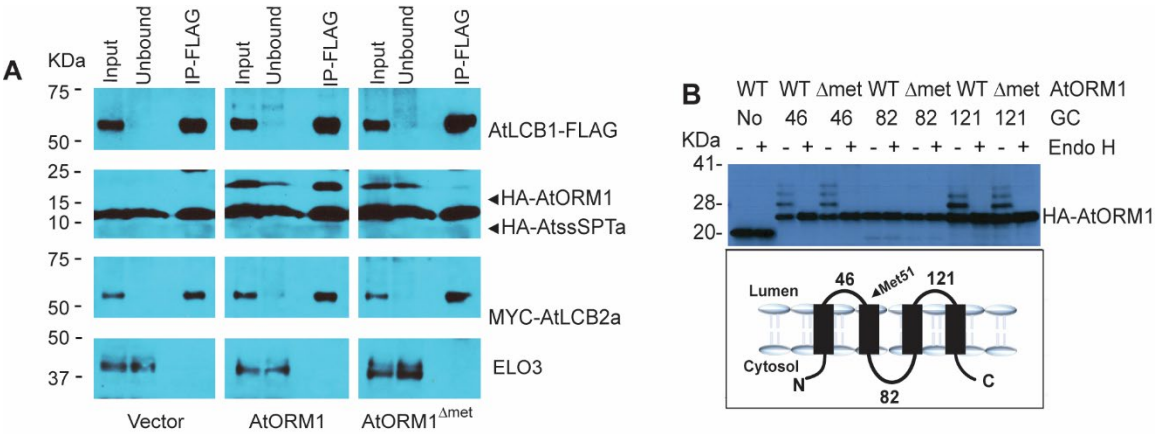

Figure 3.7 AtORM1$^{\Delta Met51}$ Fails to Regulate SPT Activity and Does Not Interact with LCB1.

(**A**) Coimmunoprecipitation of FLAG-tagged AtLCB1 in *S. cerevisiae* expressing AtLCB1-FLAG, MYC-AtLCB2a, HA-AtssSPTa, and either HA-AtORM1 or HA-AtORM1DMet51. Solubilized *S. cerevisiae* microsomes were incubated with anti-FLAG beads, and protein was eluted with FLAG peptide. Solubilized microsomes (Input), unbound and bound (IP-FLAG) were analyzed by immunoblotting. ELO3, an integral ER membrane protein, was used as a negative control. (**B**) Topology mapping of AtORM1DMet51. GCs were inserted after the indicated amino acids, and the GC-tagged proteins were expressed in *S. cerevisiae*. Increased mobility following treatment of microsomes with endoglycosidase H (Endo H) revealed that the GCs at residues 46 and 121 are glycosylated and therefore reside in the lumen of the ER. However, the GC at residue 82 is not glycosylated, indicating that residue 82 is located in the cytosol. AtORM1$^{\Delta Met51}$ retains the topology of wild-type (WT) ORM1.

We inserted glycosylation cassettes into the two predicted ER luminal loops (at amino acids 46 and 121) and into the cytosolic loop between the second and third transmembrane domains (at amino acid 82) and expressed the proteins in *S. cerevisiae* along with reconstituted Arabidopsis SPT. The analysis showed that the cassettes in the predicted luminal domains were glycosylated, while the cassette in the predicted cytosolic domain was not (Figure 3.7B). Thus, we conclude that ORM1 with the Met51 deletion retains the topology of wild-type ORM1.

3.5 Discussion

Among the gene-edited ORM variants identified in our studies was a mutant that contained an in-frame deletion of Met-51 combined with a homozygous knockout of ORM2 (*orm1*$^{\Delta met/\Delta met}$ *orm2*$^{-/-}$). Seeds from this mutant were viable, in contrast to *orm1*$^{-/-}$

orm2$^{-/-}$; however, the plants did not advance beyond the seedling stage and had strong developmental defects. Like the *orm1*$^{-/-}$ *orm2*$^{-/-}$ seeds, the *orm1*$^{\Delta met/\Delta met}$ *orm2*$^{-/-}$ seedlings hyperaccumulated ceramides with C16 fatty acids. These seedlings also accumulated aberrant sphingolipids including DoxSA containing ceramides, GlcCer containing nonhydroxylated fatty acids, and IPCs, all of which were nearly absent from wild-type seedlings. Cells from the *orm1*$^{\Delta met/\Delta met}$ *orm2*$^{-/-}$ seedlings displayed gross defects in membrane and organellar structures as well as apparent autophagosome-like structures. The early cell death displayed by the *orm1*$^{\Delta met/\Delta met}$ *orm2*$^{-/-}$ seedlings can be attributed to the activation of PCD pathways, as indicated by the high transcript levels of pathogenesis- and senescence-related genes that have been shown to be activated by the accumulation of LCB and ceramides. Notably, Met-51 is predicted to occur at a position that is adjacent to the second transmembrane domain of ORMs, but is not a conserved residue across eukaryotic ORM or ORMDL proteins (Supplemental Figure 9 in Appendix 1). Using S. *cerevisiae* mutants containing the Arabidopsis SPT complex, we determined that the ORM1 Met51 mutant has greatly reduced interaction with Arabidopsis LCB1, which is required for ORM-induced suppression of SPT activity. Given that Met-51 is not conserved in eukaryotes, it is likely that LCB1 does not directly interact with this residue. Instead, the lack of this amino acid likely produces a conformational change at the second transmembrane domain of ORM that impedes its regulatory interaction with the first transmembrane domain of LCB1. The maintenance of the topology of ORM1$^{\Delta Met51}$ in microsomal membranes was verified by endoglycosidase H digestion studies using the mutant ORM1 protein carrying glycosylation cassettes. To date, no residues or structural features in ORMs have been identified that are associated with their interaction with the

LCB1/ LCB2 heterodimer of SPT. Our findings point to the possible interaction of the first transmembrane domain of LCB1 with the second transmembrane domain of ORM as the basis for SPT regulation. Additional structural studies are required to fully elucidate these potential regulatory interactions between ORM and LCB1.

Our results also revealed transcriptional mechanisms for maintaining sphingolipid homeostasis upon the enhanced production of LCBs in the *orm1*$^{\Delta met/\Delta met}$ *orm2*$^{-/-}$ mutant. *LOH2* and *LOH3* (encoding the functionally distinct ceramide synthases), *SPHK2* (enconding a LCB kinase) and *DPL1* (encoding the last step in LCB degradation) were transcriptionally upregulated in the mutant. Notably, upregulating *LOH2* expression was associated with the preponderance of ceramides containing C16 fatty acids and dihydroxy LCBs (the principal products of LOH2 ceramide synthase activity) in free ceramides and GlcCer, including nhGlcCer, which accumulated in *orm1*$^{\Delta met/\Delta met}$ *orm2*$^{-/-}$ seedlings but were detected at only low concentrations in the wild type and ORM1 and ORM2 single mutants. These findings are consistent with our previous report that LOH2 activity is upregulated in Arabidopsis ORM RNAi plants, presumably as a pathway for reducing cytotoxicity of free LCBs and ceramides (which are metabolized to GlcCer; Kimberlin et al., 2016). No changes were detected in LCB1 or ssSPTa transcript levels in the *orm1*$^{\Delta met/\Delta met}$ *orm2*$^{-/-}$ mutant, indicating that the transcriptional regulation of genes for SPT complex proteins is not a pathway for maintaining sphingolipid homeostasis in response to deregulated LCB biosynthesis. Instead, the expression of genes involved in the catabolism of LCBs increased approximately six- to sevenfold (*SPHK2* and *DPL1*) in this mutant, suggesting that an unknown mechanism is activated in response to increased ceramide and/or LCB levels.

AUTHOR CONTRIBUTIONS

A.G.S., G.H., T.M.D., and E.B.C. designed the study; A.G.S., G.H., Y.L. J.E.M. and R.E.C. performed the experiments and analyzed the data, along with G.H., T.M.D., and E.B.C.; and A.G.S., G.H., T.M.D., and E.B.C. wrote the article.

3.6 References

Breslow, D.K., Collins, S.R., Bodenmiller, B., Aebersold, R., Simons, K., Shevchenko, A., Ejsing, C.S., and Weissman, J.S. (2010). Orm family proteins mediate sphingolipid homeostasis. Nature 463: 1048–1053.

Bi, F.C., Liu, Z., Wu, J.X., Liang, H., Xi, X.L., Fang, C., Sun, T.J., Yin, J., Dai, G.Y., Rong, C., Greenberg, J.T., Su, W.W., Yao, N. (2014) Loss of ceramide kinase in Arabidopsis impairs defenses and promotes ceramide accumulation and mitochondrial H_2O_2 bursts. Plant Cell. (8):3449-67.

Coursol, S., Fan, L.M., Le Stunff, H., Spiegel, S., Gilroy, S., and Assmann, S.M. (2003). Sphingolipid signalling in Arabidopsis guard cells involves heterotrimeric G proteins. Nature 423: 651–654.

Gable, K, Gupta, SD, Han, G, Niranjanakumari, S, Harmon, JM, and Dunn, TM (2010). A disease-causing mutation in the active site of serine palmitoyltransferase causes catalytic promiscuity. J Biol Chem 285: 22846–22852.

Han, G., Gupta, S.D., Gable, K., Bacikova, D., Sengupta, N., Somashekarappa, N., Proia, R.L., Harmon, J.M., and Dunn, T.M. (2019). The ORMs interact with transmembrane domain 1 of Lcb1 and regulate serine palmitoyltransferase oligomerization, activity and localization. Biochim. Biophys. Acta Mol. Cell Biol. Lipids 1864: 245–259.

Han, S., Lone, M.A., Schneiter, R., and Chang, A. (2010). Orm1 and Orm2 are conserved endoplasmic reticulum membrane proteins regulating lipid homeostasis and protein quality control. Proc. Natl. Acad. Sci. USA 107: 5851–5856.

Kimberlin, A.N., Han, G., Luttgeharm, K.D., Chen, M., Cahoon, R.E., Stone, J.M., Markham, J.E., Dunn, T.M., and Cahoon, E.B. (2016). ORM expression alters sphingolipid homeostasis and differentially affects ceramide synthase activity. Plant Physiol. 172: 889–900.

Kimberlin, A.N., Majumder, S., Han, G., Chen, M., Cahoon, R.E., Stone, J.M., Dunn, T.M., and Cahoon, E.B. (2013). Arabidopsis 56- amino acid serine palmitoyltransferase-interacting proteins stimulate sphingolipid synthesis, are essential, and affect mycotoxin sensitivity. Plant Cell 25: 4627–4639.

Markham, J.E., and Jaworski, J.G. (2007). Rapid measurement of sphingolipids from Arabidopsis thaliana by reversed-phase highperformance liquid chromatography coupled to electrospray ionization tandem mass spectrometry. Rapid Commun. Mass Spectrom. 21: 1304–1314.

Markham, J.E., Molino, D., Gissot, L., Bellec, Y., Hématy, K., Marion, J., Belcram, K., Palauqui, J.C., Satiat-Jeunemaître, B., and Faure, J.D. (2011). Sphingolipids containing very-long-chain fatty acids define a secretory pathway for specific polar plasma membrane protein targeting in Arabidopsis. Plant Cell 23: 2362–2378.

Magnin-Robert M, Le Bourse D, Markham J, Dorey S, Clément C, Baillieul F, Dhondt-Cordelier S. (2015) Modifications of Sphingolipid Content Affect Tolerance to Hemibiotrophic and Necrotrophic Pathogens by Modulating Plant Defense Responses in Arabidopsis. Plant Physiol. 169:2255-74.

Li, J., Yin, J., Rong, C., Li, K.E., Wu, J.X., Huang, L.Q., Zeng, H.Y., Sahu, S.K., and Yao, N. (2016). Orosomucoid proteins interact with the small subunit of serine palmitoyltransferase and contribute to sphingolipid homeostasis and stress responses in Arabidopsis. Plant Cell 28: 3038–3051.

Liang, H., Yao, N., Song, J.T., Luo, S., Lu, H., and Greenberg, J.T. (2003). Ceramides modulate programmed cell death in plants. Genes Dev. 17: 2636–2641.

Luttgeharm, K.D., Chen, M., Mehra, A., Cahoon, R.E., Markham, J.E., and Cahoon, E.B. (2015a). Overexpression of Arabidopsis ceramide synthases differentially affects growth, sphingolipid metabolism, programmed cell death, and mycotoxin resistance. Plant Physiol. 169: 1108–1117.

Luttgeharm, K.D., Kimberlin, A.N., Cahoon, R.E., Cerny, R.L., Napier, J.A., Markham, J.E., and Cahoon, E.B. (2015b). Sphingolipid metabolism is strikingly different between pollen and leaf in Arabidopsis as revealed by compositional and gene expression profiling. Phytochemistry 115: 121–129.

Roelants, F.M., Breslow, D.K., Muir, A., Weissman, J.S., Thorner, J. (2011) Protein kinase Ypk1 phosphorylates regulatory proteins Orm1 and Orm2 to control sphingolipid homeostasis in *Saccharomyces cerevisiae*. Proc Natl Acad Sci USA 108:19222–7.

Ternes, P., Feussner, K., Werner, S., Lerche, J., Iven, T., Heilmann, I., Riezman, H., and Feussner, I. (2011). Disruption of the ceramide synthase LOH1 causes spontaneous cell death in *Arabidopsis thaliana*. New Phytol. 192: 841–854.

4 Chapter 4 Investigating the physiological effects of HSAN1-like mutations in Arabidopsis.

This chapter may be part of a publication in the future.

Authors: Ariadna Gonzalez Solis, Rebecca E. Cahoon, Gongshe Han, Teresa M. Dunn, Edgar B. Cahoon.

4.1 Abstract

The deoxysphingolipids are atypical sphingolipids that are generated when serine palmitoyltransferase (SPT) condenses palmitoyl-CoA with alanine or glycine instead of serine during the synthesis. The shift in substrate specificity is associated with variants of SPT subunits that have specific point mutations. Even though great progress has been made understanding the metabolism and effects of deoxysphingolipids in the context of the hereditary sensory autonomic neuropathy type 1 (HSAN1) in humans, these atypical sphingolipids remain largely unexplored in plants.

Here we provide insights into the physiological effects in Arabidopsis caused by the incorporation of the point mutations in SPT that are associated with the accumulation of deoxysphingolipids. Our research demonstrated that the changes in SPT resulted in early senescence and resistance to the cell death triggered by the mycotoxin Fumonisin B1.

4.2 Introduction

Serine palmitoyltransferase (SPT) catalyzes the first reaction of sphingolipid biosynthesis by condensing L-serine with palmitoyl-CoA to form sphingoid bases or long chain bases (LCBs), the characteristic backbone of all sphingolipids. The core SPT is a heterodimer formed by LCB1 and LCB2 subunits, additional regulatory proteins like ssSPT and ORM proteins interact with the core SPT and have an impact on its activity

(Tamura et al., 2001; Chen et al., 2006; Dietrich et al., 2008; Kimberlin et al., 2013; Kimberlin et al., 2016). Based on studies of *Saccharomyces cerevisiae* it is known that the active site of SPT is localized at the dimer interface, and LCB1 stabilizes the complex (Gable et al., 2002). Moreover, several studies in Arabidopsis have shown knock-out mutants for the *LCB2* (*LCB2a* and *LCB2b*) and *LCB1* genes are not viable, emphasizing the importance of sphingolipids as essential components of plant cells (Tamura et al., 2001; Chen et al., 2006; Dietrich et al., 2008).

In humans, eight missense mutations in SPTLC1 and four mutations in the SPTLC2 subunits (LCB1 and LCB2 ortologues, respectively), are associated with Hereditary Sensory and Autonomic Neuropathy 1 (HSAN1), a rare dominantly inherited degenerative disorder caused by the accumulation of unusual deoxysphingolipids (Penno et al., 2010). All the HSAN1 mutations characterized to date induce a shift in the substrate specificity of SPT from L-serine to L-alanine or glycine giving rise to 1-deoxyshinganine (1-deoxySA; m18:0) or 1-deoxymethylsphinganine (1-deoxymetylSA: m17:0). These atypical LCBs can get N-acylated by ceramide synthases to form ceramides; however, the lack of the hydroxyl group in C1 position precludes the formation of more complex glycosylated sphingolipids. The missing hydroxyl group also hampers the degradation of deoxyLCBs by the canonical pathway that requires phosphorylation at C1 to form the catabolic phosphorylated intermediates.

Interestingly, out of the context of HSAN1, 1-deoxysphingolipids were also detected in a mammalian cell line treated with the ceramide synthase inhibitor Fumonisin B1 (FB1) (Zitomer *et al.*, 2009). In this study the accumulation of canonical LCBs was

accompanied with 1-deoxySA suggesting that the wild-type SPT is also capable of using alanine and glycine as substrates.

The study of SPT regulation requires a robust, sensitive and reproducible method to measure its activity. In mammalian cells and yeast, SPT activity is usually measured by a radioactivity-based assay using ^{3}H or ^{14}C-serine as substrate that gets incorporated into 3-ketosphinganine (Williams et al., 1984). However, measuring the activity in plants is still problematic due to the low activity in *in vitro* assays. Evidence in yeast shows the non-degradable deoxySA could serve as a strategy to measure SPT activity as this LCB accumulates and is not degraded (Chapter 3) (Gable et al., 2010; Kimberlin et al., 2016).

For this study, we hypothesize that incorporating the HSAN1 mutations into Arabidopsis SPT would allow the production of deoxysphingolipids, which could be used as a readout for SPT activity. Moreover, the characterization of transgenic plants expressing mutations in LCB1 would allow us to examine the physiological effects of the unusual sphingolipids that until now have not been explored in plants.

Here we describe the incorporation of the mutated versions LCB1^{C144W} and LCB1$^{C144W\ V155D}$ into Arabidopsis resulting in early senescence hallmarks. We also determined that these plants are resistant to the mycotoxin FB1. Although we did not detect a significant accumulation of deoxyceramides in the transgenic plants compared to wild type, we observed that m18:0 and m18:1 were incorporated to ceramides containing C16 fatty acids. Future work will focus on the detection of potential degradation products of deoxysphingolipids and their subcellular localization.

4.3 Materials and Methods

4.3.1 Plant Materials and Growth Conditions

Arabidopsis (*Arabidopsis thaliana*) Columbia-0 (Col-0) was used as the wild-type reference in this study. Arabidopsis seedlings were grown on Murashige and Skoog (MS) medium supplemented with 1% (w/v) Sucrose and 0.8% (w/v) agar, pH 5.7, with 16-h-light (100 mmol/ m^{-2} s^{-1})/8-h-dark conditions at 22°C. The light source for growth chamber–grown seedlings was supplied by standard wide-spectrum fluorescent bulbs type F32/841/ ECO 32 W (maximum intensity, 480 to 570 nm). For Arabidopsis plants in soil, seeds were sown, and after 2 d of stratification at 4°C, plants were grown at 22°C with 16-h-light (100 mmol/ m^{-2} s^{-1})/8-h-dark conditions.

4.3.2 HSAN1 LCB1 Generation and Transformation

Two versions of the HSAN1 mutations were generated in *AtLCB1* using QuikChange Site-Directed Mutagenesis Kit (Stratagene), $LCB1^{C144W}$ an $LCB1^{C144W\ V155D}$. The mutated versions of LCB1 were then cloned into the vector pBinGlyRed3 under the native LCB1 promoter (~1kb). The Binary vectors were transformed into *Agrobacterium tuumefaciens* GV3101 by electroporation. Heterozygous LCB1 mutants (SALK_077745) were used to create transgenic plants by the floral dip method (Clough and Bent, 1998). Red seeds were screened using a green LED light and a red2 camara filter to identify transformed Arabidopsis seeds harboring the vector expressing DsRed.

4.3.3 Arabidopsis Mutant Genotyping

The T-DNA SALK_077745 insertion line was acquired from the Arabidopsis Biological Resource Center. Individual plants from a mixed population of seeds were screened by

PCR using the primers P1+P3. The wild-type allele was amplified using P2+P3; Supplemental Table 1 in Appendix B.

4.3.4 Sphingolipid Extraction and Analysis

Sphingolipids were extracted as described in Markham and Jaworski (2007). Briefly, 35-d-old Arabidopsis leaves were collected for biological replicates. The plant tissue was lyophilized, and 10 to 30 mg of tissue was homogenized and extracted with isopropanol:heptane:water (55:20:25, v/v/v). Internal standards for the different sphingolipid classes were added. The supernatants were dried and de-esterified with methylamine in ethanol:water (70:30, v/v). The lipid extract was re-suspended in tetrahydrofuran:methanol:water (5:2:5, v/v/v) containing 0.1% (v/v) formic acid. The sphingolipid species were analyzed using a Shimadzu Prominence ultra-performance liquid chromatography system and a 4000 QTRAP mass spectrometer (AB SCIEX). Data analysis and quantification were performed using the software Analyst 1.5 and MultiQuant 2.1 as described by Markham and Jaworski (2007) and Kimberlin et al. (2013).

4.3.5 Alanine and Fumonisin B1 Treatment

Selected red seeds were sown on MS medium supplemented with 5 mM Alanine (Acros Organics) or 0.4 μM Fumonisin B1 (Sigma).

4.3.6 RNA Isolation and Quantitative RT-PCR

RNA was extracted from 12- to 15-d-old Arabidopsis seedlings grown on solid MS medium. Each replicate corresponds to pooled seedlings from independent plates. RNA extraction was performed using an RNeasy Kit (Qiagen) according to the manufacturer's protocol. The isolated RNA (1mg) was treated with DNase I (Invitrogen). cDNA

conversion was performed with a RevertAid cDNA synthesis kit (Thermo Fisher Scientific). SYBR Green was used as the fluorophore in a qPCR supermix (Qiagen). PP2AA3 was used as internal reference genes. qPCR was performed using a Bio-Rad MyiQ iCycler qPCR instrument. The thermal cycling conditions were an initial step of 95°C for 10 min followed by 45 cycles at 95°C for 15 s, 60°C for 30 s, and 72°C for 30 s. Primers used in this study are listed in Supplemental Table 1, Appendix B.

4.4 Results

4.4.1 SPT Amino Acids Associated with HSAN1 are Conserved in Arabidopsis

Two frequent mutations that cause HSAN1 in humans are C133W and V144D. The human SPTLC1 and Arabidopsis LCB1 share 44 % identity with each other. Based on the sequence alignment Cysteine 144 in Arabidopsis corresponds to C133 in human SPTLC1 and it is located in a conserved region (Figure 4.1). Similarly, the Valine residue in position 155 that corresponds to V144 in human. Mutating the Cysteine to Tryptophan and Valine to Aspartic acid, should confer the structural shift to allow the use of alanine and glycine to generate deoxysphingolipids.

Figure 4.1 Partial alignment of *Arabidopsis thaliana* AtLCB1 and *Homo sapiens* HsSPTLC1 protein sequences.

The arrows indicate two residues associated with HSAN1 phenotype, C133 and V144 in human and the corresponding C144 and V155 in Arabidopsis.

Given that the complete knockout of LCB1 is lethal (Chen et al., 2006), for this study we sought to complement the LCB1 heterozygous mutants with a construct expressing $LCB1^{C144W}$ or $LCB1^{C144W/V155D}$ under the native LCB1 promoter. In a previous work it was showed that a construct containing the wild-type AtLCB1 under the control of the upstream native promoter was sufficient to complement the SALK_077745 T-DNA mutant (Chen et al., 2006). With a successful complementation we would expect the levels of deoxysphingolipids to accumulate and this could be used as strategy to measure SPT activity. However, after three and four generations complementation was not achieved (Tables 1 and 2; Supplemental Figure 1 in Appendix B). Therefore, the rest of the experiments in this study were performed using transgenic lines expressing the mutated LCB1 versions in a wild-type or a heterozygous background. Considering that these mutations are dominant in the context of HSAN1 (Dawkins et al., 2001), we expect that even with a copy of the wild-type LCB1 the mutated version will still promote the generation of deoxysphingolipids.

Table 1 Segregation analysis of progeny from $LCB1^{C144W}$ transgenic lines

	Progeny Genotype (Observed/Total)		
Parent genotype	*AA*	*Aa*	*aa*
T2 *Aa*	19/33 57.6%	14/33 42.4%	0/33 0%
T3 *Aa*	56/58 96.6%	2/58 3.4%	0/58 0%

Table 2 Segregation analysis of progeny from $LCB1^{C144W\ V155D}$ transgenic lines

	Progeny Genotype (Observed/Total)		
Parent genotype	*AA*	*Aa*	*aa*
T2 *Aa*	3/21 14.3%	18/21 85.7%	0/21 0%
T3 *Aa*	33/52 63.5%	19/52 36.5%	0/52 0%
T4 *Aa*	11/25 44%	14/25 56%	0/25 0%

4.4.2 Arabidopsis HSAN1 Mutants Showed Early Senescence, Delayed Flowering and Resistance to FB1.

To examine the phenotype of the transgenic lines, seeds were grown in solid MS medium. Both lines tested showed low germination rates ~26 % when expressing LCB1^{C144W} and ~ 54 % for LCB1$^{C144W/V155D}$. Moreover, the transgenic seedlings developed pale/yellow leaves compared to the wild type (Figure 4.2A). We also observed pale wild-type seedlings growing on medium supplemented with alanine and a stronger effect on the transgenic plants (Figure 4.2B).

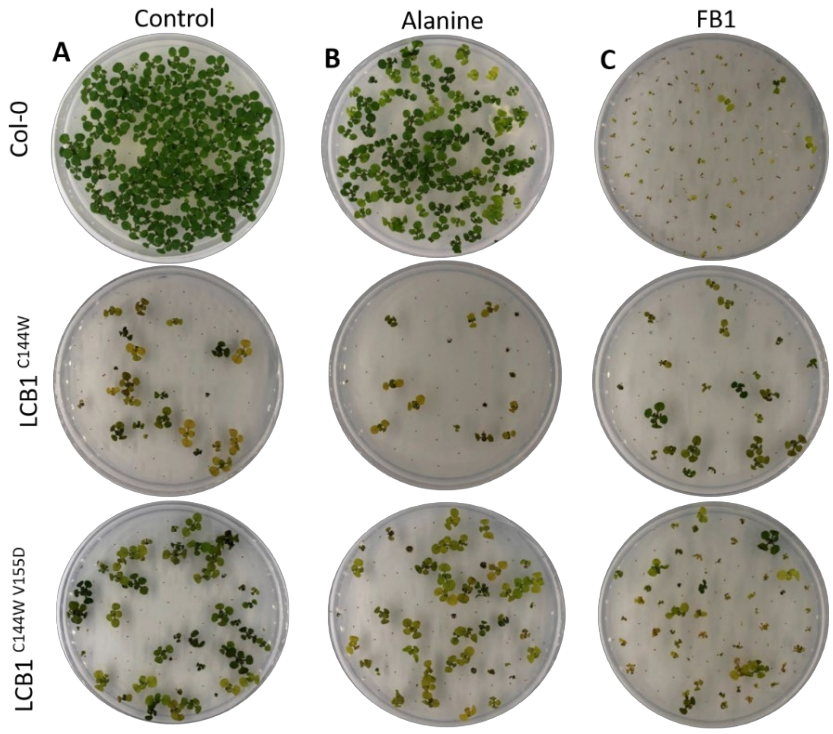

Figure 4.2 Representative images of 15-day-old wild-type, LCB1^{C144W} and LCB1$^{C144W/V155D}$ seedlings.

(**A**) MS medium, (**B**) MS medium supplemented with 5 mM Alanine, and (**C**) MS medium supplemented with 0.4 μM FB1.

Interestingly, even though wild-type plants were sensitive to FB1, the seedlings expressing LCB1 with mutations showed resistance to the toxin but still showed pale-

yellow leaves (Figure 4.2C). When transferred to soil the transgenic plants recovered the green appearance but showed delayed flowering and early senescence features (Figure 4.3 A and Supplemental Figure 1 in Appendix B).

Chlorotic and green leaves were used for sphingolipid extractions to measure the canonical species and deoxyceramides. Sphingolipid profiling revealed that, even though there was not a significant change in the levels of m18:0 and m18:1-containing ceramides compared to wild type these deoxyLCBs were preferentially coupled with C16 fatty acids (Figure 4.3B). In addition, the chlorotic leaves accumulated C16 fatty acid containing-ceramides compared to the normal green leaves (Figure 4.3C).

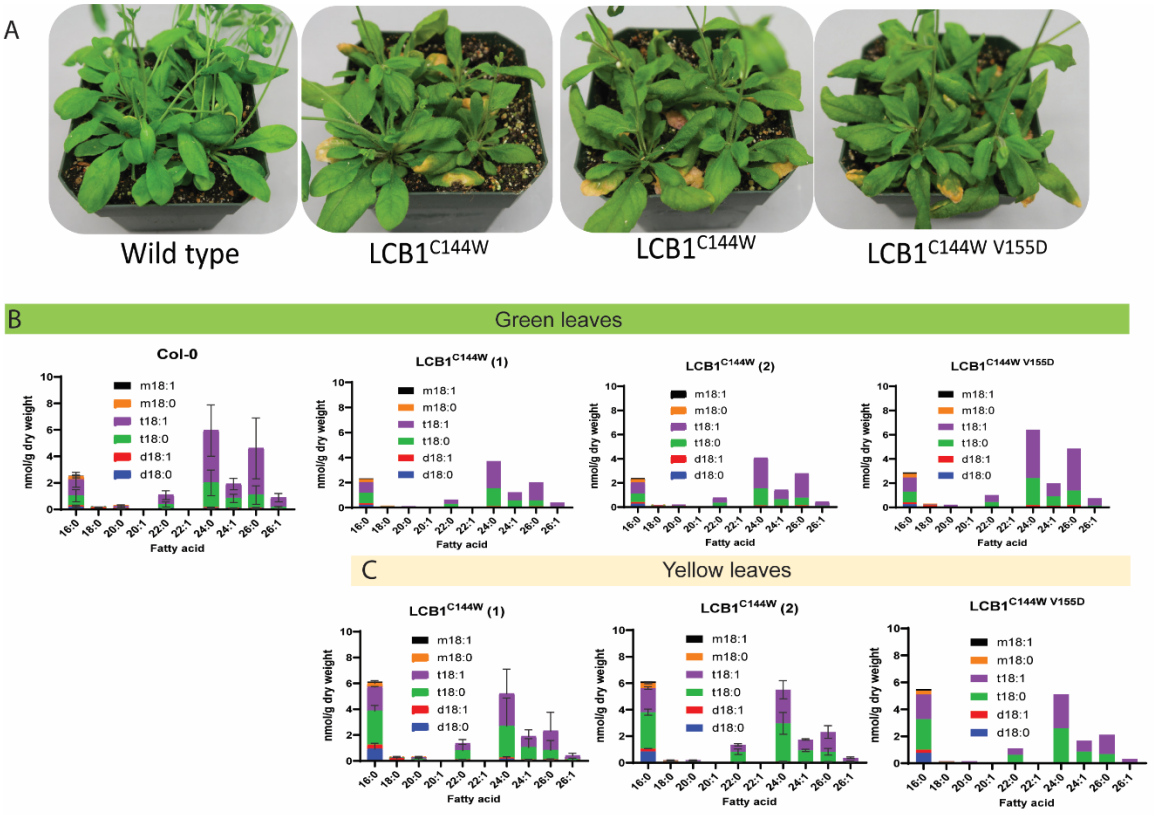

Figure 4.3 Ceramides and Deoxyceramides Profiles.

(**A**) Forty-day old wild-type plants and transgenic lines expressing LCB1^{C144W} and LCB1$^{C144W/V155D}$. Ceramide molecular species compositions representing the exact pairings of LCB and fatty acid for the wild-type and the indicated transgenic lines in (**B**) green leaves and in (**C**) yellow/pale leaves. Shown are representative values of one plant or the mean ± SD n=3.

4.4.3 Expression of Genes Associated with Senescence and Sphingolipid Biosynthesis and Homeostasis

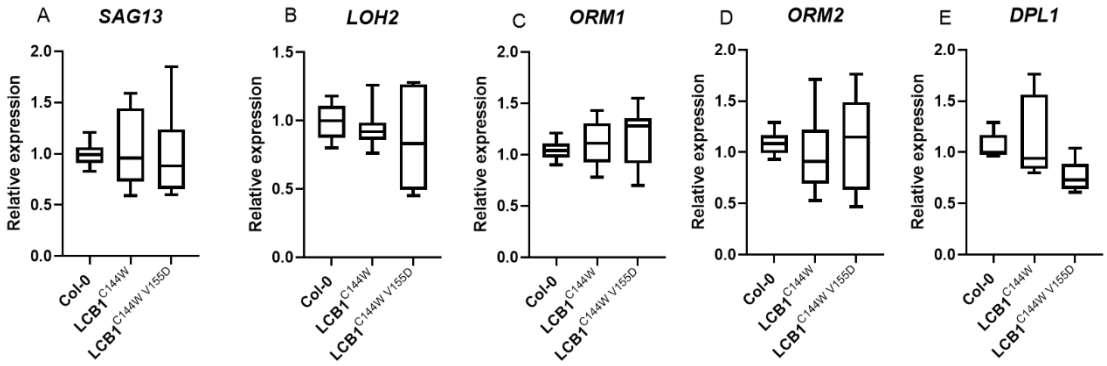

Figure 4.4 Expression of Genes Associated with Senescence and Sphingolipid Biosynthesis, Catabolism, and Homeostasis.

15 day-old wild-type plants and transgenic lines expressing LCB1^{C144W} and LCB1$^{C144W/V155D}$, were used to examine gene expression by q-PCR to monitor the expression of **(A)** senescence-related 13 *SAG13,* **(B)** ceramide synthase *LOH2* **(C)** *ORM1* **(D)** *ORM2* and (**E**) *DPL1*. *PP2AA3* transcript levels were used as a control. Specific primers used for this analysis are shown in Supplemental Table 1 in Appendix B. Gene expression levels are normalized to those in wild-type seedlings. Values are the mean ± SD (n=9). There are no significant differences based on one-way ANOVA followed by Tukey´s multiple comparisons test.

Given that the plants expressing HSAN1-like mutations showed early senescence and accumulation of C16 ceramides we then examined the expression *SAG13*, a senescence-related gene, and *LOH2*, the gene encoding the ceramide synthase that preferentially N-acylates C16 fatty acids with LCBs to form ceramides. Our results revealed no significant changes in the expression of these genes among the wild-type and transgenic lines evaluated (Figures 4.4A and 4.4B). Similarly, the expression of *ORM* genes, regulators of SPT activity; and *DPL1*, encoding the lyase that catabolizes LBCs, did not change in the transgenic plants compared to wild-type (Figures 4.4C- 4.4E).

4.5 Discussion

For this work, we hypothesized that the incorporation of the HSAN1 mutations into the Arabidopsis LCB1 SPT subunit would enhance the production of deoxysphingolipids in the plants. DeoxySA (m18:0) is normally present at very low concentrations in the wild-type and can be increased 60-fold in the *orm1*$^{\Delta met/\Delta met}$ *orm2*$^{-/-}$ mutant where SPT activity is deregulated (Chapter 3). We picked C144W and V155D because they are among the most frequent mutations in the context of HSAN1 and these residues are in a highly conserved region of LCB1 that is predicted to be a catalytic domain (Bode et al., 2016). Failure to complement the *Atlcb1*$^{+/-}$ mutant with LCB1^{C144W} or LCB1 $^{C144W/V155D}$ suggests the detrimental effects of these point mutations. Additional confirmation was provided by the low germination rate of the progeny of heterozygous plants expressing the mutations in LCB1. Notably, the germinated seeds gave rise to plants with an early senescence phenotype, which was also observed in wild-type seedlings growing with alanine supplementation. It has been shown that the formation of deoxysphingolipids is modulated by the availability of alanine and serine. Increased alanine concentration enhances the production of deoxysphingolipids in a HSAN1 mouse model and in mutant-expressing HEK293 cells (Garofalo et al., 2011; Bode et al., 2016). Therefore, one possible explanation is that wild-type SPT can use alanine as substrate for the production of deoxysohingolipids when this amino acid is in excess. In this context it will be important to perform sphingolipid measurements for the detection of the free deoxyLCBs (m18:0, m18:1) and their incorporation into ceramides in seedling grown with excess alanine and serine. In this case, we would expect serine enrichment to alleviate the senescence phenotype in the transgenic plants.

Our findings showed that the senescence phenotype persisted in adult transgenic plants and it was also associated with delayed flowering. Despite the observed phenotypes, the adult transgenic plants did not accumulate deoxyceramides compared to wild type. Yet, the detected deoxyLCBs were preferentially coupled with C16 fatty acids to form deoxyceramides. This suggests channeling through the LOH2 ceramide synthase which has substrate specificity for the more common dihydroxy LCBs. In contrast, mouse fibroblasts incorporated supplemental m18:0 to a variety of acyl-CoAs from C16 to C24:1; while m18:1 was preferentially acylated to VLCFA (Alecu *et al.*, 2017). Examination of gene expression showed no changes in *LOH2* transcript levels in the transgenic plants compared to wild type; perhaps other regulatory mechanisms at the protein level could take place to favor the increase of C16 ceramides in chlorotic leaves. Moreover, it will be interesting to determine if C16 ceramide accumulation also occurs during senescence in wild-type plants.

Consistent with our findings, in mammalian cells the HSAN1-like mutations have been linked to the aging process and induced expression of senescence markers (Lone et al., 2019). Even though, gene expression analyses showed no differences in the transcript levels of the senescence-related gene *SAG13,* it is necessary to complement the analysis with other markers.

Until recently, deoxysphingolipids have been considered dead-end metabolites due to the lack of the hydroxyl group at C1 position for canonical degradation. However, a recent report described multiple polyunsaturated and polyhydroxylated forms of deoxySA as catabolic downstream products (Alecu et al., 2017). It is possible that in plants deoxysphingolipids are also degraded to other hydroxylated structures as a cellular

detoxification process that requires further investigation. Another important aspect related to the cellular effects of deoxysphingolipids is their subcellular localization. A study revealed that an alkyne-click labelled deoxySA initially localizes to mitochondria and it is later detected in Golgi and ER (Alecu et al., 2017). The localization of these lipids to mitochondria induces changes in morphology and reduced ATP generation (Alecu et al., 2017). Future work will focus on determining possible downstream products of deoxysphingolipids in plants and their potential roles related to mitochondrial dysfunction and senescence.

It is important to note that the effect of two HSAN1-related mutations, like in LCB1 $^{C144W/V155D}$, has not been investigated before; however, our current findings suggest there is no synergistic effect when compared to the single mutation LCB1 ^{C144W}.

Out of the context of HSAN1, mammalian cells treated with FB1, a ceramide synthase inhibitor, accumulated deoxySA showing that wild-type SPT was able to synthesize this unusual structures (Zitomer et al., 2011). Moreover, FB1 treatment caused an increase in deoxySA in HEK293 cells expressing SPTLC1^{C133W} and this was accompanied with a reduced SPT activity (Bode et al., 2016). Consistent with this, our results showed transgenic seedlings expressing LCB1^{C144W} and LCB1 $^{C144W/V155D}$ were resistant to the cell death induced by FB1, possibly due to a decrease in SPT activity and reduced levels of canonical cytotoxic LCBs. In order to elucidate if ORM proteins could be associated with SPT regulation under FB1 treatment, we performed gene expression analyses. Our results rule out the possibility of transcriptional regulation of ORM, but leave open other options like specific ceramide species interacting with ORMs to exert the regulation of SPT activity.

One of the objectives of the present study was to introduce the HSAN1 mutations in the Arabidopsis LCB1 to examine the feasibility of using deoxySA levels as a readout for SPT activity. In yeast, this strategy has been successful and the concentration of this atypical LCB has been used as an indirect measurement of activity (Gable et al., 2010). In the case of Arabidopsis, more work is needed to determine if the free deoxyLCBs (m18:0, m18:1) can be used for this purpose. Especially, it will be important to determine the dynamics of the catabolic pathways. In addition, it will be interesting to explore if the ORM proteins are involved in the regulation of SPT activity in response to the production of deoxysphingolipids.

AUTHOR CONTRIBUTIONS

A.G.S., G.H., T.M.D., and E.B.C. designed the study; A.G.S. and R.E.C. performed the experiments and analyzed the data.

4.6 References

Alecu, I., Othman, A., Penno, A., Saied, E.M., Arenz C., von Eckardstein, A., Hornemann, T. (2017) Cytotoxic 1-deoxysphingolipids are metabolized by a cytochrome P450-dependent pathway, J. Lipid Res. 58:60–71.

Alecu, I., Tedeschi, A., Behler, N., Wunderling, K., Lamberz, C., Lauterbach, M.A., Gaebler, A., Ernst, D., Van Veldhoven, P.P., Al-Amoudi, A., Latz, E., Othman, A., Kuerschner, L., Hornemann, T., Bradke, F., Thiele, C., Penno, A. (2017) Localization of 1-deoxysphingolipids to mitochondria induces mitochondrial dysfunction, J. Lipid Res. 58:42–59.

Bode, H., Bourquin, F., Suriyanarayanan, S., Wei, Y., Alecu, I., Othman, A., Von Eckardstein, A., Hornemann, T. (2016) HSAN1 mutations in serine palmitoyltransferase reveal a close structure-function-phenotype relationship, Hum. Mol. Genet. 25:853–865.

Chen, M., Han, G., Dietrich, C.R., Dunn, T.M., and Cahoon, E.B. (2006). The essential nature of sphingolipids in plants as revealed by the functional identification and characterization of the Arabidopsis LCB1 subunit of serine palmitoyltransferase. Plant Cell 18: 3576–3593.

Clough, S.J., and Bent, A.F. (1998). Floral dip: A simplified method for Agrobacterium-mediated transformation of *Arabidopsis thaliana*. Plant J. 16: 735–743.

Dawkins JL, Hulme DJ, Brahmbhatt SB, Auer-Grumbach M, Nicholson GA. (2001) Mutations in SPTLC1, encoding serine palmitoyltransferase, long chain base subunit-1, cause hereditary sensory neuropathy type I. Nat Genet. 27:309-12.

Duan, J., & Merrill, A. H., Jr (2015). 1-Deoxysphingolipids Encountered Exogenously and Made de Novo: Dangerous Mysteries inside an Enigma. J Biol Chem, 290:15380–15389.

Dietrich, C.R., Han, G., Chen, M., Berg, R.H., Dunn, T.M., and Cahoon, E.B. (2008). Loss-of-function mutations and inducible RNAi suppression of Arabidopsis LCB2 genes reveal the critical role of sphingolipids in gametophytic and sporophytic cell viability. Plant J. 54: 284–298.

Gable, K., Slife, H., Bacikova, D., Monaghan, E., and Dunn, T.M. (2000). Tsc3p is an 80-amino acid protein associated with serine palmitoyltransferase and required for optimal enzyme activity. J. Biol. Chem. 275: 7597–7603.

Gable, K., Han, G., Monaghan, E., Bacikova, D., Natarajan, M., Williams, R., Dunn, T. M. (2002) Mutations in the yeast LCB1 and LCB2 genes, including those corresponding to the Hereditary Sensory Neuropathy type I mutations, dominantly inactivate serine palmitoyltransferase J. Biol. Chem. 277:10194–10200.

Gable, K., Gupta, S.D., Han, G., Niranjanakumari, S., Harmon, J. M., Dunn, T.M. (2010) A Disease-causing Mutation in the Active Site of Serine Palmitoyltransferase Causes Catalytic Promiscuity J. Biol. Chem., 285:22846–22852.

Garofalo, K., Penno, A. and Schmidt, B.P. (2011) Oral L-serine supplementation reduces production of neurotoxic deoxysphingolipids in mice and humans with hereditary sensory autonomic neuropathy type 1. J. Clin. Invest. 14–16.

Hanada, K. (2003) Serine palmitoyltransferase, a key enzyme of sphingolipid metabolism. Biochim. Biophys. Acta 1632:16−30

Kimberlin, A.N., Han, G., Luttgeharm, K.D., Chen, M., Cahoon, R.E., Stone, J.M., Markham, J.E., Dunn, T.M., and Cahoon, E.B. (2016). ORM expression alters sphingolipid homeostasis and differentially affects ceramide synthase activity. Plant Physiol. 172: 889–900

Kimberlin, A.N., Majumder, S., Han, G., Chen, M., Cahoon, R.E., Stone, J.M., Dunn, T.M., and Cahoon, E.B. (2013). Arabidopsis 56- amino acid serine palmitoyltransferase-interacting proteins stimulate sphingolipid synthesis, are essential, and affect mycotoxin sensitivity. Plant Cell 25: 4627–4639.

Lone, M.A., Santos, T., Alecu, I., Silva, L.C., Hornemann, T. (2019) 1-Deoxysphingolipids. Biochim Biophys Acta Mol Cell Biol Lipids.1864:512-521

Markham, J.E., and Jaworski, J.G. (2007). Rapid measurement of sphingolipids from *Arabidopsis thaliana* by reversed-phase highperformance liquid chromatography coupled to electrospray ionization tandem mass spectrometry. Rapid Commun. Mass Spectrom. 21: 1304–1314.

Penno, A., Reilly, M.M., Houlden, H., Laura, M., Rentsch, K., Niederkofler, V., Stoeckli, E.T., Nicholson, G., Eichler, F., Brown, R.H. Jr., von Eckardstein A., Hornemann T. (2010) Hereditary sensory neuropathy type 1 is caused by the accumulation of two neurotoxic sphingolipids, J. Biol. Chem. 285:11178−11187.

Rotthier, A., Penno, A., Rautenstrauss, B., Auer-Grumbach, M., Stettner, G.M., Asselbergh, B., Van Hoof K., Sticht, H., Levy, N., Timmerman, V., Hornemann, T., Janssens K. (2011) Characterization of two mutations in the SPTLC1 subunit of serine palmitoyltransferase associated with hereditary sensory and autonomic neuropathy type I, Hum. Mutat. 32:E2211−E2225.

Tamura, K., Musuhashi, M., Hara-Nishimura, I., and Imai, H. (2001). Characterization of an Arabidopsis cDNA encoding a subunit of serine palmitoyltransferase, the initial enzyme in sphingolipid biosynthesis. Plant Cell Physiol. 42:1271–1281.

Williams, R. D., E. Wang, and A. H. Merrill, Jr. (1984) Enzymology of long-chain base synthesis by liver: characterization of serine palmitoyltransferase in rat liver microsomes. Arch. Biochem. Biophys. 228:282–291.

Zitomer, N.C., Mitchell, T., Voss, K.A, Bondy, G.S., Pruett, S.T., Garnier-Amblard, E.C., Liebeskind, L.S., Park, H., Wang, E., Sullards, M.C., Merrill Jr A.H., Riley R.T. (2009) Ceramide synthase inhibition by fumonisin B1 causes accumulation of 1-deoxysphinganine: a novel category of bioactive 1-deoxysphingoid bases and 1-deoxydihydroceramides biosynthesized by mammalian cell lines and animals, J. Biol. Chem. 284:4786–4795.

5 Chapter 5 Towards Building a Kinetic Model of Sphingolipid Biosynthesis under FB1 Treatment and Pathogen Infection.

This chapter may be part of a publication in the future.

Authors: Ariadna Gonzalez Solis, Adil Alsiyabi, Jennifer E. Markham, Edgar B. Cahoon, Rajib Saha.

5.1 Abstract

The fungal mycotoxin FB1 and the avirulent pathogen *Pseudomonas syringae* pv. tomato *avrRpm1* elicit a rapid increase in LCBs and their phosphorylated forms in Arabidopsis. In the case of FB1 treatment, this buildup of LCBs is the consequence of the inhibition of ceramide synthases that condense LCBs and fatty acids for the formation of ceramides. In contrast, the main mechanisms of the accumulation of LCBs are not known during pathogen infection. Here we characterize the Arabidopsis cell suspension culture as a system for the generation of a metabolic model that will allow a better understanding of the changes in sphingolipid network in the context of FB1 treatment and pathogen infection.

5.2 Introduction

In addition to the structural roles of glycosphingolipids (GlcCer and GIPCs) in membrane formation and function; sphingolipid biosynthetic intermediates (LCBs and ceramides) have been recognized as important mediators of physiological processes in plants. Phosphorylated long chain bases (LCBs-P) participate in the ABA-mediated signaling pathway that regulate stomatal closure (Ng et al., 2001; Coursol et al., 2003, 2005; Townley et al., 2005). Whereas several studies revealed LCBs and ceramides as inducers of programmed cell death (PCD). This association has been shown in Arabidopsis

mutants that accumulate ceramides (Liang et al., 2003; Bi et al., 2014); with exogenously applied LCBs and ceramides (Lachaud et al., 2010, Alden et al., 2011) or with Fumonisin B1 (FB1) treatment (Stone et a., 2000; Shi et al., 2007; Saucedo-García et al., 2011). FB1 is a sphingosine-analogue mycotoxin produced by Fusarium species. It is widely known as a potent inhibitor of ceramide synthases that triggers the accumulation of LCBs (Abbas et al., 1994). Recent evidence suggests this mycotoxin exerts a more effective inhibition on Class II ceramide synthases (LOH1 and LOH3) that generate ceramides with VLCFA, than Class I (LOH2) which preferentially produces C16-containing ceramides (Markham et al., 2011; Ternes et al., 2011; Luttgeharm et al., 2016). Therefore, the PCD induced by FB1 is presumably due to the accumulation of LCBs and C16 ceramides.

A successful immune response in plants often includes the hypersensitive response (HR), a form of rapid programmed cell death (PCD) occurring in a limited area at the site of infection (Balint-Kurti, 2019). This suicide of infected cells is thought to limit the spread of biotrophic pathogens that rely on the plant cell machinery for proliferation (Mur et al., 2010). Given the similarities of FB1- and pathogen- induced PCD it is believed that LCBs and ceramides are part of the large array of signaling networks involved in plant resistance (Berkey, 2012). Notably, infection of Arabidopsis with the avirulent pathogen *Pseudomonas syringae* pv. tomato *avrRpm1* triggers the accumulation of LCB phytosphingosine (t18:0) (Peer at al., 2010). Furthermore, the ceramide accumulation in *acd5* and *acd11* mutants is associated with salicylic acid- dependent upregulation of defense-related genes (Brodersen et al., 2002). However, the mechanisms for the induction of LCB and ceramides during pathogen attack are not known. It is possible that

the immune response mechanisms are linked to an altered regulation of SPT to induce *de novo* synthesis of sphingolipids (Takahashi et al., 2009). Alternatively, catabolic reactions including the degradation of more complex sphingolipids like GIPCs and GlcCer could give rise to enhanced levels of free LCBs and ceramides.

In this work, we characterized the Arabidopsis T87 cell line as a system to perform metabolic labeling to determine the changes in sphingolipid levels in response to FB1 and pathogen infection. This system will be used to generate data to create a kinetic model that will allow a better understanding of the changes in the metabolic network. The combination of experimental testing and *in silico* analysis will allow refinement of the model to make predictions of cell responses under different perturbations.

5.3 Materials and Methods

5.3.1 Plant Material and Growth Conditions.

An undifferentiated and photoautotrophic *Arabidopsis thaliana* T87 cell suspension culture, established from the ecotype Columbia (Axelos et al., 1992), was used in this study. Cells were cultured in NT-1 liquid medium (Murashige and Skoog medium with vitamins, 30 g/l sucrose, 1 mM KH_2PO_4, 1mg/l thiamine, 100mg/l myo-inosytol and 2 µM 2,4-dichlorophenoxyacetic, pH 5.8 adjusted with KOH) at 22 °C and 120 rpm on a shaking platform under continuous light conditions (100µmol/ m^{-2} s^{-1}). Every 7 days 1 ml of mother cell suspension was transferred into 50 ml of fresh medium.

5.3.2 Stable Isotope Labeling

T87 Arabidopsis cells were cultured in NT-1 liquid medium containing $K^{15}NO_3$ and $^{15}NH_4{}^{15}NO_3$ (Cambridge Isotope Labs) under the same conditions described above.

5.3.3 Fumonisin B1 Treatment

The cells were grown for 2 d first in NT-1 medium and then FB1 (Sigma-Aldrich) was added for a final concentration of 1μM. The cells were sampled for analysis after 1, 2, 4, 6, 12, 24, 48 and 72 h. Control cells were also sampled at the same point of time. Cells were harvested by centrifugation at 400g for 5 min and lyophilized prior to sphingolipid analysis.

5.3.4 Sphingolipid Extraction and Analysis.

Sphingolipids were extracted as described in Markham and Jaworski (2007). Briefly, 10 to 30 mg of lyophilized cells were homogenized and extracted with isopropanol:heptane:water (55:20:25, v/v/v). Internal standards for the different sphingolipid classes were added. The supernatants were dried and deesterified with methylamine in ethanol:water (70:30, v/v). The lipid extract was re-suspended in tetrahydrofuran:methanol:water (5:2:5, v/v/v) containing 0.1% (v/v) formic acid. The sphingolipid species were analyzed using a Shimadzu Prominence ultra-performance liquid chromatography system and a 4000 QTRAP mass spectrometer (AB SCIEX). The incorporation of the ^{15}N into sphingolipid was detected with a +1 m/z shift in the mass of both the precursor and the product ion in sphingolipid MRMs. Data analysis and quantification were performed using the software Analyst 1.5 and MultiQuant 2.1 as described by Markham and Jaworski (2007), Kimberlin et al. (2013).

5.4 Results

A time-course sphingolipid profiling was conducted to characterize the response of the Arabidopsis cells to FB1. The accumulation of free LCBs was observed from two hours of treatment with the mycotoxin and was sustained over all the time points analyzed

(Figures 5.1A-C and 2A-H). Free LCBs, mainly d18:0 and t18:0, accumulated 17-fold during the first six hours of treatment compared to the control (Figure 5.1A-C and 5.2A-D). While after 24, 48 and 72 hours, the phosphorylated forms (LCB-P), d18:0-P and t18:0-P, reached levels of 36- 203- and 280-fold, respectively, compared to the control (Figures 5.1B-C and 5.2A-H). In addition, treatment with FB1 resulted in a reduction of ~half the amount of the original level of ceramides at two hours and was maintained until six hours post treatment. We observed an increase in C16 ceramides at 24 hours after exposure to FB1.

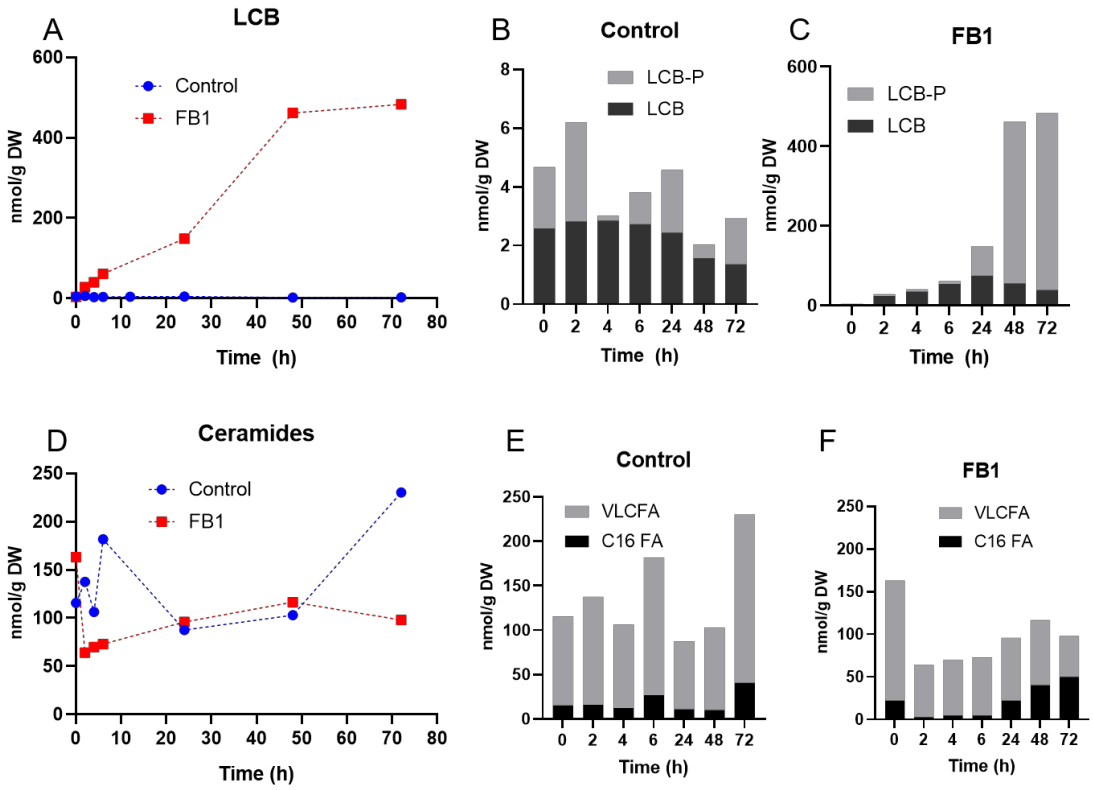

Figure 5.1 Time course sphingolipid profiling of Arabidopsis T87 cells after treatment with 1µM FB1.

(A) Total levels of free LCBs and the phosphorylated forms (LCB-P). Distribution of free or phosphorylated LCBs at the different time points analyzed for **(B)** control and **(C)** 1µM FB1. **(D)** Total levels of ceramides. Distribution of ceramides containing **(E)** very long chain fatty acids (VLCFA) or **(F)** C16 fatty acids. Time 0 h corresponds to the basal levels before FB1 addition.

To establish if the stable isotope labeling with ^{15}N is a suitable method to detect changes in fluxes of sphingolipids, we first determined the growth rate of the Arabidopsis cells in medium where the nitrogen sources have been replaced with ^{15}N. According to the results the ^{15}N medium did not affect the growth of the cells (Figure 5.3A). Next, to determine if we can detect the label going to sphingolipids we measured labeled LCBs and ceramides after 18 hours of growing in ^{15}N medium. We observed an incorporation of the isotope into LCBs and ceramides in cells and this incorporation was blocked with the SPT inhibitor, myriocin.

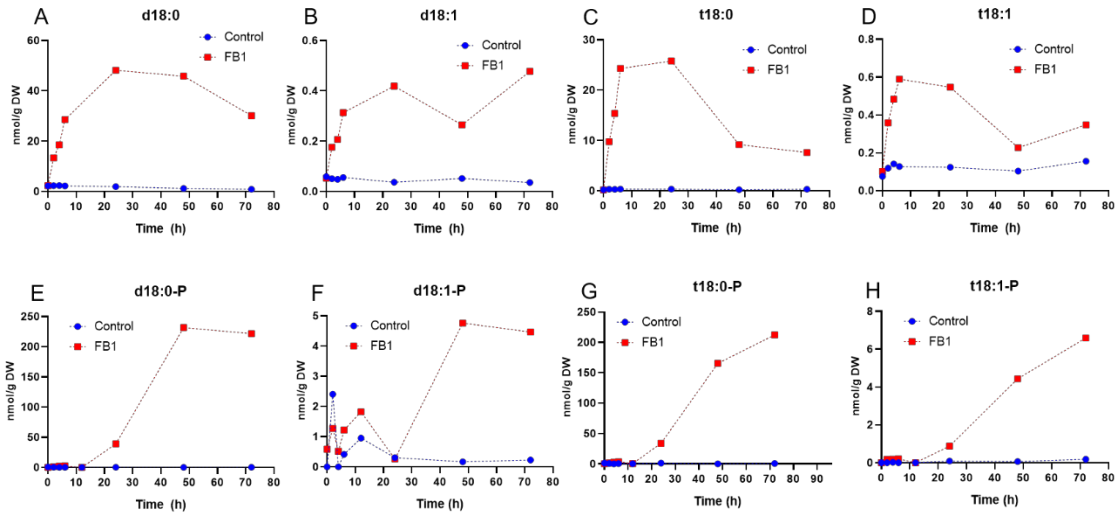

Figure 5.2 Time course profiling of LCBs and LCB-P.

Time course analysis of the indicated (**A-D**) free LCBs and (**E-H**) phosphorylated LCBs (LCB-P) levels in Arabidopsis T87 cells after treated with 1μM FB1.

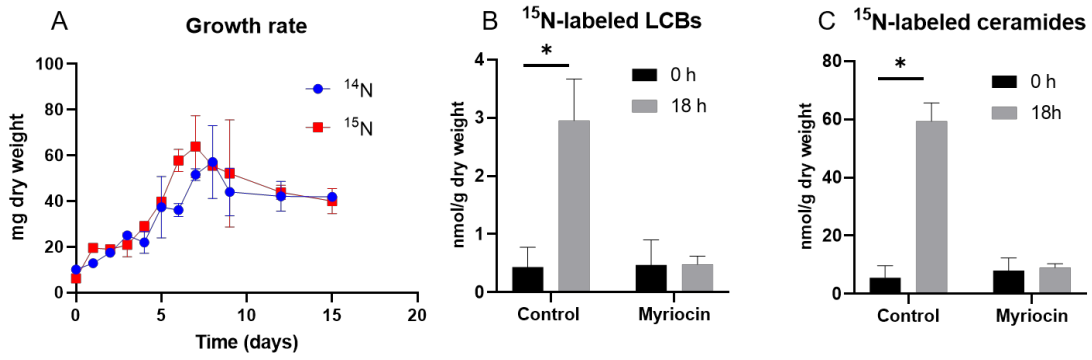

Figure 5.3 Labeling of Sphingolipids with the Stable Isotope Nitrogen 15.

(A) Growth curve of T-87 cells cultured with nitrogen 14 (^{14}N) or the stable isotope nitrogen 15 (^{15}N). Values are the mean ±SD (n=3). **(B)** Incorporation of ^{15}N into ceramides and LCBs of wild type cultured cells treated with DMSO as control and 1 nM myriocin for 18 hours. Values are the mean ±SD (n=3). Asterisks denote statistical significance when $P < 0.01$ in Students' T Test.

5.5 Discussion

For our studies, we chose the photoautotrophic Arabidopsis T87 cell culture because it has a short doubling time (2.7 days), produces large amount of tissue and it is a good system to perform *in vivo* labeling with reduced biological variation.

Consistent with previous studies performed in plants (Saucedo-Garcia et al., 2011; Peer et al., 2010), treatment of the Arabidopsis cell suspension with FB1 elicited a rapid accumulation of free LCBs and the phosphorylated forms. Moreover, as expected, we observed a reduction in ceramide levels following FB1 exposure and a subsequent accumulation of C16 ceramides at longer times (>24 h). These results confirm the early response of the cells to FB1 and validate it as a good system for the labeling studies.

We could also detect the incorporation of the nitrogen 15 isotope into LCBs and ceramides via flux through SPT in short-term experiments, thus this is a cost effective and accurate procedure that can be used in quantitative profiling to apply to a kinetic model. The rate at which ^{15}N appears in sphingolipids will be used to calculate the fluxes

trough each step of the pathway using a reaction network that comprises all the metabolic transformations involved in sphingolipid biosynthesis in Arabidopsis (Alsiyabi et al., 2010 under revision). Especially, this labeling approach will be very informative to estimate sphingolipid turnover rates. The kinetic model will allow us to make predictions of how the flux of sphingolipid metabolites is regulated in response environmental responses.

AUTHOR CONTRIBUTIONS

A.G.S., J.E.M, R.S., and E.B.C. designed the study; A.G.S. and J.E.M. performed the experiments and analyzed the data.

5.6 References

Abbas, H.K., Tanaka, T., Duke, S.O., Porter, J.K., Wray, E.M., Hodges, L., Sessions, A.E., Wang, E., Merrill, A.H. Jr, Riley, R.T. (1994) Fumonisin- and AAL-toxin-induced disruption of sphingolipid metabolism with accumulation of free sphingoid bases. Plant Physiol 106(3):1085–1093.

Alden, K.P., Dhondt-Cordelier, S., McDonald, K.L., Reape, T.J., Ng, C.K., McCabe, P.F., and Leaver, C.J. (2011). Sphingolipid long chain base phosphates can regulate apoptotic-like programmed cell death in plants. Biochem. Biophys. Res. Commun. 410: 574–580.

Axelos, M., Curie, C., Mazzolini, L., Bardet, C., and Lescure, B. (1992) A protocol for transient gene expression in *Arabidopsis thaliana* protoplasts isolated from cell suspension cultures. Plant Physiol. Biochem. 30:123– 128.

Balint-Kurti P. (2019) The plant hypersensitive response: concepts, control and consequences. Mol Plant Pathol. 20:1163-1178.

Berkey, R., Bendigeri, D., Xiao, S. (2012) Sphingolipids and plant defense/disease: the "death" connection and beyond. Front. Plant Sci. 3:68.

Bi, F.C., Liu, Z., Wu, J.X., Liang, H., Xi, X.L., Fang, C., Sun, T.J., Yin, J., Dai, G.Y., Rong, C., Greenberg, J.T., Su, W.W., Yao, N. (2014) Loss of ceramide kinase in Arabidopsis impairs defenses and promotes ceramide accumulation and mitochondrial H_2O_2 bursts. Plant Cell. (8):3449-67.

Brodersen P, Petersen M, Pike HM, Olszak B, Skov S, Odum N, Jørgensen LB, Brown RE, Mundy J. (2002) Knockout of Arabidopsis ACCELERATED-CELL-DEATH11 encoding a sphingosine transfer protein causes activation of programmed cell death and defense. Genes and Development 16: 490–502.

Coursol, S., Fan, L-M., Le Stunff, H., Spiegel, S., Gilroy, S., Assmann SM. (2003) Sphingolipid signalling in Arabidopsis guard cell involves heterotrimeric G proteins. Nature 423: 651–654.

Coursol, S., Le Stunff, H., Lynch, D.V., Gilroy, S., Assmann, S.M., Spiegel, S. (2005) Arabidopsis sphingosine kinase and the effects of phytosphingosine-1-phosphate on stomatal aperture. Plant Physiol. 137: 724–737.

Kim, J.K., Harada, K., Bamba, T., Fukusaki, E., Kobayashi, A. (2005) Stable isotope dilution-based accurate comparative quantification of nitrogen-containing metabolites in *Arabidopsis thaliana* T87 cells using in vivo (15)N-isotope enrichment. Biosci Biotechnol Biochem. 69:1331-40.

Lachaud, C., Da Silva, D., Cotelle, V., Thuleau, P., Xiong, T.C., Jauneau, A., Briere, C., Graziana, A., Bellec, Y., Faure, J.D. et al. (2010) Nuclear calcium controls the apoptotic-like cell death induced by d-erythro-sphinganine in tobacco cells. Cell Calcium 47: 92–100.

Liang, H., Yao, N., Song, J.T., Luo, S., Lu, H., and Greenberg, J.T. (2003). Ceramides modulate programmed cell death in plants. Genes Dev. 17: 2636–2641.

Luttgeharm, K.D., Cahoon, E.B., Markham, J.E. (2016) Substrate specificity, kinetic properties and inhibition by fumonisin B1 of ceramide synthase isoforms from Arabidopsis. Biochem J. 473:593-603.

Markham, J.E., Molino, D., Gissot, L., Bellec, Y., Hématy, K., Marion, J., Belcram, K., Palauqui, J.C., Satiat-Jeunemaître, B., and Faure, J.D. (2011). Sphingolipids containing very-long-chain fatty acids define a secretory pathway for specific polar plasma membrane protein targeting in Arabidopsis. Plant Cell 23: 2362–2378.

Mur, L.A., Aubry, S., Mondhe, M., Kingston-Smith, A., Gallagher, J., Timms-Taravella, E., James, C., Papp, I., Hörtensteiner, S., Thomas, H., Ougham, H. (2010) Accumulation of chlorophyll catabolites photosensitizes the hypersensitive response elicited by *Pseudomonas syringae* in Arabidopsis. New Phytol. 188:161-74.

Ng, C.K.Y., Carr, K., McAinsh, M.R., Powell, B., Hetherington, A.M. (2001) Drought-induced guard cell signal transduction involves sphingosine-1-phosphate. Nature 410: 596–599.

Peer, M., Stegmann, M., Mueller, M.J., and Waller, F. (2010). *Pseudomonas syringae* infection triggers de novo synthesis of phytosphingosine from sphinganine in *Arabidopsis thaliana*. FEBS Lett. 584: 4053–4056.

Saucedo-García M, Guevara-García A, González-Solís A, Cruz-García F, Vázquez-Santana S, Markham JE, Lozano-Rosas MG, Dietrich CR, Ramos-Vega M, Cahoon EB, Gavilanes-Ruíz M. (2011) MPK6, sphinganine and the LCB2a gene from serine palmitoyltransferase are required in the signaling pathway that mediates cell death induced by long chain bases in Arabidopsis. New Phytol. 191:943-57.

Shi, L., Bielawski, J., Mu, J., Dong, H., Teng, C., Zhang, J., Yang, X., Tomishige, N., Hanada, K., Hannun, Y.A. et al. (2007) Involvement of sphingoid bases in mediating reactive oxygen intermediate production and programmed cell death in Arabidopsis. Cell Research 17: 1030–1040.

Stone, J.M., Heard, J.E., Asai, T., Ausubel, F.M. (2000) Simulation of fungal mediated cell death by fumonisin B1 and selection of fumonisin B1-resistant (*fbr*) Arabidopsis mutants. Plant Cell 12: 1811–1822.

Takahashi, Y., Berberich, T., Kanzaki, H., Matsumura, H., Saitoh, H., Kusano, T., Terauchi, R. (2009) Serine palmitoyltransferase, the first step enzyme in sphingolipid biosynthesis, is involved in nonhost resistance. Molecular Plant–Microbe Interactions 22: 31–38.

Ternes, P., Feussner, K., Werner, S., Lerche, J., Iven, T., Heilmann, I., Riezman, H., and Feussner, I. (2011). Disruption of the ceramide synthase LOH1 causes spontaneous cell death in *Arabidopsis thaliana*. New Phytol. 192: 841–854.

Townley, H.E., McDonald, K., Jenkins, G.I., Knight, M.R., Leaver, C.J. (2005) Ceramides induce programmed cell death in Arabidopsis cells in a calcium-dependent manner. Biological Chemistry 386: 161–166.

Wang W, Yang X, Tangchaiburana S, Ndeh R, Markham JE, Tsegaye Y, Dunn TM, Wang GL, Bellizzi M, Parsons JF et al. (2008) An inositolphosphorylceramide synthase is involved in regulation of plant programmed cell death associated with defense in Arabidopsis. Plant Cell 20: 3163–3179.

6 APPENDIX A

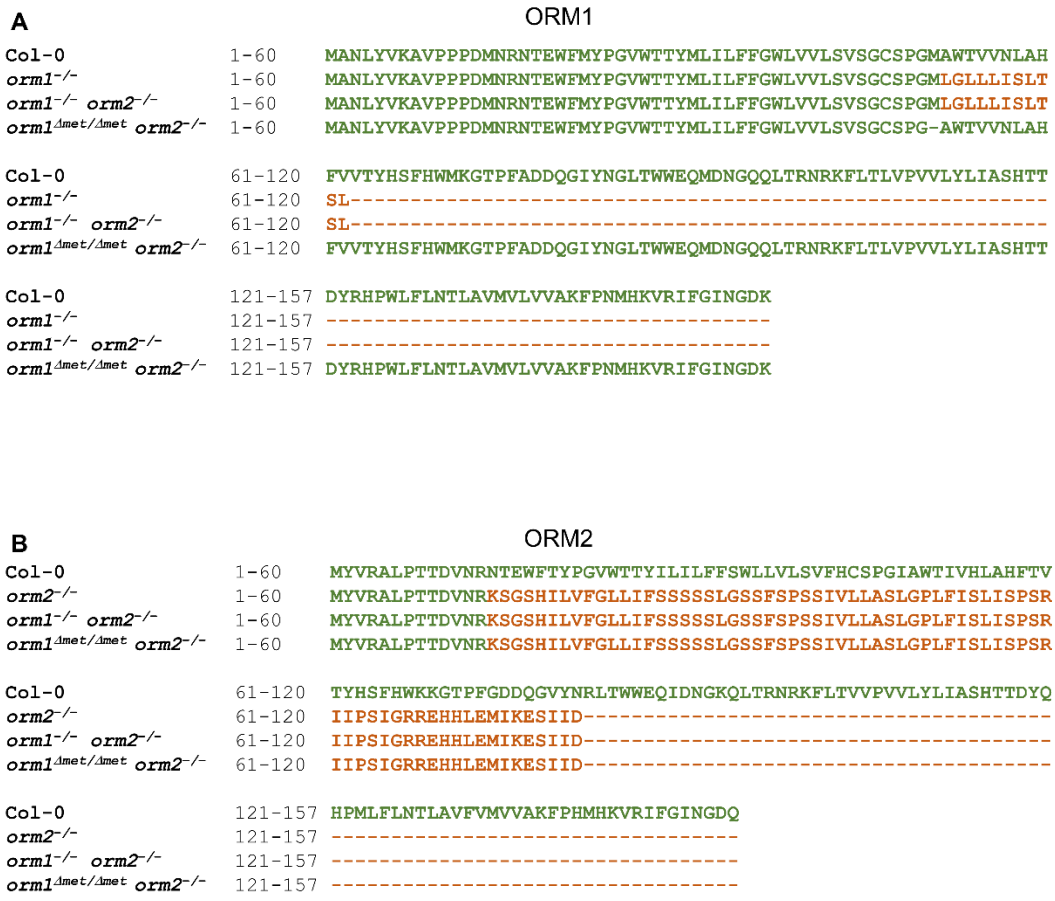

Supplemental Figure 1. Predicted Protein Sequences of ORMs in the CRISPR/Cas9 Mutants.

Predicted protein sequences based on indels. **(A)** ORM1, for the single mutant *orm1*$^{-/-}$ and the double knockout *orm1*$^{-/-}$ *orm2*$^{-/-}$, the deletion of one nucleotide in the first exon resulted in a frameshift in the coding sequence that produced premature termination. In the case of *orm1*$^{\Delta met/\Delta met}$ *orm2*$^{-/-}$ the deletion of three nucleotides resulted in the elimination of a methionine residue at position 51. **(B)** ORM2, for the single mutant *orm2*$^{-/-}$ and double mutants, the deletion of four nucleotides caused a frameshift and premature termination of the polypeptide.

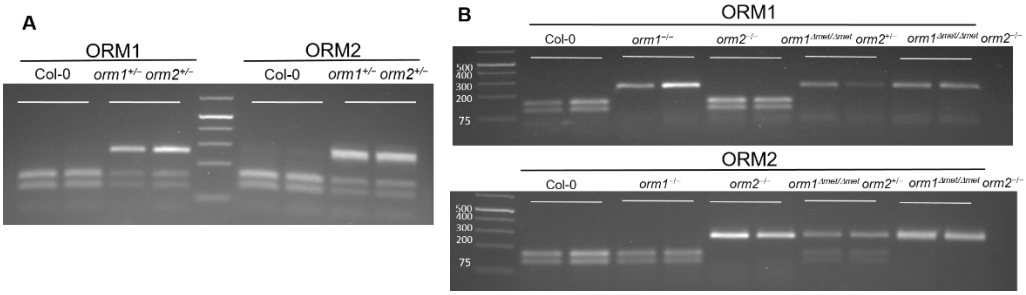

Supplemental Figure 2. PCR/Digestion-based Genotyping of CRISPR/Cas9 ORM Mutants.

The DNA fragment encompassing the CRISPR target site was amplified by PCR (Primers P5-P8) and digested with *BslI* (*ORM1*) or *DraIII* (*ORM2*).
(A) Representative genotyping results of wild-type Col-0 and $orm1^{+/-}$ $orm2^{+/-}$.
(B) Representative genotyping results of wild-type Col-0, $orm1^{-/-}$, $orm2^{-/-}$, $orm1^{\Delta met/\Delta met}$ $orm2^{+/-}$ and $orm1^{\Delta met/\Delta met}$ $orm2^{-/-}$. In wild-type plants, the DNA is completely digested at the restriction site. In homozygous plants, the restriction site was lost by CRISPR/Cas9-induced mutation, resulting in undigested DNA. In heterozygous plants, the restriction site is present in one gene copy, resulting in partial digestion.

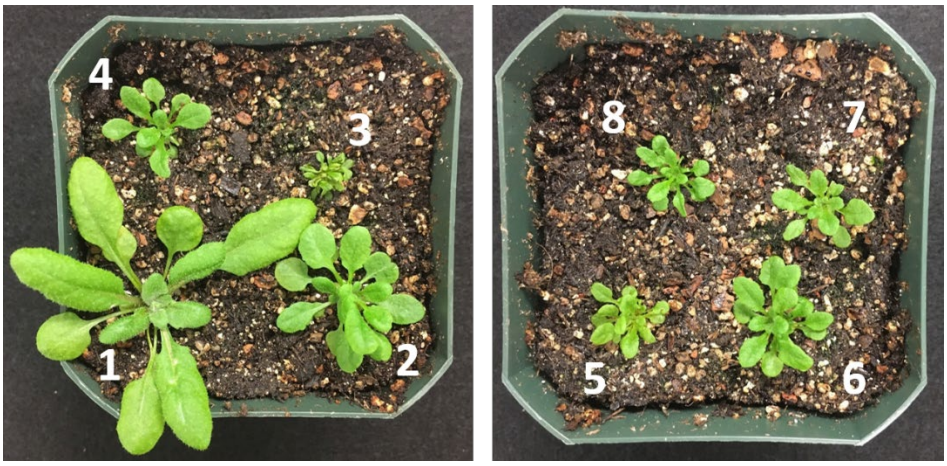

Supplemental Figure 3. Complementation of *orm1*$^{\Delta met/\Delta met}$ *orm2*$^{-/-}$.

(1) Wild-type plant, **(2-8)** *orm1*$^{\Delta met/\Delta met}$ *orm2*$^{-/-}$ plants complemented with a codon optimized version of *ORM1* under the control of its native promoter.

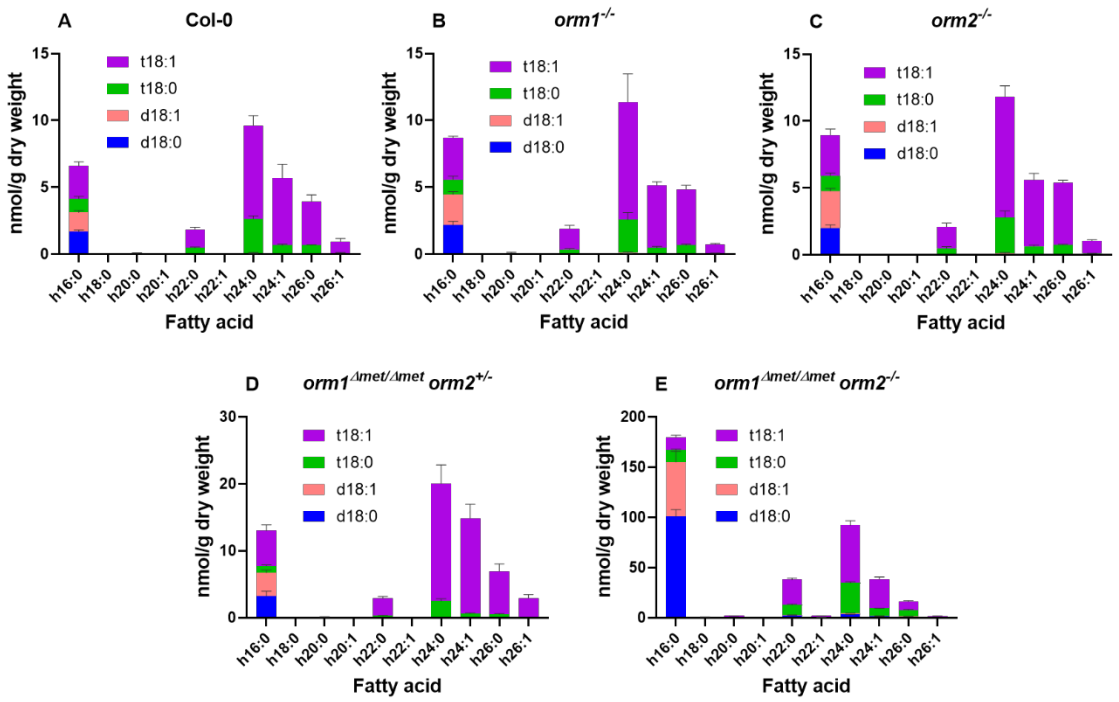

Supplemental Figure 4. Ceramide Compositions with Hydroxylated Fatty Acids in *ORM* Mutants.

Concentrations of ceramides with hydroxylated fatty acids (hCer) are presented according to the composition of LCB (d18:0, d18:1, t18:0, t18:1) and hydroxylated (h) fatty acid for **(A)** wild-type Col-0, **(B)** *orm1*$^{-/-}$, **(C)** *orm2*$^{-/-}$, **(D)** *orm1*$^{\Delta met/\Delta met}$ *orm2*$^{+/-}$ and **(E)** *orm1*$^{\Delta met/\Delta met}$ *orm2*$^{-/-}$. Bars show averages of four to six replicates consisting of 12 to 15-day-old pooled seedlings grown on different plates. Error bars represent the standard error of the mean.

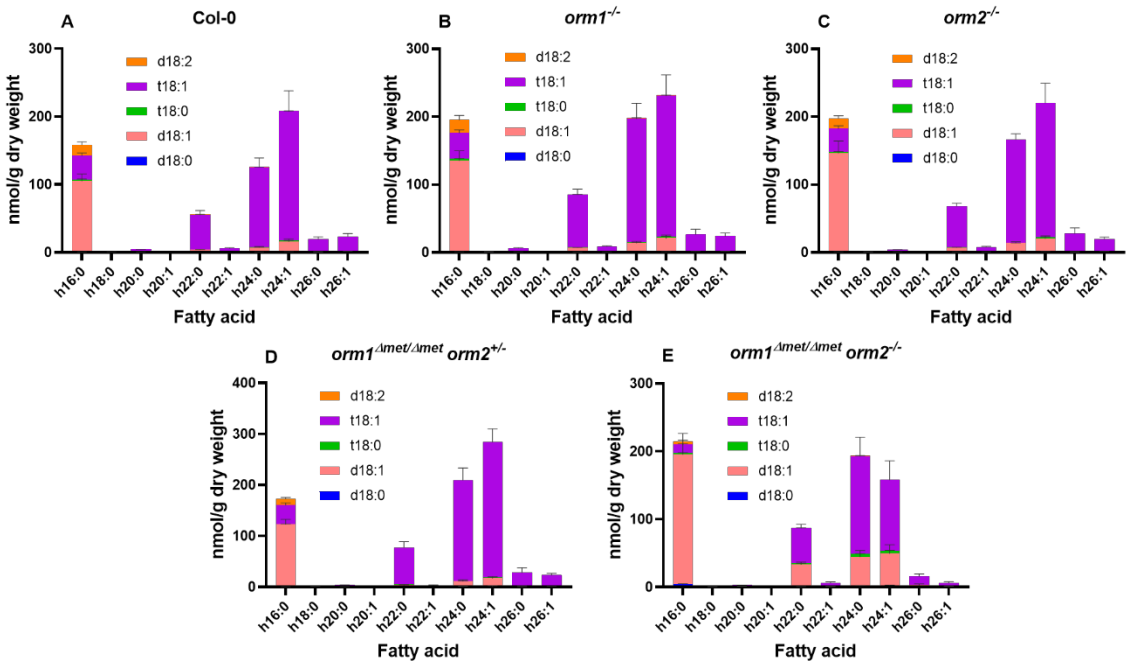

Supplemental Figure 5. Glucosylceramide Compositions in *ORM* Mutants.

Glucosylceramide (GlcCer) concentrations are presented according to the composition of LCB (d18:0, d18:1, t18:0, t18:1) and hydroxylated (h) fatty acid for **(A)** wild-type Col-0, **(B)** *orm1*$^{-/-}$, **(C)** *orm2*$^{-/-}$, **(D)** *orm1*$^{\Delta met/\Delta met}$ *orm2*$^{+/-}$ and **(E)** *orm1*$^{\Delta met/\Delta met}$ *orm2*$^{-/-}$. Bars show averages of four to six replicates consisting of 12 to 15-day-old pooled seedlings grown on different plates. Error bars represent the standard error of the mean.

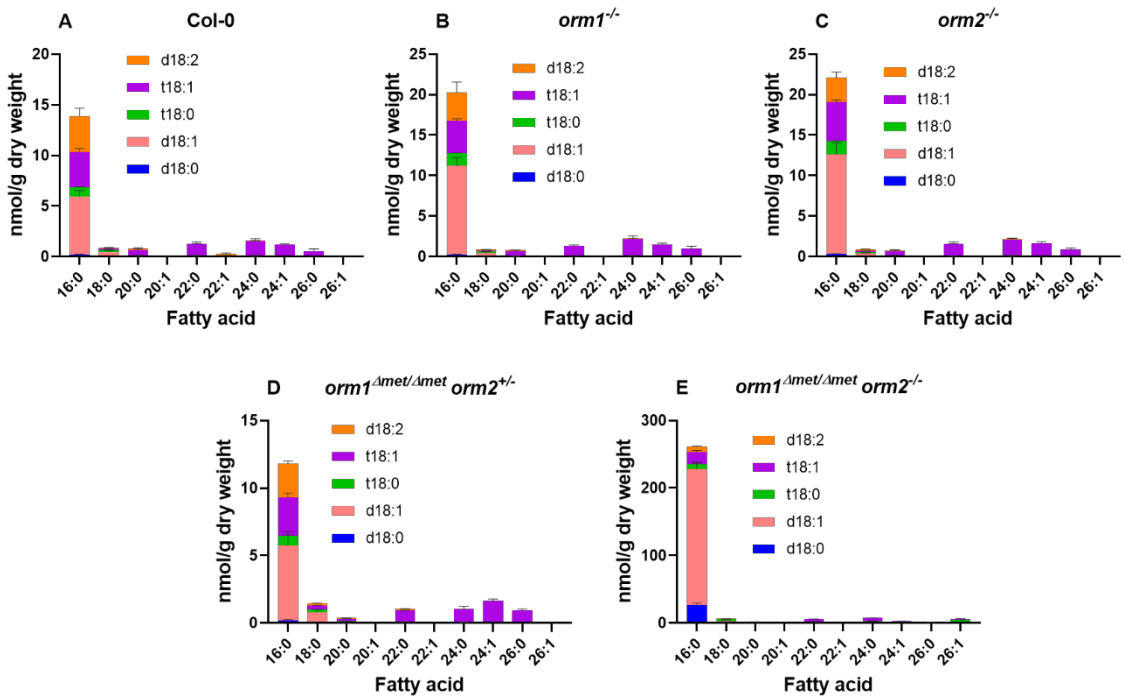

Supplemental Figure 6. Composition of Glucosylceramides Containing Non-Hydroxylated Fatty Acids in *ORM* Mutants.

Concentrations of glucosylceramides containing non-hydroxylated fatty acids (nh-GlcCer) are presented according to the composition of LCB (d18:0, d18:1, t18:0, t18:1) and fatty acid for **(A)** wild-type Col-0, **(B)** *orm1*$^{-/-}$, **(C)** *orm2*$^{-/-}$, **(D)** *orm1*$^{\Delta met/\Delta met}$ *orm2*$^{+/-}$ and **(E)** *orm1*$^{\Delta met/\Delta met}$ *orm2*$^{-/-}$. Bars show averages of four to six replicates consisting of 12 to 15-day-old pooled seedlings grown on different plates. Error bars represent the standard error of the mean.

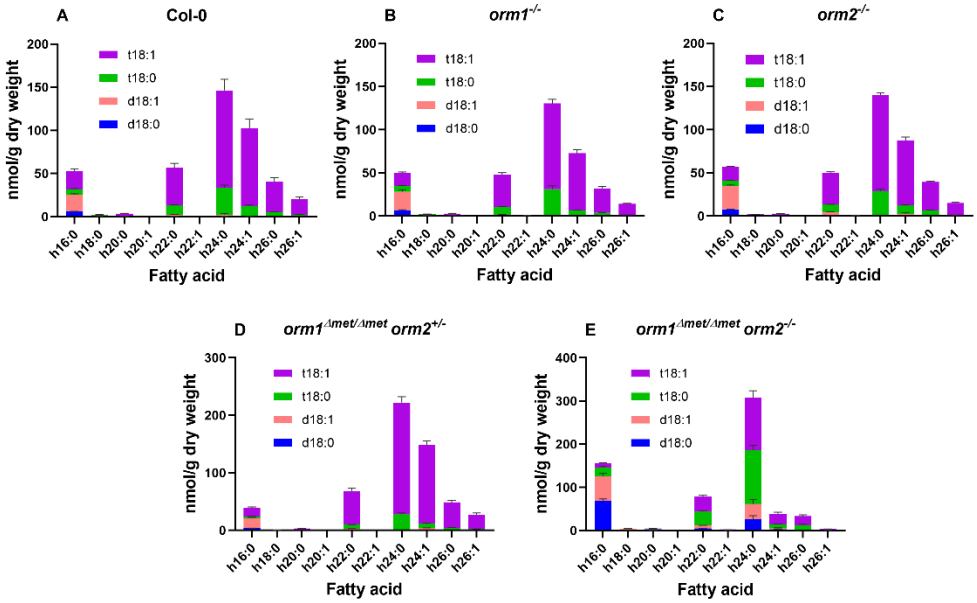

Supplemental Figure 7. Glycosylinositolphosphoceramide Compositions in *ORM* Mutants.

Glycosylinositolphosphoceramide (GIPC) concentrations are presented according to the composition of LCB (d18:0, d18:1, t18:0, t18:1) and the hydroxylated (h) fatty acid for **(A)** wild-type Col-0, **(B)** *orm1*$^{-/-}$, **(C)** *orm2*$^{-/-}$, **(D)** *orm1*$^{\Delta met/\Delta met}$ *orm2*$^{+/-}$ and **(E)** *orm1*$^{\Delta met/\Delta met}$ *orm2*$^{-/-}$. Bars show averages of four to six replicates consisting of 12 to 15-day-old pooled seedlings grown on different plates. Error bars represent the standard error of the mean.

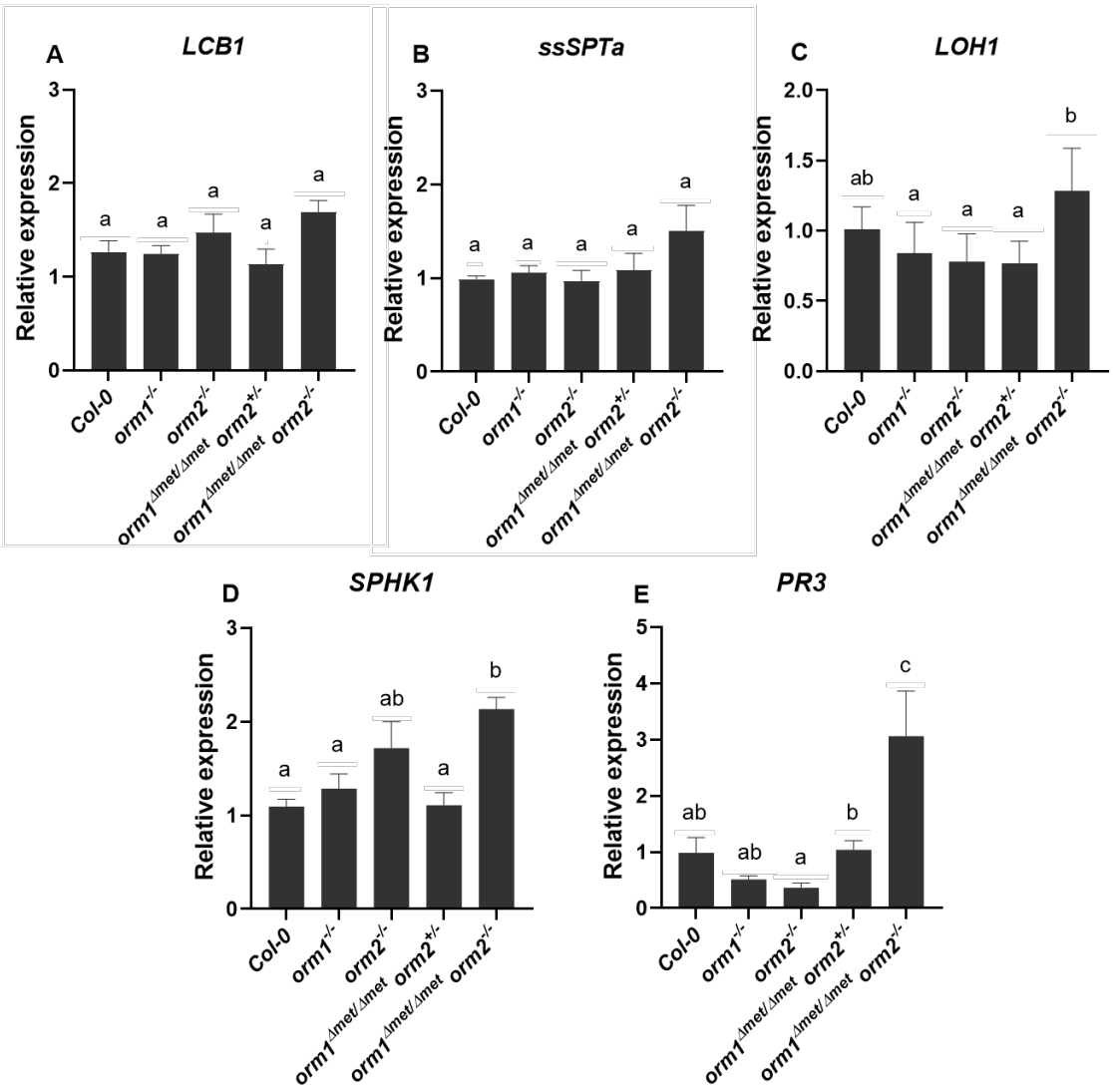

Supplemental Figure 8. Expression of Genes Associated with Sphingolipid Biosynthetic and Catabolic Pathways and Pathogenesis.

Wild-type, *orm1*$^{-/-}$, *orm2*$^{-/-}$, *orm1*$^{\Delta met/\Delta met}$ *orm2*$^{+/-}$ and *orm1*$^{\Delta met/\Delta met}$ *orm2*$^{-/-}$ seedlings (12-day-old plants) were used to examine gene expression by qPCR to monitor genes encoding enzymes in the sphingolipid biosynthetic and catabolic pathways: **(A)** *LCB1*, **(B)** *ssSPTa*, **(C)** ceramide synthase gene *LOH1,* **(D)** sphingosine kinase 1 gene *SPHK1;* and the selected pathogenesis-related gene **(E)** basic chitinase *PR3*. *PP2AA3* transcript levels were used as a control for the sphingolipid genes and *UBIQUITIN* for the pathogenesis-related genes. Specific primers used for this analysis are shown in Supplemental Table 1. Gene expression levels are normalized to those in wild-type seedlings. Values are the mean ± SD (n=6-12). Different letters indicate significant difference based on one-way ANOVA followed by Tukey's multiple comparisons test (P≤0.05).

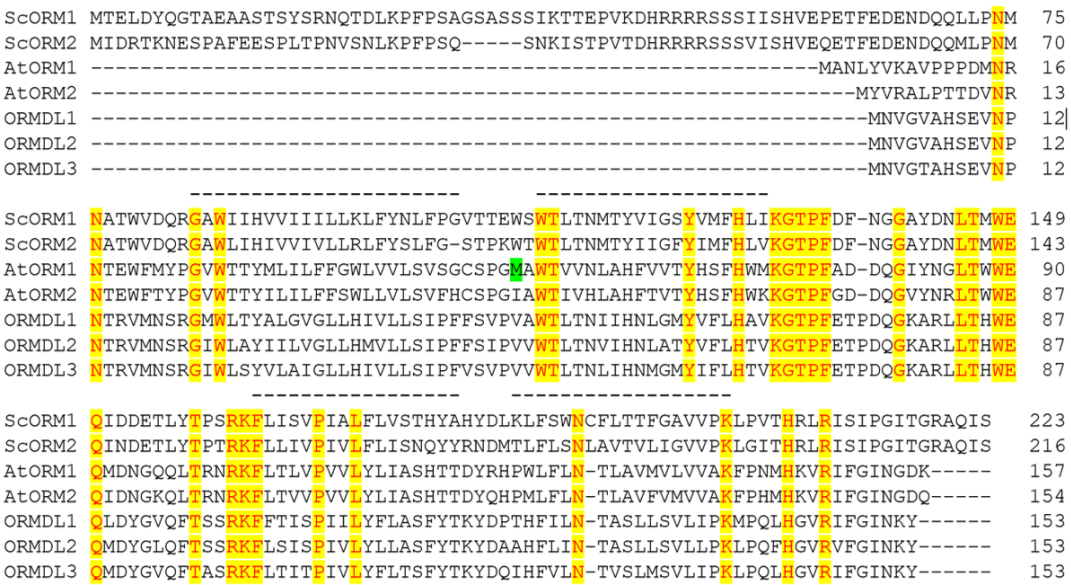

Supplemental Figure 9. Amino Acid Sequence Alignment of ORM Proteins.

Protein sequences from *Saccharomyces cerevisiae* (*Sc*), *Arabidopsis thaliana* (*At*) and *Homo sapiens* (ORMDL). The dashed lines indicate putative transmembrane domains. Methionine 51 in AtORM1 is highlighted (green) as well as conserved amino acids (yellow).

Supplemental Table 1. Primer Sequences Used for Cloning, RT-PCR, qPCR, and Genotyping.

Primer	Primer Name	Sequence	
P1	ORM1-BsF	5'-ATATATGGTCTCGATTGTTGTTCCCCTGGAATGGCTGTT-3'	Cloning *Bsa*I
P2	ORM1-F1	5'-TGTTGTTCCCCTGGAATGGCTGTTTTAGAGCTAGAAATAGC-3'	Cloning
P3	ORM2-R1	5'-AACCTCTGTGTTCCGATTCACACAATCTCTTAGTCGACTCTAC-3'	Cloning
P4	ORM2-BsR	5'-ATTATTGGTCTCGAAACCTCTGTGTTCCGATTCACACAA-3'	Cloning *Bsa*I
P5	ORM1-F	5'-GAAATGGCGAATCTGTATG-3'	Genotyping
P6	ORM1-R	5'-CATCATCTAATTTAAAGTCAC-3'	Genotyping
P7	ORM2-F	5'-CTTGCTCAACGACGATTCAT-3'	Genotyping
P8	ORM2-R	5'-GAGGAGATCGGGAATAATAC-3'	Genotyping
P9	Cas9-F	5'-CTGTTCGTCGAGCAGCACAAGCATT-3'	Cas9 check
P10	Cas9-R	5' TTCCCAATGCCATAATACTCAAACTCAG-3'	Cas9 check
P11	A_OptORM1F	5'-ATGCGAATTCATGGCGAATCTGTATGTGA-3'	Cloning *Eco*RI
P12	B_OptORM1r	5'-CAGTCCATGCCATACCTGGAGAGCAACCAGAG-3'	Overlapping PCR
P13	C_OptORM1f	5'-CTCTGGTTGCTCTCCAGGTATGGCATGGACTG-3'	Overlapping PCR
P14	D_OptORM1R	5'-ATGCTCTAGATTATTTATCACCATTG-3'	Cloning *Xba*I
P15	ORM1promoterF	5'-ATGCGGATCCCTTTGGCTGCACTCCTCTCT-3'	Cloning *Bam*HI
P16	ORM1promoterR	5'-ATGCGAATTCTTCTTCTTCAATCAGATCGGATCG -3'	Cloning *Eco*RI
P17	PP2AA3 (At1g13320)	QuantiTect Qiagen QT00857220	qPCR
P18	LOH1 (At3g25540)	QuantiTect Qiagen QT00779331	qPCR
P19	LOH2 (At3g19260)	QuantiTect Qiagen QT00774949	qPCR
P20	LOH3 (At1g13580)	QuantiTect Qiagen QT00857402	qPCR
P21	LCB1 (At4g36480)	QuantiTect Qiagen QT00727251	qPCR
P22	ssSPTa (At1g06515)	QuantiTect Qiagen QT01712004	qPCR
P23	DPL1qpcr-F	5'-GCTTGGTCAACTGGCTCTTA-3'	qPCR
P24	DPL1qpcr-R	5'-GGGATCTGGTACCCAAGTTTAC-3'	qPCR
P25	Sphk1-qpcr-F	5'-AGACCTTGGTTGAGAAAGGAGGAG-3'	qPCR
P26	Sphk1-qpcr-R	GATGGAACTTATCGGACCAAAGCT	qPCR
P27	Sphk2-qpcr-F	CGGTGGACAGAGTATGGACTCC	qPCR
P28	Sphk2-qpcr-R	GCAGCAGATTCCTCCTGCCT	qPCR
P29	PRXc-qpcr-F	5'-CAACATCGTCCACTTGGACAATCTT-3'	qPCR
P30	PRXc-qpcr-R	5'-CCTGCCAAAGTGACAGATTGTTGAG-3'	qPCR
P31	PR2-qpcr-F	5'-AGCCTCACCACCAATGTTGATGAT-3'	qPCR
P32	PR2-qpcr-R	5'-GTTCTCGATGTTCTGCATTGCTTGT-3'	qPCR

P33	PR3-qpcr-F	5’-AACGGTCTATGCTGCAGCGAGTT-3’	qPCR
P34	PR3-qpcr-R	5’-GCGCTCGGTTCACAGTAGTCTGA-3’	qPCR
P35	FMO-qpcr-F	5’-CGTATTCGAAGCCTCGGATTCAGTC-3’	qPCR
P36	FMO-qpcr-R	5’-GGTATTCTTGGAACGTCGCCGTATT-3’	qPCR
P37	SAG13-qpcr-F	5’-GAAACTCAGCTTCAAGAACGCTTACGTG-3’	qPCR
P38	SAG13-qpcr-R	5’-TCGCCCATTCGCAAGCTAAGTTT-3’	qPCR

Underlined sequences correspond to the restriction enzyme sites.

7 APPENDIX B

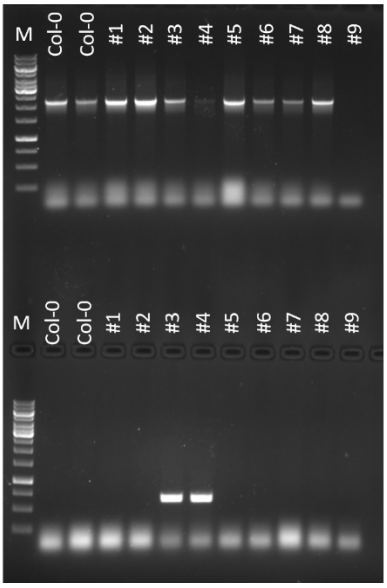

Supplemental Figure 1. Amplification with gene specific primers (P2+P3 Supplemental Table 1, Appendix B) indicate wild type LCB1, while amplification with T-DNA primers (P1+P3) indicate the presence of the T-DNA. A PCR product amplified with both primer sets indicates heterozygous line. Amplification with only gene specific primers corresponds to wild type.

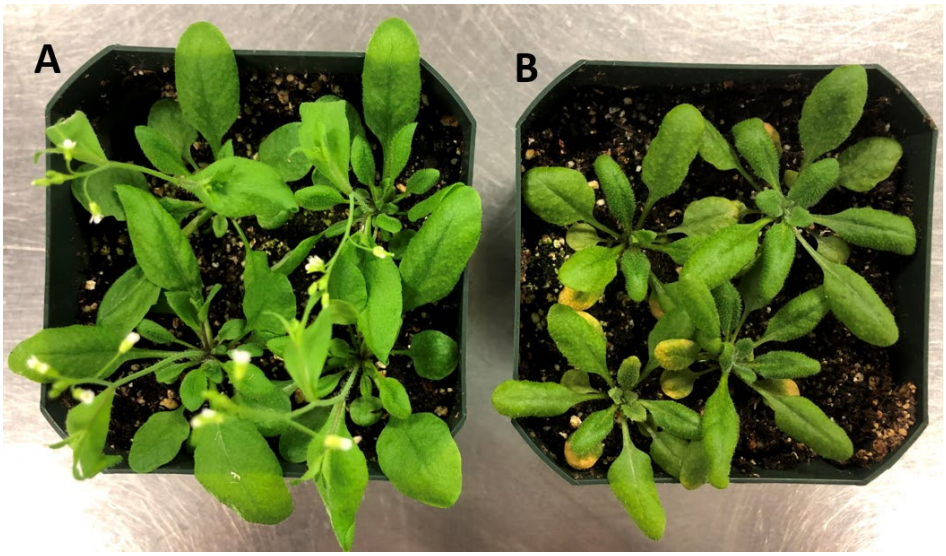

Supplemental Figure 2. 30 days-old representative plants **(A)** Col-0 and **(B)** LCB1^{C144W}

Supplemental Table 1. Primer Sequences Used for Genotyping and qPCR.

Primer	Primer Name	Sequence	
P1	Lb1a	5'-TGGTTCACGTAGTGGGCCATCG-3'	Genotyping
P2	F1	5'-GATGGCTTCATGTAATGTTTGTACTTTC-3'	Genotyping
P3	R	5'-TGGTGGCTCATGCTTCATGTC-3'	Genotyping
P4	PP2AA3 (At1g13320)	QuantiTect Qiagen QT00857220	qPCR
P5	LOH2 (At3g19260)	QuantiTect Qiagen QT00774949	qPCR
P6	SAG13-qPCR-F	5'-GAAACTCAGCTTCAAGAACGCTTACGTG-3'	qPCR
P7	SAG13-qPCR-R	5'-TCGCCCATTCGCAAGCTAAGTTT-3'	qPCR
P8	ORM1-qPCR-F	5'-AATGGTCAACAGCTTACCCGCAA-3'	qPCR
P9	ORM1-qPCR-R	5'-TATGCGATGCAATCAAGTACAGAACAAC-3'	qPCR
P10	ORM2-qPCR-F	5'-TTGATAATGGCAAGCAGCTTACACGTA-3'	qPCR
P11	ORM2-qPCR-R	5'-ATCAAGTACAAGACAACAGGAACAACGG-3'	qPCR